LIÈGE université
Gembloux
Agro-Bio Tech

Assessing soil cracks' dynamics in relation to mucilage application and soil hydraulic properties under different soil management practices in Wallonia Belgium, using image analysis

Njaka Andriamanantena RALAIZAFISOLOARIVONY

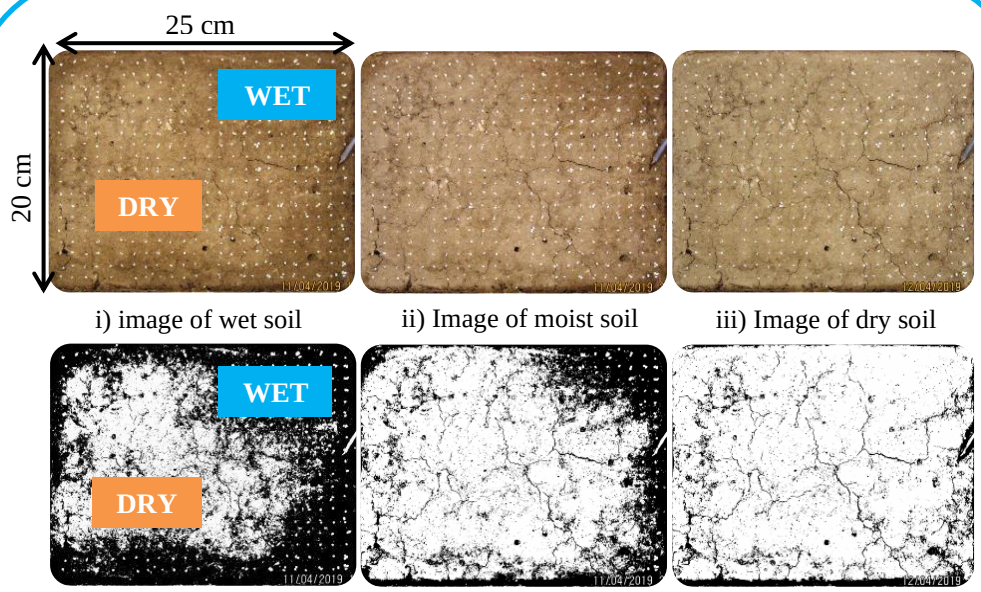

i) image of wet soil ii) Image of moist soil iii) Image of dry soil

**The black pixels indicated the wetter part of the sample*

iv) Binary image of wet soil v) Binary image of moist soil vi) Noisy binary image of dry soil

COMMUNAUTÉ FRANÇAISE DE BELGIQUE
UNIVERSITÉ DE LIÈGE – GEMBLOUX AGRO-BIO TECH

ASSESSING SOIL CRACKS' DYNAMICS IN RELATION TO MUCILAGE APPLICATION AND SOIL HYDRAULIC PROPERTIES UNDER DIFFERENT SOIL MANAGEMENT PRACTICES IN WALLONIA BELGIUM, USING IMAGE ANALYSIS

Njaka Andriamanantena RALAIZAFISOLOARIVONY

Dissertation originale présentée en vue de l'obtention du grade de docteur en sciences agronomiques et ingénierie biologique

Promoteur: Prof. Aurore DEGRÉ et Co-Promoteur: Prof. Robert CHARLIER
Année civile : 2022

Résumé

La fissuration du sol est un phénomène largement observé sur les parcelles agricoles. Plusieurs observateurs ont affirmé que ce phénomène peut avoir des impacts tant positifs que négatifs sur la dynamique de l'eau contenue dans le sol. En effet, la fissuration peut affecter la rétention d'eau et la perméabilité en eau du sol. De plus le séchage excessif du sol induit chez les plantes un stress hydrique pouvant nuire à la productivité agricole. Les mécanismes de la fissuration du sol restent cependant flous. Les effets de la fissuration sur les caractéristiques du sol sont difficiles à évaluer. Cela est dû au fait qu'une compréhension approfondie du phénomène nécessite à la fois une connaissance des fissures (par analyse d'images) et de l'hydrologie du sol. L'étude s'avère d'autant plus complexe si des paramètres agricoles tels que le travail du sol et la gestion des résidus sont ajoutés à la recherche. Pourtant, la connaissance du processus de fissuration du sol dans le cadre d'une gestion agricole réelle (labour + gestion des résidus) contribuerait à améliorer la productivité des cultures.

Le premier défi majeur de cette recherche concerne la méthodologie adoptée pour obtenir des informations sur la dynamique de la fissuration. Bien que des études sur l'analyse des fissures aient été menées, les analyses des fissures sur des sols agricoles non perturbés sont rares. L'analyse d'images numériques (RVB et bidimensionnelle) est une méthode scientifiquement et techniquement approuvée, qui bénéficie de l'utilisation des logiciels libres de droits ImageJ et PCAS. Ces logiciels s'améliorent rapidement grâce à l'évolution de la technologie mais aussi de l'interaction croissante avec des utilisateurs et scientifiques. La qualité et la précision des résultats (fissuration) dépendent cependant principalement des modes d'acquisition, de manipulation et de traitement des images. En étudiant plusieurs techniques spécifiques à l'analyse des fissures, nous avons pu adopter une approche améliorée et semi-automatisée qui nécessitait l'utilisation de ROI (Region Of Interest). Celle-ci consiste à faire converger l'analyse de l'image sur les zones probables de fissuration afin de réduire les effets de contraste du fond de l'image.

L'objectif de cette thèse est d'analyser la dynamique des fissures en lien avec les propriétés hydriques du sol et l'utilisation du mucilage, dans des conditions contrastées de pratiques agricoles et de gestion des résidus. Les résultats ont montré que l'étendue de la fissuration diffère significativement selon les traitements adoptés, à savoir RTRI (Labour réduit avec incorporation de résidus), CTRO (Labour conventionnel avec exportation de résidus) et DS (Sol perturbé). De plus, le fait de remanier le sol (juste après le labour du sol) multiplie la fissuration de plus de 5 à 6 fois (Crack intensity factor (CIF) : 0,3 % pour le CTRO, 0,5 % pour le RTRI et 3 % pour le DS). Cela montre l'importance de la période de labour ainsi que de la structure du sol. Enfin, d'autres paramètres tels que l'agrégation du sol, la cohésion des particules du sol, la matière organique, la teneur en fibres et la densité du sol (porosité) affectent intrinsèquement la formation et la propagation des fissures. C'est la raison pour laquelle les sols labourés (CTRO) présentaient moins de fissures que les sols à labour réduit (RTRI). La courbe de fissuration croît rapidement sur les échantillons

perturbés car ils n'ont que deux périodes (B et C) au lieu de trois pour les NDS (échantillons non perturbés). La longueur et la surface de la fissure sont statistiquement plus élevées sur DS >> RTRI > CTRO.

Le résultat a également révélé que l'amorçage de la fissure nécessite une succion négative plus forte et une teneur en eau plus faible dans DS>>CTRO>RTRI. La progression de la fissure (en longueur et en surface) augmente presque linéairement avec la succion jusqu'à atteindre 300 kPa pour le DS, et plus de 15 000 kPa pour le NDS. La succion au-dessus de 5000 kPa a été extrapolée à partir des courbes d'ajustement de van Genuchten (modèle monomodal) et Durner (modèle bimodal). La teneur en eau critique (environ 20 % Wc) est atteinte à la fin de la période de séchage à taux d'évaporation constant (CRP : évaporation maximale). Après cette période, le développement des fissures commence à s'accélérer sur les NDS (RTRI et CTRO). La distribution de la taille des pores ainsi que la courbe de Krisher démontrent l'importance des pores > 50 µm (et des fissures) sur la perméabilité du sol et sur l'évaporation. La courbe de rétention (SWRC) et la courbe de distribution des pores (PSD) indiquent le moment où la fissuration débute. La structure du sol ainsi que la gestion agricole affectent la progression des fissures. Et comme les fissures affectent le mouvement des fluides dans le sol, elles devraient également affecter les fonctions de rétention et de conductivité pendant le séchage. L'effet de la perturbation du sol semble plus important que le changement des pratiques agricoles en ce qui concerne la formation de fissures et l'hydrodynamique des sols.

Enfin, nos premiers résultats sur l'utilisation de mucilage (Chitosan (CHI), Tragacanthe (TRA) et Xanthane (XAN)) montrent que le mécanisme de séchage du sol en est modifié. Ces substances rhizosphériques peuvent absorber de manière significative l'eau et augmenter la capacité de rétention d'eau du sol (jusqu'à 75-80 % en volume pour le TRA et le XAN). L'utilisation de mucilages (Xan, TRA) à la dose de 3,6g/kg permet de diminuer la densité de fissuration ainsi que l'entropie de probabilité de (9 % et 1 %) et (59 % et 12 %) respectivement. Ces deux types de mucilage ont également retardé l'initiation des fissures de 5h. Le Xanthane contribue à réduire les fissures même à faible quantité (0,9 g/kg) tandis que le TRA perd sa capacité de contrôle à dose similaire. D'autre part, l'utilisation du CHI donne des résultats similaires au sol de référence (REF) à n'importe quelle teneur. En augmentant la température de 25 °C à 50 °C, la formation de fissures augmente sous REF/CHI tout en diminuant avec TRA/XAN. TRA/XAN réduit la formation de fissures et la dimension fractale, indiquant une diminution de la complexité de la fissure.

Grace au traitement et à l'analyse d'images, cette thèse met en évidence certains paramètres affectant la fissuration des sols (pratiques agricoles et utilisation des mucilages), ainsi que les influences probables de la fissuration sur les propriétés hydro-pédologiques.

Abstract

Soil cracking is a common phenomenon dominating the agricultural field. Several observers affirmed that this phenomenon can have positive or negative impacts on the soil hydrodynamic including water retention, soil water permeability, and soil desiccation which in turn adversely affect the crop productivity. However, the mechanisms of soil cracking remain unclear and its effect on soil water characteristics is hard to measure and quantify. This is due to the fact that a deep understanding requires both knowledge of crack analysis (image analysis) and soil hydrology. The study is more complex and scarcer if agricultural parameters such as tillage and residue management are added into the research. Yet, knowing soil cracking process under actual agricultural management (tillage + residue management) will help improving crop productivity.

The first major challenge in this research concerns the methodology adopted in order to obtain information on the dynamics of cracking. While crack analysis has been conducted before; detailed crack observations under undisturbed agricultural soils are rare. Digital image analysis (RGB and two-dimensional) is a promising option because it is proven scientifically and technically acceptable thanks to the open-source software ImageJ and PCAS. These software evolve rapidly due to evolution of technology and growing interaction between users and scientific members. However, the quality and the accuracy of the results (cracking) reside mainly on the modality of image acquisition, manipulation and processing. By investigating several techniques specific to crack analysis, we were able to adopt an improved and semi-automated approach that required the use of ROI (Region Of Interest). This consists of converging the image analysis on the probable areas of cracking in order to reduce the contrasting effects of the image background.

The objective of this thesis is to analyse crack dynamics in connection with soil water properties and mucilage application; under contrasting conditions of agricultural practice and residue management. The results showed that the extent of cracking differs significantly among the adopted treatments, namely RTRI (Reduced tillage with residue incorporation), CTRO (Conventional tillage with residue exportation) and DS (Disturbed soil). In addition, disturbing the soil (as right after tillage) increases cracking more than 5-6 times (CIF: 0.3 % for CTRO, 0.5 % for RTRI and 3 % for DS). This shows the importance of the ploughing period as well as the soil structure. Finally, other parameters such as soil aggregation, cohesion of soil particles, organic matter, fibre content, and soil density (porosity) intrinsically affect the cracks formation and propagation. This is the reason why tilled soil (CTRO) exhibited less cracking than reduced tillage soils (RTRI). Cracking curve grows quickly on disturbed samples as they only have two periods (B and C) instead of three for NDS (undisturbed samples). The length and the area of crack are statistically higher on DS >> RTRI > CTRO.

The result also revealed that initiating crack requires stronger negative suction and lower water content in DS>>CTRO>RTRI. Crack progression (in length and area) increases almost linearly with suction until reaching 300 kPa for DS, and more than

15 000 kPa for NDS. The suction above 5000 kPa was extrapolated form fitting curves of van Genuchten (monomodal model) and Durner (bimodal model). The critical water content (around 20% Wc) is attained at the end of the constant rate period (CRP: maximum evaporation). After this period, crack development commences to accelerate on NDS (RTRI and CTRO). The pore size distribution as well as the Krisher's curve demonstrate the importance of pore > 50µm (and cracks) on soil permeability and likely on evaporation. The retention curve (SWRC) and the pore distribution curve (PSD) revealed the moment of the onset of cracking. Soil structure as well as the agricultural management affect the crack progression. And as cracks affect the fluid movement in the soil, they also should affect the retention and conductivity functions during desiccation. The effect of soil disturbance seems more important than change in agricultural practices as far as crack formation and soil hydrodynamic is concerned.

Finally, some preliminary result on mucilage (Chitosan (CHI), Tragacanth (TRA), and Xanthan (XAN)) application shows that the drying mechanism of soil has been affected by mucilage. Those rhizospheric substances can absorb significantly water and increase the water retention capacity of the soil (up to 75-80 % in volume for TRA and XAN). The use of mucilages (Xan, TRA) at a dose of 3.6g/kg permit a decrease of cracking density as well as the probability entropy by (9 % and 1%), and (59 % and 12 %), respectively. Those two types of mucilage deferred as well the crack initiation by 5h. Xanthan continue to maintain its effect on crack restriction even at lower quantity (0.9 g/kg) while TRA loses its controlling capacity at similar dose. On the other hand, the effect of CHI is almost similar to reference soil (REF) at any dose. By increasing the temperature from 25 °C to 50 °C, crack formation is increasing under REF/CHI while decreasing with TRA/XAN. TRA/XAN reduces the crack disorder and the fractal dimension indicating a decrease of the crack complexity (in pattern).

This dissertation highlights some parameters affecting soil cracking (agricultural practices and use of mucilages), as well as the probable influences of cracking on the hydro-pedological property by means of image processing and analysis.

Acknowledgement

The submission of this PHD thesis is the fruit of four long years of research study. I am very grateful for a number of friends and colleagues in encouraging me to start the work, persevere through tough time and difficulty, and submit this dissertation in partial fulfilment of the requirements for the Doctor in Agronomical Sciences and Biological Bioengineering Degree at Gembloux Agro-Bio Tech, University of Liège (Belgium).

This thesis could not take place without the fund from Liège University during the first year and the FRIA fellowship (FNRS, Belgium) from the second year onward. I would like to express my profound gratitude to my supervisors Professor Aurore Degré and Professor Robert Charlier who constantly give their guidance, technical support, scientific advice and correction in order to achieve our study goal. Their seriousness, trust and dedication made this dissertation possible. I also thankful to the thesis committee members including Prof. Angélique Léonard, Prof. Toye Dominique, and Prof. Benoît Mercatoris for their precious time, advice and commitment throughout the year despite odds and circumstances. Special thanks to Dr. Eléonore Beckers, Dr. Erwan Plougonven, Dr. Vincent Leeman, Prof. Yves Brostaux, and Prof. Bernard Bodson for their available time explaining X-ray devices, computer programming, crack/image processing, statistical/data analysis and mucilage extraction. Their help facilitate a lot the data analysis and the conduct of this study.

I am very delightful to mention the name of the staff at the department Soil-Water-Plant Continuum group at Gembloux Agro-Bio Tech (GxABT): Mrs. Katia Berghmans, Mr. Stéphane Becquevort, Mr. Gilles Swerts, Mr. Daniel Baes, Mr. Alain Debacq, Prof. Sarah Garré, Prof. Gilles Colinet, and Dr. Vincent Cantreul. I am very thankful for their friendship, technical help, and constant support and availability. I don't forget as well the team of Robert Charlier, the team of Angélique Léonard, the team of Benoît Mercatoris and the team of Tea-Time Games. It is always entertaining to meet, eat together and discuss with you all during break time and in the field. Thanks to all my closest officemate and friends, Kien Tran, Jinjing Lu, Maud Grandy, Shengping Li, Pirlot Clémence, Souer Agathe N'Kweso for their sharing, laugh and help during my Ph.D. study time. Thanks to my countrymate: Aladin Danoary, Ando sy Holy, Noro Romuald and all churchmate for their sincere love and pray. May God bless you all.

Last but not least, I want to express my earnest gratitude to my wonderful wife (Aina Ranaivojaona) and my son Ralaizafisoloarivony Tony; your existence and support made my life full of wonder and plenty of love. Finally, I would like to acknowledge with gratitude the support and love of my family: my mother (Ralalasoa Sabine), my sister (Ralaizafisoloarivony Tojosoa), my nephew (Tsinjo), my niece (Vohary), my mother-in-law (Ralaiarinosy Julia), my brother-in-law (Miandra Ada), and all other family members (in Madagascar and in Europe) who kept motivating me to continue and achieve this doctoral study.

Table of contents

List of figures

Chapter 1

Chapter 2

Chapter 3

Chapter 4

Chapter 5

Chapter 6

List of tables

List of abbreviations and symbols

AGU	α-1,3-glucan
BD	Soil bulk density
CHDK	Canon Hack Development Kit
CHI	Chitosan,
CIF	Crack intensity factor
CRP	Constant Rate Period
CT	Conventional tillage
CTRO	Conventional tillage with residue-out
DF	Degree of freedom
DS	Disturbed samples
F,	F (Fisher) Statistic or F value,
FAO	Food agricultural organisation
Fd	Fractal dimension
H	Probability entropy
FRP	Falling Rate Period
IR	Infrared
Lg-RTRI/CTRO/DS	crack length for RTRI/CTRO/DS
MICP	Microbial induced calcite precipitation
Mp	Megapixel
N/A	Not applicable
NDS	undisturbed sample
NT	No-tillage
PCAS	Pores/Particles and Cracks Analysis System
PGA	Polygalacturonic acid
pH	Potential hydrogen
Pr>F	p-value
PSD	Pore size distribution
qmax	Maximum drying rate,
R2	Determination coefficient)
REF	reference soil (
REML	Restricted maximum likelihood
RGB	Red Green Blue
RH	Relative humidity
RMSE	Root mean square error)

ROI	Region of interest
RTRI	Reduced tillage with residue-in
SOC	Soil Organic Carbon
SWRC	Soil water retention curve
TC	Total carbon
TOC	Total organic carbon
TRA	Tragacanth
UK	United Kingdom
VBA	Visual Basic for Applications
Wc	Water content
Wcrit	Critical water content
Wcrit	Critical water content
Wd-RTRI/CTRO/DS	Crack width for RTRI/CTRO/DS.
XAN	Xanthan
SEM	Scanning electron microscope
ROI	Region of interest
RMSE	Root Mean Square Error
Lcr	Critical contact length
SCC	Soil-shrinkage curve
MICP	Microbial induced calcite precipitation
GPR	Ground penetration radar
ERT	Electrical resistivity tomography
EMI	Electromagnetic induction
pF	suction in logarithmic scale
Ks	Saturated hydraulic conductivity
1D,2D,3D	One, two, and three dimension

CHAPTER 1

Overall introduction showing the study research objectives

1. General overview of the study research

1.1 Soil properties in relation to soil functions and ecosystem services

Based on agricultural science, soil constitutes numbers of materials integrating minerals, stone/rock, water and air that mixes together with living (macro and micro-fauna, flora) and dead organic matter. Soil covers series of functions and services which guaranty the subsistence of humans and other lifeform into existence. Its functions can be subdivided into many groups according to the European Commission's soil protection strategy (EC 2006). Primarily, soil (depending on their types and characteristics) offers physical support medium for agricultural production (food, fibre, biomass, crop yield, horticulture, bioenergy, timber wood, forage); a good environmental support for natural plant populations and vegetation growth; anchor for plant roots; natural protector of seeds; efficient bed for seed germination and dispersal; and niches for species in the terrestrial ecosystems (including worms, fungi and bacteria); and permanent habitat for other living creatures and gene pools. Soil is also a source of raw materials, and the physical and cultural environment, for humans. It is archive of geological and archaeological heritage.

Secondly, soil participates in water cycling by collecting/keeping water for plant and organisms, regulating water infiltration, filtering and purifying surface/deep water, equilibrating soil water according to atmospheric water/gases demand. Soil absorbs water and preserves water as much as possible from surface evaporation. Associated with soil water movement, the role of soil is also to assure nutrient cycling starting from storing nutrients, preventing nitrate leaching or gas exchange, and assuring transmission/transport of water and nutrients (available) to plant roots. Along with this regulation function, soil helps transforming/degrading pollutants compounds, buffering organic and inorganic compounds including toxic organic pollutants, antibiotics or pesticides, trace elements etc. It includes acidity buffering; for example, buffering of nitrogen oxides. Soil plays key role in regulating greenhouse gases by storing and sinking carbon pool and other substances. Therefore, it aids regulating the earth's temperature and averting global warming.

Of course, soil relays on its properties (physical: structure, texture, etc; chemical: pH, SOC, etc) to fulfil its function. In agricultural soils, these soil properties (especially soil structures) are the results of several years of physical/chemical/biological (fauna, flora) construction where individual particles of sand, silt, clay, and organic matter group together to form small crumbs to large blocks of aggregates (or peds). The relationship between (i) soil properties, (ii) soil functions and (iii) ecosystem services as well as (iv) field of benefit is summarised in the Figure 1-1 bellow. The graph portrays that change in one parameter could influence the overall stability of the entire system. For example, soil in its intact/undisturbed structure resists against erosion (water) while helping nutrient/water retention and cycling. In the opposite, soil with poor structure (compacted soil) affects the soil water-holding capacity, and reduces nutrient uptake to crop. Soil structural

degradation puts in danger the soil processes such as sorption, degradation, heat/gas exchange, nutrient leaching and water flow.

Soils functions are threatened by a variety of processes which could be detrimental for the ecosystem services. Many of the following soil threats are identified in Europe. One of the prime threats affecting soil function are coming from natural and human origin. Human activities and different management practices play important role in soil function. For instance, change in land-use may enhance the greenhouse gas emission. For example, conversion of grasslands/forests land into agricultural land declines the C input and depletes the SOC stock in a very short period of time (Freibauer et al., 2004). Intensive tillage practices disrupt the soil aggregates, reduce the soil porosity, compact the soil and degrade the overall soil structure. In many cases, it accelerates surface runoff and soil erosion, clogs soil pores, disrupts water infiltration and affects water cycle. In the contrary, reduced tillage and continual addition of soil organic matter tends to increase the soil microbial biomass, enhance the species activities and diversity, and improve the soil structure (micro and microporosity) and nutrient/water cycling.

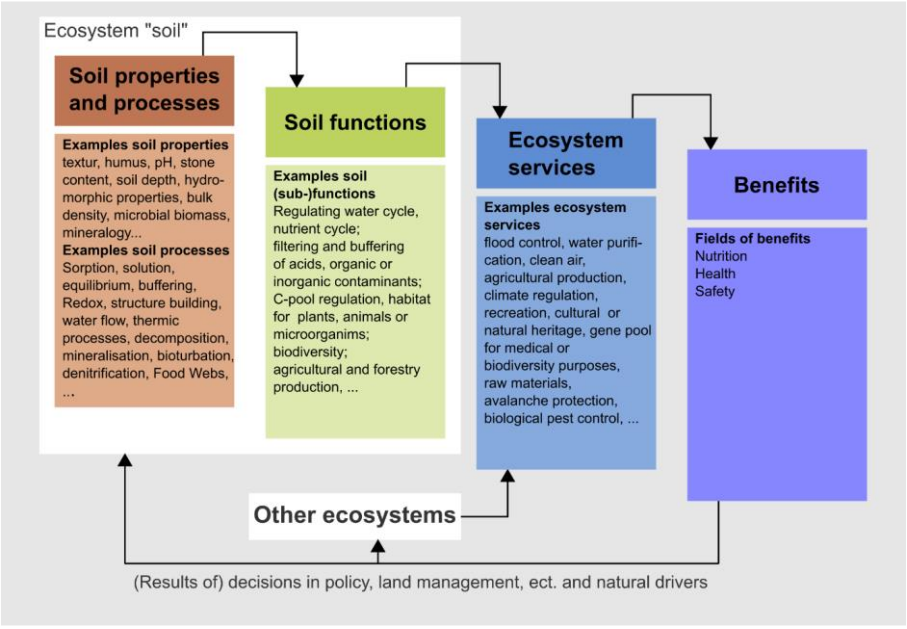

Figure 1-1 Assessment of the contributions of soil functions to ecosystem services using the cascading framework developed by Haines-Young and Potschin (2008)

Natural factor (as climate change) associated with human activities (change in land-use, tillage, organic matter exportation etc) deteriorate also the soil function and the ecosystem services. For instance, climate variation (temperature, rainfall, solar radiation) combined with tillage without additional of residue may accelerate the

organic matter mineralization and damage the soil physical, chemical and biological characteristics. It can drive the mechanisms of soil erosion, runoff, leaching and soil structural degradation etc. Decrease in organic matter can affect the soil structural stability and the soil water infiltration and storage. Currently, due to severe drought (with rising temperature) in many parts of the world including Europe, desiccation cracking becomes a serious threat especially for poorly managed soil since it opens the soil surface, allows pollutants to trespass the soil and divert from the soil buffering capacity. Cracking may also destroy the crop rooting system, and essentially affect the soil hydraulic properties (soil water infiltration, storage, suction, and soil water evaporation). This study wants to elucidate more on this effect of cracking (in conjunction with agricultural practices) on soil hydraulic properties knowing that the global warming is becoming more drastic in the near future. Understanding the actual mechanisms involved in agricultural soil cracks formation becomes therefore of major importance. The reciprocal impact of cracks on soil hydrodynamic functions as well.

1.2 Introduction to desiccation cracking

1.2.1 Definition of cracks

By definition, cracking is a drying-induced natural phenomenon in soil and other specimen (slurry, paste, pure clay, etc) as a result of various parameters including intrinsic (soil physical, biological and chemical properties) and extrinsic (temperature, RH, rainfall, seasonal variations) conditions. According to Oxford dictionary, cracking is equivalent to breaking (apart), opening and fracturing. Cracks are found to originate from internal energy imbalance inside soil due to non-uniform distribution of moisture, temperature and compaction (Hulimka et al., 2019). Cracking is controlled by soil properties such as shear strength, tensile strength, compression modulus and surface energy (Morris et al., 1992). Figure 1-2 bellow illustrates the forming cracks after rainfall event in the field of study (Gembloux).

Figure 1-2: Cracking formation observed in the field of study after rainfall

1.2.2 Different types of cracks

In general, there are two ways to classify cracks. The first way consists of categorizing cracks into four different types: shrinkage, thermal, tensile, and fracture cracks (Hulimka et al., 2019). Shrinkage cracking is the main type of cracking when wet soil starts losing its water and tensile forces take place in the drying surface. The stress is released by forming shrinkage cracks. Thermal cracking is due to thermal stress of the soil during freezing-thawing or wetting-drying. Tensile cracking is caused by overburden pressures due to structure, rain/ice/snow, vegetation etc. Fracture cracking is the resulting cracks from a mixture of shrinkage/thermal stress and pore water pressure. This can arrive during change in moisture, temperature, rainfall/snow/ground-water fluctuation. This study is focused on shrinkage cracking, however; other types of cracking could intervene in the process. For example, there could be effect of thermal cracking during wetting and drying, or tensile cracking due to increase of soil tensile stress. The second classification spread cracks according to their morphology and characteristics: size, shape/geometry, surface roughness, intensity and length/width (Qi et al., 2020). Various terminologies are used for characterising cracks such as: crack pattern and size which indicates the morphology and the size of the surface cracks. This includes length, depth, width, and area. Crack clod is a portion of soil isolated by cracks.

1.3 Why do we need to study cracks and what are their consequences?

Cracks are widespread in nature. Therefore, cracks attract attention among several disciplines including agricultural soil science. It will be the focus of this thesis.

1.3.1 Cracks affect the soil property

Crack development influences the strength properties of soil. There is contradicting information concerning cracks and soil properties. Some researchers found that desiccation cracking results into a (over)consolidation of soil due to soil shrinkage characteristic (Mesri and Ali, 2002). In the opposite, the presence of micro-fissures (alters the strength) diminishes the value of shear strength of the specimen. This is due to the alteration of the soil structure. Particularly, in agricultural soils, cracks affect the mechanical strength, bulk density, soil aeration, soil salinity (salt leaching), seedling, root penetration, soil stability and aggregate size.

1.3.2 Cracks affect the soil hydrology and can be damageable for the environment

Cracks influence also the soil hydrological properties mainly the hydraulic conductivity and the water retention. The change in hydraulic conductivity seems obvious since cracks are considered as macropores in soil and the magnitude of cracks can go up to several meter depth in nature. By following this logic, this increase in soil macropore creates another range of pores which should be observed in the soil water retention curve (SWRC). Cracking soil is therefore supposed to have greater conductivity than intact soil. However, the result of experimental study is not always giving this expectation. Some contradicting results are found in the literature. Li et al.

(2012) revealed that crack may not appear in the SWRC due to its absence during soil saturation and its late appearance during drying.

Regarding the conductivity, Rayhani et al. (2007) affirmed that cracking augmented the soil hydraulic conductivity. Drumm et al. (1997), Albrecht and Benson (2001) and Zhu et al. (2018) found that cracks become a preferential flow path and increase by three orders of magnitude the hydraulic conductivity compared to intact soil. This may facilitate the movement of pollutants in the soil.

In the agricultural soils, cracks may allow water/nutrients/air to circulate, facilitate soil infiltration, soil aeration and root penetration (Li et al., 2012; Zhang et al., 2014). However, this effect of cracks on water permeability is still discussed by the scientific community.

Some authors mentioned the possible effect of cracks on soil evaporation affecting soil water storage, and soil desiccation. All this could provoke water shortage, crop nutrient deficiency, crop yield reduction, and soil/groundwater pollution (Bronswijk, 1991). The study of Yoshida and Adachi (2001) revealed that cracks can affect the field water balance. Therefore, crack formation and development could impact the efficiency of drainage, irrigation, and even evapo-transpiration.

One of the reasons which come against the idea of cracks increasing the water permeability, is the fact that soil shrinks before forming cracks (Cornelis et al., 2006; Mishra et al., 2008; An et al., 2020). This implies that the soil decreases in porosity and therefore in permeability. Therefore, this invites us to investigate and to understand (in the following section) how crack (and its characteristics) evolve in agricultural soil, which factors control cracks, and what are the effects of cracks in the agricultural system.

1.4 How does crack initiate and propagate?

1.4.1 Crack initiation

According to Zeng et al. (2019), crack initiation is commonly guided by tensile failure mechanism (Tang et al., 2011b). When water-saturated soil is exposed to heat, water film at the surface layer starts to evaporate to the atmosphere (Figure 1-3). At this time, there is no structural change inside the sample and this early water loss does not affect the soil stress–strain states. Upon further drying, water removal increases from the surface while water–air meniscus is developing between soil particles (Figure 1-3b, c). Capillary suction augments in the upper soil layer. This suction and effective stress between soil particles continue to escalate during desiccation. This brings to shrinkage and consolidation of the sample. The decreasing of water content raises the soil tensile stress (Figure 1-3d) between soil particles and compels them to squeeze next to each other. There is enormous change in sample's volume especially for soil containing swelling clay (montmorillonite, smectite etc) (Tollenaar et al., 2017).Tensile stress develops therefore at the surface layer. According to mode-I failure, cracks forms when the tensile strength of the soil is below the tensile stress (Zeng et al., 2019) (Figure 1-3e).

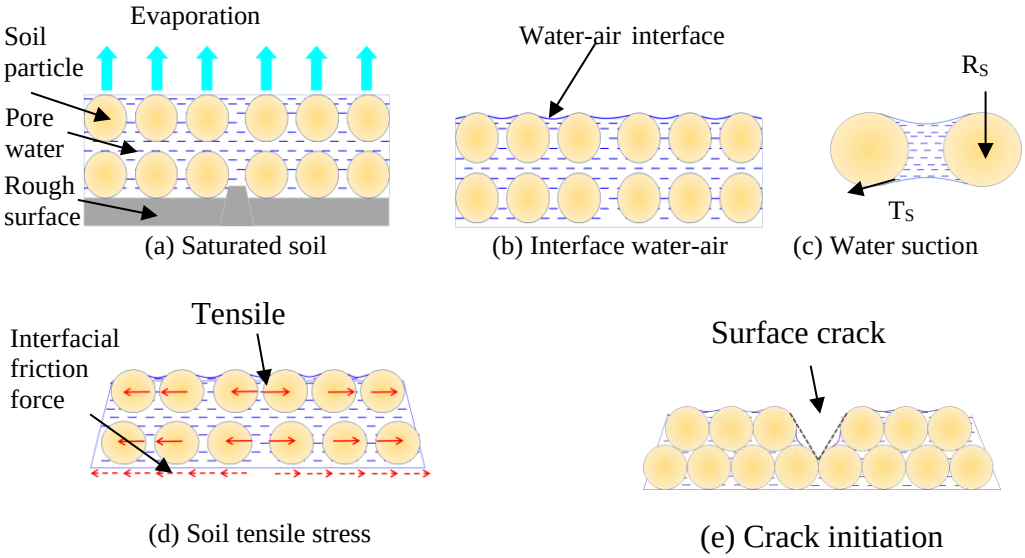

Figure 1-3 Process illustrating soil drying kinetic and crack formation (Zeng et al., 2019)

1.4.2 Where does crack initiate?

Apart from this tensile failure theory, authors reported various mechanisms of crack initiation. Tang et al. (2011b) observed that crack initiates in a particular (convex or concave areas), defected (air-filled micro-pores) and weak area. This is an area where water drained faster and air bubble forms due to cavitation and decrease of water vapor pressure of the specific point compared to the surrounding environment (Peron et al., 2009). The difference in deformation of a weak area causes the concentration of the soil stress on it (Nahlawi and Kodikara, 2006).

The result is still controversial among researchers concerning the weak area and crack initiation. Some detected crack inception at the edges of weak area (Scherer, 1990) while other reported it on the centre of the weak area (protrudes downward or laterally) (Corte and Higashi, 1960). Others pointed out the possible role of micro-cracks as a precursor for crack initiation or that crack initiates from the soil basal to the surface (Weinberger, 1999). According to Shin and Santamarina (2011), crack could be triggered by shrinkage distortion due to small soil variation (composition difference, aggregation).

The distribution of the suction (from tensile stress) and the pore pressure progression were pointed out by Tang et al. (2008) as the origin of cracks. Tang et al. (2021) reported that locating and determining crack initiation is under debate despite its importance in solving problematics in various field of research.

It is important to mention that most of those studies utilised disturbed sample, leaving rooms for studying undisturbed sample from field.

1.4.3 Crack propagation

Cracks continue to propagate after crack initiation. According to Tang et al. (2021), the progression of cracks follows three steps:

(i) Random cracks start at each weak point (or edge, or boundary), protrude towards the inner part of the surface and end at intersection. They are called primary cracks which are wide in size.

(ii) The next group of cracks (or secondary cracks) progress from the previous cracks and end when reaching another primary crack. They are thinner in size and form polygonal clods with the primary cracks. Thinner third cracks could form in linear or curved form. The term "sub-cracks" includes secondary and tertiary cracks (Style et al., 2011; Zeng et al., 2019).

(iii) The last step of crack stabilisation consists of widening (expanding) cracks without further new forming cracks (Nahlawi and Kodikara, 2006; costa et al., 2013).

Crack clod morphology forms different pattern of three types of polygons: triangle, quadrilateral (primary shape) and pentagon. Secondary cracks form orthogonal to primary crack. However, the crack intersection can be in "Y", "T" or "+" shape depending on the constraint in the sample (Lakshmikantha et al., 2009; Tollenaar et al., 2017).

1.5 What are the factors influencing crack formation?

The literature related to cracks formation is dominated by studies on disturbed clay soils. In this paragraph, we try to equilibrate with other factors, less investigated but relevant when dealing with agricultural soils with contrasted structures. Indeed, cracking is triggered by great diversity of factors including: clay type and clay content, but also soil structure, soil water content, soil suction, sample geometry, boundary conditions etc (Tang et al., 2021).

1.5.1 Clay content and type of containing clay

1.5.1.1 The type of clay

Sridharan and Jayadeva (1982) found that clay type determines the distance between clay layers and affect the soil void ratio. Among other types of phyllosilicates, Smectite and Illite present the greatest shrinkage strains (> 15%) while Kaolinite and quartz present a neutral effect (Albrecht and Benson, 2001). Soil with high swelling-shrinking capacity was due to significant percentage of smectite as reported by Tay et al., (2001), Vail et al. (2020). Tang et al. (2008) found that crack area percentage and crack width were important in soil with higher plasticity index. Cracking was around 15% in montmorillonite enriched-sample while only 10% for samples containing illite. Omidi et al. (1996) found that samples containing Smectite exhibited higher volumetric deformation of up to 15 %, followed by 10 % of volumetric deformation for samples with illite. Baer et al. (2009) and Wang et al. (2020) reported on clay soil

site (in agricultural field) that crack area and fractal dimension (of crack area) increase with smectite content but less influence on fractal-dimension (Fd) of crack edge.

1.5.1.2 Clay content

At similar type of clay, crack formation increases with the clay percentage. Kleppe and Olson (1985) discovered that crack ceased to take place at 88% of sand regardless of the clay type and water content. By consequence, sample containing 20% of clay (bentonite) shrunk significantly compared to the one with 10% (Tay et al., 2001). The work of Rayhani et al. (2008) revealed that samples with high clay content (30-45%) could increase its hydraulic conductivity by 10-20 times during drying-wetting cycle due to crack formation. Therefore, soil with high clay content is more prone to shrinkage deformation and intensive cracking formation. The loess soil of Belgium contains significant amount of high swelling clays (Smectite and Illite 12-20%)(Gentile et al., 2009; Parvin et al., 2017) making the agricultural soil prone to cracking.

1.5.2 Soil structure

1.5.2.1 Soil structure

Soil structure describes the arrangement of soil particles (or granules) that clump, bind together, and form aggregate, affecting the soil pores space, distribution and networking (Gao et al., 2017). Natural aggregate is called ped, whereas clod designates a mass of soil that is formed artificially. The aggregation of soil particles comes with various process and reaction such as: flocculation (of clay, colloid), cementation (by carbonate production, colloidal clay, sugar, biopolymers), precipitation (Fe-Al-Mg oxides, carbonates and silicates), interaction via by-product of organisms (biofilms, fungal hyphae, glycoproteins, organic glue), ionic bridging between charged particle, complexes interaction between organic–inorganic compounds (complex clay-humus interaction, calcium humate combination), other bounding (covalent bound, metallic bound, hydrogen bound etc) between mineral and organic compounds (Bronick and Lal, 2004; Yost et al., 2014; Ye et al., 2020)(Figure 1-4).

Some physical phenomenon and activity (agricultural practices) affect the soil structure because they push the soil particles to get closer (or away) such as during tillage, machinery trespassing, freezing and thawing, wetting and drying, and root insertion and expansion (growth). For instance, the work of Gao et al. (2017) showed that soil structure under reduced tillage (RT) presented bimodal pores (macro and micropores) while only monomodal pores (micropores) for conventional tillage (CT). Aggregate stability was increased when passing from CT to three years of no-tillage (NT) on loamy soil (Nunes et al., 2020). However, the bulk density was slightly decrease especially bellow the ploughing depth (Schlüter et al., 2018). Compared to conventional tillage, Daraghmeh et al., (2009) found that reduced tillage improved soil structure through a combination of increased soil organic matter, reduced soil bulk density and increased proportion of larger aggregates.

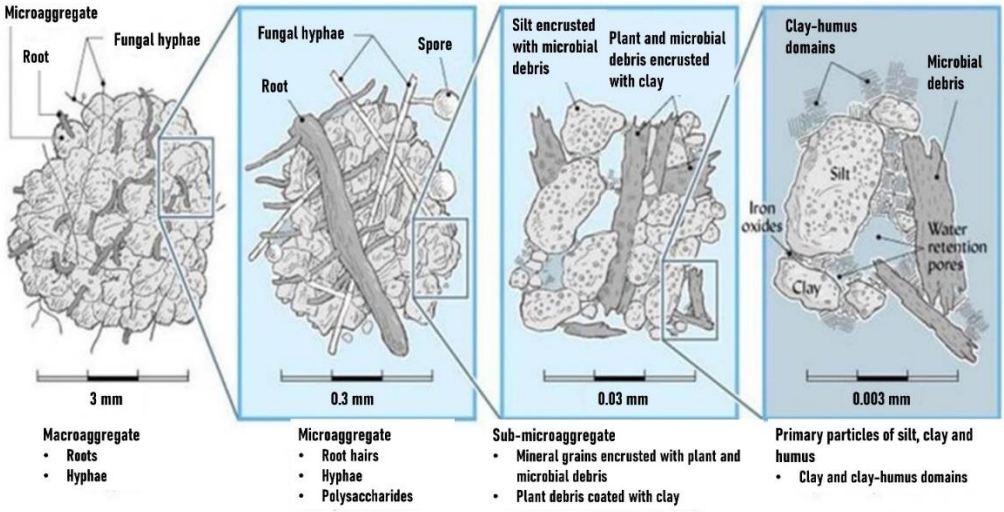

Figure 1-4 Soil aggregate size and composition. (Source: Yost et al., 2014)

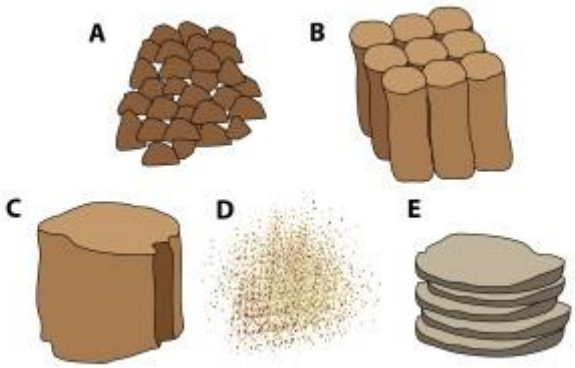

Figure 1-5 Different types of soil structure: a) blocky, b) columnar, c) massive, d) single grain, e) platy. (Source :https://www.qld.gov.au/environment/land/management/soil/soil-properties/structure)

Therefore, the formation and stability of soil structure and aggregates depends on: (a) Organic matter (including crop residue) which improves the soil structure by producing sticky substances (during decomposition of organic matter) crucial for sandy soil, and reducing the strong cohesive force of clay soil (Zhou et al., 2020). (b) Tillage (cultivation) which breaks down large clods and aggregates into smaller fragments (Gao et al., 2017; Schlüter et al., 2018). (c) Plant roots which create crumb structure and produce cementing agent to bind soil particles (Hudek et al., 2017). (d) Soil organism (micro-macro fauna, flora) that mixes soil with organic compounds and create burrow (Degrune et al., 2017). (e) Wetting-drying which produces crack that

breaks soil into clods of various size ((Tang et al., 2020; Xu et al., 2021). Soil structure is classified by type (shape), class (size) of peds, stability, and grade (strength of cohesion) of aggregates (Galloway et al., 2018). The structure can be classified as granular (highly permeable), aggregated (highly permeable), blocky (moderately permeable), columnar or prismatic (moderately permeable), platy (low permeable), and massive (low permeable) (Figure 1-5).

1.5.2.2 Soil density

The drying process results into shrinkage and restructuring of soil particles. Soil structure is therefore important during drying because samples with different structures will lead to different cracking output. The work of Corte and Higashi (1960) and Demagistri et al. (2018) compared the crack formation of saturated slurry samples versus compacted samples. They found that compacted samples took time to form cracks. Compacted samples had lower evaporation rate and vapour diffusion. The critical water content (for crack initiation) was lower than the loose soil. Albrecht and Benson (2001) found that compacted samples presented lower volumetric shrinkage strain and few cracks. Desiccation cracking was important in flocculated structured samples compared to dispersed structured samples (Fang and Chane, 2016). Soil density varies in the field depending on the agricultural practices. According to Gao et al. (2017), reduce tillage helps the soil to keep its natural structure and density in contrast with conventional tillage. However, the soil density is very low just after the tillage; but it compacted quickly as time goes by. This difference in density could affect crack formation.

1.5.3 Soil water content

The effect of water content on cracks and vice versa is complex and not clear; this induces many controversial reports. As initial water content was a key factor for cracks initiation for some researchers (Auvray et al., 2014); other authors declared that it did not bring any change in cracking water content (i.e., water content at crack initiation) (Li et al., 2014). The study of Li and Zhang (2011) found that crack pattern is linked to initial water content and drying time. The work of Gargiulo et al. (2015) elucidates that the effect of water content on cracks is complexly associated with other parameters (soil structure, etc). Moisture removal can go from easy linearly pattern to more difficult curved trend (with time).

1.5.4 Water suction

Suction is also known as the matric capillary pressure. Swelling, shrinkage and any change in volume of soil are mainly controlled by suction. The critical suction at crack initiation depends mainly on: the soil tensile strength, the initial stress state, the total and effective stress paths, and the stress history of the soil (Konrad and Ayad, 1997). Increase in matric suction increases (non-linearly) the shear strength of the soil (Vanapalli et al., 1996). Study by Pouya et al. (2019) showed that imposing suction on specimen reduces significantly its crack initiation time. Analytical calculation was proposed by Vo et al., (2017) to predict the critical suction. Since at a certain moment of the drying, air replaces water in the porous media, this air-water interface pushes cracks to initiate. Haruna and Gofar (2012) reported that suction increase almost

linearly with decreasing evaporation. Tang et al. (2021) agreed that there are few studies linking soil tensile strength, suction and desiccation cracks. However, according to the same authors in-depth comprehensive understanding of crack progression with suction and soil tensile strength is still missing.

1.5.5 Sample boundary condition

At sample scale, boundary conditions should play major role in soil cracking since it can constrain the free-soil shrinkage (or displacement) (Peron et al., 2009; Zeng et al., 2019). Various possible factors may occur such as constraint due to the form (geometry), size, thickness, interfacial friction, etc.

1.5.5.1 Sample geometrical characteristics

Many researchers were interested in the geometry of the sample due to its important and direct effect on crack formation. The shape, size, thickness, and aspect ratio are the major factors considered in the study. The experiment of Lakshmikantha et al. (2009) on cohesive disturbed soil compared circular and rectangle samples with varying diameters 84-119cm. Prat et al. (2006) found that larger samples (disturbed clay soil) presented denser (length per unit area), longer but thinner cracks. On the other hand, thicker samples (from 10 to 20mm of undisturbed loam soil) result in higher crack area percentage but short in length (Prat et al., 2008; Shit et al., 2015). However, the study of Tang et al., (2008) on the same disturbed clay soil from 5-8-11 mm concluded that crack length, width, and clod are enhanced in thicker samples. They assumed that the thickness modifies the stress state of the sample which in turn changes the water movement and thermal energy dispersion. Following the same idea, Nahlawi and Kodikara (2006) proved that thicker sample (slurry clay soils) tends to have reduced desiccation rate. This comes from the fact that water takes more time to evaporate at the surface for thicker samples. The soil upper layer desiccates faster than the bottom one. Tang et al. (2008) reported enhanced crack spacing, width and area of clods from thicker sample. The aspect ratio (thickness versus surface area) should play a major role according to Lakshmikantha et al. (2018). The authors collected sample of increasing aspect ratio (1.5-4.5 and fixed thickness 15 mm). The study revealed a decreasing desiccation rate with increasing aspect ratio.

The direct relationship between crack thickness and crack formation can be illustrated by the work of Zeng et al. (2019). From two-dimensional scheme (Figure 1-6), the first process is the formation of horizontal shrinkage (assuming that the sample is homogeneous) as water evaporates on the soil surface. An increasing frictional forces F is opposing the soil shrinkage between the soil basal and the grid (rough surface). This force is linked with the interfacial friction forces $f(\mu)$ and the contact length L. As a result, another horizontal tensile stress σ, distributed in the thin soil (thickness d), is created in the specimen. The tensile stress σ is replaced by the tensile strength σ_{cr} (critical) of the soil during the crack initiation. Therefore, at a given interfacial friction, the critical contact length (L_{cr}) (that activates crack initiation) increases with the soil thickness and vice-versa. Therefore, thicker soil necessitates higher tensile stress to activate cracks (Figure 1-6). By the time the contact length decreases as a result of new crack formation, the tensile stress becomes too weak to

trigger further crack propagation. Desiccating cracks attain therefore their maximum development (Lakshmikantha et al., 2009; Tang et al., 2010; Guo et al., 2018). The critical length corresponds to the length of clods and the length of crack between nodes. Maximum crack formation ended up normally to a formation of nodes and clods (Tang et al., 2008; Shit et al., 2015; Somasundaram et al., 2018; DeCarlo and Caylor, 2019).

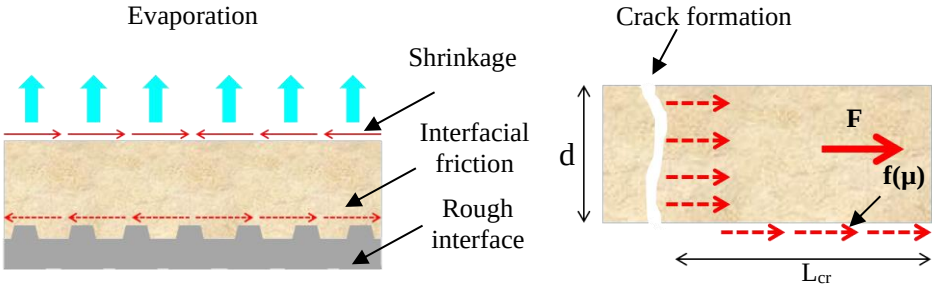

(a) Soil shrinkage during evaporation

(b) Critical state at crack initiation

Figure 1-6 Illustration of soil cracking in relation to soil stress and thickness (Zeng et al., 2019)

1.5.5.2 Bottom interfacial boundary

The contact between the sample and its interfaces is crucial for crack behaviour in the laboratory environment as well as in the field. Friction is necessary to initiate and propagate cracks. The intensity and the type of the friction at the bases of the sample determines the amount/size of the forming cracks. For instance, use of grooved plate, notched plate, and glass bases increase crack formation (in intensity, area, length, clods) than smooth plate, Teflon plate, and wood bases (Nahlawi and Kodikara, 2006; Peron et al., 2009, Al-Jeznawi Marcelo Sanchez Abbas Al-Taie, 2021). Lakshmikantha et al. (2018) reported thinner cracks under smooth contact surface compared to rough surface. The experiment of Sanchez (2011) revealed that cracks formed orthogonal crack patterns (forming crack cells) when desiccated under uniform grooved plates. However, Lakshmikantha et al. (2018) found that the form and the aspect of the friction grid (grid whether circular or squared grid) did not influence the crack intensity. Increasing of the friction does not always increase the intensity of the forming cracks. The work of Decarlo and Shokri (2014) found a decreasing of crack length and density when increasing the roughness (friction) of a substrate. The same authors reported a decreasing time to reach full crack development with decreasing friction. Finally, cracks could start from the sample basal and extend to the sample surface since the friction is located at the bottom of the sample (Weinberger, 1999; Guo et al., 2018).

1.6 How to monitor and measuring crack dynamics?

1.6.1 Experimental approach for analysing cracks

Study on crack can be subdivided into two main components: study done on small scale or under laboratory experiment; and/or study conducted in the large field scale. It is difficult to investigate crack on large scale field because it is hard to control all the extrinsic environmental parameters (temperature, air humidity, rainfall, wind, etc.). Nevertheless, there are few researchers analysing crack formation under freeze-thawing (Konrad and Ayad, 1997), under mud (puddling) (Weinberger, 1999); or under wet-dry cycle of silt/clay soil (Lu et al., 2021). Most of the other analyses are conducted under laboratory conditions. Cracks are analysed based on two different approaches including soil mechanic approach and the fracture mechanics.

The common method used in agricultural science is the mechanical approach. It consists of observing the desiccation process, the crack formation and its propagation inside container which is specific for the study. In some circumstances, crack initiation and crack growth are monitored by camera. Currently, digital image associated with image processing and analysis become the main method which is used to measure and quantify cracks. Digital crack analysis become a central study in large varieties of disciplines inside agricultural science such as agricultural and irrigation management, soil science and hydrology, crop science, etc (Tang et al., 2010; Cheng et al., 2020). The technique can be very accurate and adapted to the laboratory or even in the field (Auvray et al., 2014). Digital crack assessment is conducted during the process of drying or at the end of the drying. Various researchers utilised specific methods to estimate crack characteristics and distribution in soil samples or in the field. Basically, the analysis is made in 2D showing the surface cracks (DeCarlo and Caylor, 2019). However, several scanning of soil at different depth could give extrapolated 3D images of soil (Al-Awsi et al., 2015). The extracted cracks (from digital images) are characterised from different features: number of intersection/nodes, number of branches, number and shape of clods, crack width, crack length, crack depth, crack intensity factor (CIF), crack area and crack size distribution (Bordoloi et al., 2019). Recent improvement on image analysis and photogrammetry permit assessment of more complicated information as fractal dimension, crack probability density etc (Tang et al., 2010; Cheng et al., 2020).

Different intrinsic or extrinsic parameters are considered along the process such as: temperature, relative humidity, sample thickness, soil friction (adhesion at the bottom contact surface), water/moisture content, water suction, cycle of wetting-drying, desiccation speed etc. For example, the work of Corte and Higashi (1960) considers some variables: disturbed soil thickness 7cm (60x84cm), contact surface (different adhesion characteristics), wetting-drying, initial water content of 40-60%, dry density 1.5-1.8g/cm3 at 22°C, and RH 30-40%. (Lloret et al., 1998): cylinder 38mm x 76mm thickness, dry density 1.53g/cm3; 25cmx4cm(thick) 50% Water content. RH 60%. (Albrecht and Benson, 2001): different type of soils, compacted at different pressure. Temperature 20°C.

1.6.2 Procedures to extract crack information from digital images

Until now, there is no standard procedure specific for crack analysis based on digital image processing. The majority of researchers follows the procedure elaborated by Tang et al., (2008) and its derivative (Tang et al., 2010; Al-Dakheeli et al., 2018; Cheng et al., 2020). This includes image correction (perspective, feature matching), noise removal (despeckle, outlier), filtering (median, Gaussian), segmentation (thresholding), binary (erode, dilate), skeletonization (thinning), and cracks characteristic identification. The image processing can be achieved using commercial graphics software such as Adobe Photoshop, Matlab or some other open-source image processing program such as ImageJ, PCAS (Pores/Particles and Cracks Analysis System). PCAS was developed to assess cracks characteristics (number, size, shape, geometry, crack skeleton, probability, clod, fractal dimension) (Liu et al., 2011; Liu et al., 2020). The main drawback in crack analysis program is that there are few or no scripts specific for agricultural/ soil science. Researchers need to adapt their analysis according to their study objective. For instant, the actual software (PCAS, script in Matlab and ImageJ) are specific for geotechnical/ engineering problem. Generally, the program is developed to assess cracks from dam/concrete, slurry, landfill soil, or disturbed soil.

Most crack analysis is not adapted to intact agricultural soil which should behave differently compared to disturbed specimen used in engineering study.

1.7 How was desiccation cracking controlled in previous studies?

Crack control is widely addressed in geotechnical engineering; however, it does not bring much attention in the agricultural science. To come against crack formation, various substances were mixed (added) with soil (e.g., lime) in order to increase the soil strength and their mechanical characteristics. In order to efficiently control cracks in soil, literature proposes three main techniques: mechanical, physical, and biochemical procedures (Mitchell et al., 2005; Ikeagwuani and Nwonu, 2019).

1.7.1 Controlling cracks using chemical or mineral product

The first mechanical technique uses commonly lime and ash. They were used to improve the soil quality by strengthening the soil structure against excess shrinkage and thus the crack formation (Al-Taie et al., 2016). Ash is found to stabilize clay soil and able to reduce the crack formation (Şenol, 2012). The use of chemical stabilizer does not always offer positive effects. Some authors reported an increase of soil shrinkage and crack propagation due to soil liming (Jayanthi and Singh, 2016). Moreover, the use of chemical product could be detrimental for the ecosystem and the environment (Cochrane et al., 2005). There is likelihood of ground-water contamination by chemical leaching.

1.7.2 Controlling cracks using fibre or frictional product

The second method consists of embedding fibre in soil as reinforcement (Chaduvula et al., 2017). The fibre performs well when there is strong interaction (friction)

between fibre and the soil matrix (Han and Gabr, 2002; Tang et al., 2010). Some authors reported that the soil adopts more ductile behaviour, less compressive (limited swelling/shrinking) and resistant to shear forces when fibres are added (Valadez-Gonzalez et al., 2009; Hejazi et al., 2012). Reduction of crack surface, and CIF from 20-40% were observed on clay reinforced with fibre (Alwahab and Alqedra, 1995; Harianto et al., 2008). Natural fibber attracts more attention such as coconut fiber (Ghavami et al., 1999), sisal (Prabakar and Sridhar, 2002), palm fiber (Taallah et al., 2014), jute (Wang et al., 2016), flax (Khelifi et al., 2015), human hair (Pillai and Ayothiraman, 2012), straw (Mousavi et al., 2012); (Wang et al., 2018), bamboo (Marto and Othman, 2011), and cane (Dang et al., 2016). Fibre is by far the best alternative to reduce crack propagation; however, some authors reported that wet-dry cycle reduces the overall effect of excessive fiber inserted into soil (Ziegler et al., 1998). Some fibre could create mechanical problem with agricultural engine (tractor, etc), and induce some chemical imbalance as far as C:N ratio is concerned. The best source of fibre is the residue incorporation into soil.

1.7.3 Controlling cracks using bio-chemical or biological product

The last technique consists of adding solution into soil in order to create a bio-mineralization process which augment the resistance to cracking. This method used mostly microbial induced calcite precipitation (MICP) method in sandy soil (to strength of collapsible sand) (Dejong et al., 2006). Few studies used other type of soil since the bacteria could not circulate easily in small pore like in clay soil (Cardoso et al., 2018; Guo et al., 2018; Li and Zhang, 2018; Vail et al., 2020). Therefore, the use and uniform mix of the bio-mineral with soil remain challenging especially for field application. Other bio-treatment methods that have positive effect on crack remediation (in clay) includes: rice hush ash (Eberemu et al., 2011), biochar (Lu et al., 2021), and biopolymer (Acharya et al., 2017). The use of mucilage could be an alternative to such product. However, there is still big gap in the knowledge of the technics, their efficiency, their behaviour under different temperature, wet-dry cycles, and their environmental effect.

2. What is missing in the knowledge of cracks in the agricultural science? What are the overall and specific objective of the study?

2.1 Cracks assessment under different land use (agricultural) practices

We observed from the literature that crack is very important since it affects the movement of air/water/solute in soil. Due to high variation in rainfall and drought as a result of climate change, cracks are no longer specific to heavy clay soil. The common luvisol found in Belgium presenting medium to high clay content is predisposed to cracking. We could notice however that study on cracks is focused on geotechnical problems and less targeting agricultural science. Consequently, most of the studies work on disturbed samples, disregarding the role of the soil structure in its hydrodynamic behaviour.

We expect that cracks progression should not have equal effect in different land use practices especially for various agricultural management/practices (such as conservation tillage and conventional tillage). Indeed, the agricultural practices modify the soil structure (porosity, aggregation), the soil composition (organic matter, organisms) and could impact the soil structural stability, the soil tensile strength, the soil hydrodynamic, and additional soil mechanical friction.

Until now, no consensus is reported concerning tillage management and cracks. For example, no-tillage (NT) system was found producing wider and deeper crack compared to conventional tillage (CT) under vertisol in India. In the contrary, in the Mediterranean rainfed of spain (Vertisol), CT created larger crack surface area and volume than in NT. Addition of organic matter (biochar, residue etc) seems affecting the cracking behaviour of soils as well. There is little information about how reduced tillage and conventional tillage associated with residue management could influence crack formation and development.

Yet, cracks were reported by farmers in the luvisol of Belgium under those agricultural practices. ***This is the prime objective of this research i.e., assess the effect of cultural practices (conventional and reduced tillage associated with residue practices) on crack formation during drying of an agricultural soil (luvisol) from Gembloux-Belgium, under controlled laboratory experiment***. ***The study is mainly conducted under laboratory environment using image processing and analysis. ANOVA and other statistical analysis helped as well to give insight on the difference between crack variables.***

As mentioned above, crack analysis has been widely developed in the geotechnical science. Most of the program and software in image analysis are meant for solving engineering problems. There is therefore a need for adapting those techniques to fit to agricultural science. Finding adapted technique for accurate crack analysis is also part of the objective of this study.

2.2 Crack progression related to soil water properties

Studying soil cracks dynamics and their characteristics might help understanding the mechanical changes in soil physical properties, and theirs direct effect on soil hydrology. Based on crack physical description (length, width, form, size, shape, and density), some researchers developed various kind of models that predict water infiltration, water evaporation, soil pollution, and landfill protection. However, it is also possible to directly link the crack properties and soil hydraulic properties. For instance, previous studies showed that increase in cracks width (from 0.64cm to 1.9 cm) rise by 15% the evaporation rate. A direct relationship between water evaporation and the number of crack nodes was also reported. The close relationship between water permeability and fractal dimension (plus crack maximum width) was observed. However, crack area/density and the soil permeability could not be associated. Recent study gave insight of a direct influence of crack propagation at any stages of water evaporation. It was suspected that crack properties (crack width, crack distance, crack depth) could participate to 50% evaporation rate variations.

In the contrary, other studies suggested a feeble effect of soil shrinkage and crack formations on the mechanism of soil evaporation since they only change the soil structure (add macropore and disturb the pore connectivity), but don't influence the soil matrix, the process of capillary rise, and the vapor diffusion.

Finding the crack parameters which could directly be connected to the soil hydrology remains complicated and not well understood. Moreover, the influence of the agricultural practices on crack formation and soil hydraulic properties (evaporation, water retention) is missing.

This is therefore the second objective of this research which is to attempt to connect the crack parameters (area, CIF, length and width) and soil hydraulic properties (water content, evaporation, water suction) under agricultural practices in Wallonia. Various correlations are built between the explained and explaining variables including the Krisher's curve which correlates water content and water evaporation. However, this study includes also the influence of crack on water retention curve (SWRC).

2.3 Addition of mucilage to control crack

When understanding the probable effect of cracks on soil hydraulic properties, it is also crucial to find out some possibility to control this phenomenon. Mechanically, crack initiate and propagate as a result of soil desiccation and excessive water suction (matrix potential) which exceeds the soil tensile strength. Therefore, controlling crack invites either increasing soil strength or limiting soil water stress (reducing water evaporation and/or holding more water). As elaborated in the literature section, previous studies focused on methods which acted mechanically against crack formation as: chemical, fibre and bio-chemical. Those techniques encounter some difficulty in terms of cost-efficiency, equipment/machinery adaptability, and environmentally not-friendly and basically can hamper agricultural activities. Therefore, it is crucial to find out easy and environmentally friendly methods to control crack formation and development.

Recent research found that root exudates such as mucilages penetrated and agglomerated soil particles surrounding the rhizosphere. As a result, the rhisospheric zones become resistant to water stress, to tensile stress due to soil dessication. Other authors confirmed this finding by applying mucilages (Chia, Xyloglucan, AGU etc.) directly to soil particles on paper and rinse them with water. The results claimed the vivid effect of Chitosan, Xanthan, Xyloglucan, and Tragacanth on soil sticking property. It could help soil structure to reduce or avert crack dynamic. Moreover, mucilages create a symbiotic relationship with the soil and microorganisms increasing the soil aggregate-formation, microbial growth, water/nutrients uptakes, and plant-soil-atmosphere interaction.

Other laboratory experiments used mucilage (Chia (*Salvia hispanica L.*, Lamiceae family) seed, Xyloglucan, polygalacturonic acid (PGA)) as analogous to root-exudates. Some exopolysaccharides (dextran and xanthan) were also utilised as microbial exudates. Little is known about the relation between the association of mucilages, soil hydrology and cracks management. ***This is therefore the third***

objective of this research which is to assess the effect of mucilage addition on crack formation and on soil hydraulic properties.

3. Outlines

The overall objective of this thesis is therefore to investigate the effect of desiccation cracking on the soil hydraulic properties in conjunction with agricultural practices of tillage and residue management in an agricultural soil. This study objective is subdivided in five different sub-sections representing specific objectives:

1) Chapter 2 is not a specific objective; however, this chapter gives additional information concerning the used methodologies which are not always detailed in the published articles; yet they are important for the reproducibility of the experiment.

2) Chapter 3 assesses the kinetic of drying of an agricultural soil under experimental and numerical investigation. This is an overview on how the soil moisture regime including: soil water retention, water content and evaporation behave during the process of desiccation. The results from numerical simulation are validated from the laboratory experiment using very accurate tools (Hyprop ©).

3) Chapter 4 covers the missing part of connecting cracking and soil hydraulic properties. This chapter aims at evoking the interaction (positive and negative) and also the neutral effect of crack on soil hydrology and vice-versa.

The manuscripts are arranged in a way that summary, abstract and introduction precede the methodology, results and discussion, and conclusion. References and annexes are placed at the end of the articles.

4) Since chapter 4 is limited in details and in discussion; chapter 5 comes to give additional information and discussions on cracks and soil hydrodynamic interaction.

5) Chapter 6 of the thesis details the possible control of cracking using mucilage. This section illustrates the effects of three types of mucilage at an increasing quantity on crack formation and propagation. Due to limited time frame, we failed to publish the article in due time despite the fact that all data are already available for analysis.

At the end of the thesis are given an overall discussion of the study followed by insightful perspectives which could ameliorate future research.

CHAPTER 2

Experimental design detailing part of the study methodology

1. Study area and sample characteristics

The study area is located in an agricultural field (50°33'51.6"N 4°42'43.5"E) in Gembloux-Wallonia-Belgium (Figure 2-1). The study area is characterised by a temperate oceanic climate (Degrune et al., 2017).

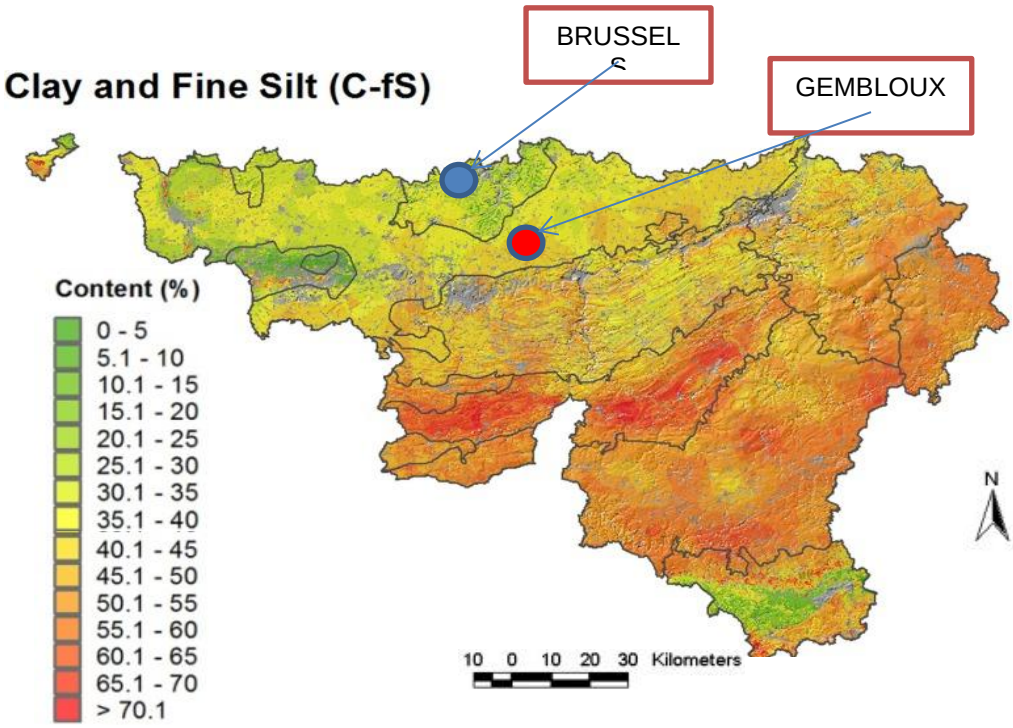

Chartin et al., 2017: fine silt-clay (Wallonia)

Figure 2-1 Chart showing the localisation of the study area and the clay and fine silt content in Wallonia-Belgium (Source: Chartin et al. (2016)).

The crop rotation is composed of cover crop (rapeseed: *Brassica napus L.*, mustard: *Brassica nigra L.*, oats: *Avena sativa L.*, and peas: *Pisum sativum L.*), maize (*Zea mays*), winter wheat (*Triticum aestivum L.*), and sugar beet (*Beta vulgaris L.*). In details, the rotation was: 2008 and 2009: rapeseed; 2010 and 2011: wheat; 2012: wheat/mustard (cover crop); 2013: faba bean; 2014: wheat/oat + peas (cover crop); 2015: maize; 2016: wheat/oat + peas (cover crop); 2017: wheat; 2018: sugar beet; 2019: maize. The preceding crop before the soil sampling was sugar beet in 2018. Shallow tillage (by tractor harrow + crosskill roller) took place prior the main tillage (by mouldboard plough) once a year around December (Winter). The detail about the cultural practices is given in the table below (Table 2-1). The cropping season starts

during winter and harvested in summer. The cover crop is installed autumn. Sometime, the field is left without cover crop in some season.

Table 2-1 Table detailing the general field operation in the study area

Season	Crop	Field_operation	Depth (cm)	CTRO	RTRI
Winter	Cover crop	Sugar lime fertilization		X	X
	Cover crop	Ploughing	-25	X	
Spring	Main crop	Sowing	-7	X	X
	Main crop	Nitrogen fertilization		X	X
	Main crop	Weeding		X	X
	Main crop	growth regulator		X	X
	Main crop	Fungicide		X	X
	Main crop	Insecticide		X	X
Summer	Main crop	Harvest		X	X
	Main crop	Residues exportation		X	
Autumn	Bare soil	Manure fertilization		X	X
	Bare soil	Stubble breaking	-10	X	X
	Cover crop	Sowing	-7	X	X

* *Bare soil: field left without crop; Three types of cover crop: mustard, oats and peas; the field is bare when there is no cover crop; RTRI: reduced tillage with residue-in; CTRO: conventional tillage with residue-out.*

Two agricultural practices including reduced tillage (RTRI) with residue-in (i.e., incorporation of residue + 5 cm shallow tillage) and conventional tillage (CTRO) with residue-out (i.e., removal of residue) (20-30 cm plough) along with disturbed samples (DS) were considered as treatment in this study. This is to emphasize the difference in terms of tillage system as well as residue management. The term residue comprises all aboveground biomass (straw, stubble, etc) whereas the underground rooting system remains in the field for both treatments. DS is an equal mix of CTRO and RTRI, dried at 40 °C, crushed and coarse elements (sand, roots, straw, etc) more than 2 mm are removed. Despite the fact that soil disturbance (DS) does not have clear agricultural meaning; this method is commonly used by researchers for cracks analysis (Auvray *et al.*, 2014; Al-Dakheeli *et al.*, 2018; DeCarlo & Caylor, 2019; Zhang *et al.*, 2020). Moreover, DS can represent the soil state just after tillage event where soil is turned and crushed. The soil is classified as a Cutanic Luvisol (WRB, 2014), composed mainly of silt (80±2 %), clay (15±1,5 %) and sand (5±2 %). The C:N ratio is between 10 and 12 (C content of 20-35 g per kg soil), and the bulk density is around 1.3-1.4 $g.cm^{-3}$.

2. Sample treatment-preparation

Soil samples are taken (November 2018) from agricultural soil in Gembloux-Belgium (Figure 2-2 a,b,c,d) before the ploughing period (December 2018). The upper 15cm of top-soils are carefully extracted from a metal box of 25 cm x 20 cm x 4cm. The bulk samples are directly wrapped with plastic bag and stored inside refrigerator (bellow 5°C). An extra soil of about 2-4 cm thickness is taken with the metal box in order to keep the soil moisture (avoid drying) and store the soil structure intact. This extra soil is levelled down to the chosen thickness of 1.6 before the onset of the experiment. A line is drawn outside the box (of 4cm thickness) at 1.6 cm from the sample base to assure the uniformity of the sample thickness. Small Level-device assures the horizontality in X and Y axis of the sample surface. Well-levelled surface would give accurate (plan) and undistort image (digital photo). Special sharp tool (made from cutter) is specially created to remove the extra soil, to level (cut) evenly the soil, and to cut sharply the soil aggregates along with some hindering elements such as fibres (roots, straw, stubble). This is an important step before the process of sample saturation (Figure 2-3 a,b,c).

a) Metal box to collect upper soil

b) Box inserted into soil

c) Box is taken with extra soil

d) Sample ready for storage in fridge

Figure 2-2 Photos showing sample collection using metal box from the field of study

3. Device preparation, wiring and connection

3.1 Tensiometer preparation and insertion

Deionized water is used during the experiment. Gas (CO_2) is removed from the water using vacuum glass for at least 72hours. Tensiometer sensors (composed of ceramic and tube) are dipped into the water while the degassing process continues to take place from the system for 72h more (Figure 2-3d). After this period, the tensiometer-tube is filled partially with water; moreover, some bubbles may still exist. Therefore, the bubble is removed by pumping degassed water from the tensiometer-ceramic using vacuum pump. The process takes around 1-2 hours depending on the quality of the degassed water. Water is then locked inside the tube while the ceramic remains inside the degassed-water all time before its insertion to the sample. Degassed water is also used to fill-up the tube located before of the pressure transducer. In order to avoid early cavitation, water is degassed using depressurised syringe. This method is copied from the process used in Hypro® device. From this technique, we observe that the tensiometer withstand strong pressure before cavitation (400-500 hPa; pF 3.5). To insert the tensiometer, hole is drilled in the middle (0.8 cm) width of the metal box (with bit of 0.4 wq<cm size) (Figure 2-3a).

In this experiment, specific spatula from Hyprop package is used to create holes in the soil prior to the tensiometer insertion. The technique consists in making the hole when the soil is fully saturated. This avoided air entering the tensiometer and at the same time, the soil becomes firm and not friable. In order to fix the tensiometer 3cm inside the sample, the tube (holding the tensiometer) is glued (using hot glue gun) to the metal box. Part of the tube is also glued to the drying chamber. This avoids vibration and detachment of the tensiometer which may affect the reading of the balance. The tensiometers are connected to transducers which are connected to a datalogger (CR800) (Figure 2-3e). Since many devices are used during the experiment, a multiplexer is necessary to accommodate all the sensors. Some of the devices are connected directly to the datalogger, others require precision resistance (10 Ohm and 10 kOhm±10 %).

a) Hole and line on the box

b) Sharp tool to cut soil and fibres

c) Level-device to check horizontality

d) Pump, vacuum glass and tensiometers

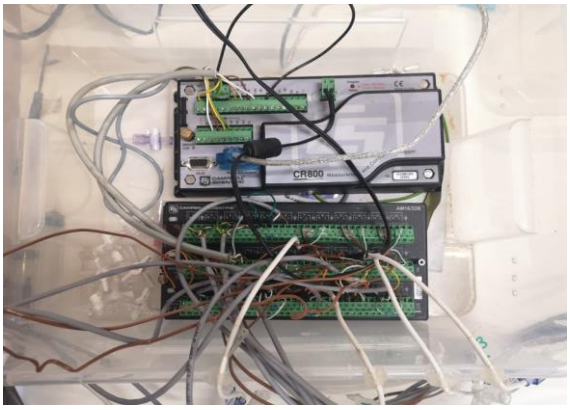

e) Datalogger (CR800 Campbell ®) connected to multiplexer and wiring to sensors

Figure 2-3 Different processes and tools for levelling soil, degassing water (vacuum pump) and controlling sensors (CR800 datalogger)

3.2 Temperature sensors

Temperature sensors (PT100) are installed 10 cm above the sample in the drying chamber, outside the chamber, on top and bellow the sample. The idea is to monitor the temperature gradient inside the sample and in the ambient/outside the ambient. Some sensors are placed above a (portion of) dry soil in order to assess the temperature of the dry sample. Relative humidity (RH) is also monitored 10 cm above the sample and outside the chamber. The temperature and RH devices are connected to Arduino and CR800 dataloggers (of Campbell Scientific ®). The thermostat has its own temperature sensor to control the temperature inside the chamber.

3.3 Lamp, camera and IR heat

The chamber is covered with black plastic film in order to circumvent any other source of luminosity to enter the chamber. Any unnecessary luminosity can defect the quality of the image. Circular white led lamp (35 W) is used to evenly enlighten the

soil surface. It is installed 1 meter above the soil surface around the Cannon camera (Canon ® version Powershot SX 520 HS ®) in the middle of the chamber (Figure 2-4a). A spirit-level is used to check the level of the cameras' objective. This is to make sure that the camera is accurately parallel to the sample surface and the resulting image is not distorted (tilt). In order to get clear and detailed images, canon camera of 12 Megapixels is used as operated in previous research (Lakshmikantha et al., 2009 etc.). Canon is also chosen among other brands due to the existence of Canon Hack Development Kit (CHDK) which is free software that can enhance the control of Canon PowerShot cameras without replacing the stock firmware.

a) Camera 12Mp + ring light

b) IR Heat Emitter and Thermostat

Figure 2-4 Cannon camera with ring-ligh, IR heat emitter and thermostat

There are many options and features available, however; the present study chooses a program known as intervalometer which works well with the CHDK. This is a computational program (written in UBASIC or Lua scripts) that controls the camera at an accurate time interval. The camera takes automatically pictures of the sample surface every 30 min throughout the entire duration of the experiment. The program is installed inside the memory card of the camera and updated each time the camera is utilized. There is a need for putting black papers around the sample in order to avoid light reflexion to the cameras' objective which may compromise the image quality. We print millimetre rulers surrounding the box (along with the black paper) that is also used to calibrate the images. The images are saved in 3000 x 4000 "Tiff" format which is equivalent to 64µm/pixel. Two IR heat emitters are installed below the level of the camera. They are oriented toward the sample in order to evenly distribute the heat on the soil surface. These heaters are adapted for image analysis since they do not emit colour on the sample surface (as the IR lamp). Thermostat detects the small change (+/- 1 °C) in temperature and adjusts the heat automatically (at around 30 °C) (Figure 2-4b).

3.4 Balance

Precision balance (Kern 0.01 g) is used in this experiment. The balance is calibrated before the experiment. The balance horizontality and its fixation are checked in order

to keep the reading quality. Any vibrating devices are installed far from the balance due to its high sensibility. The device is connected to the computer via USB port; moreover, it is programmed to send data every 5min (using data-transfer mode). The data are collected automatically using PLX-Dax ® software and saved directly to Excel ® file. The weight of all material (including sensors) is subtracted from the overall weight to obtain the sample weight. The weight of each tool (plexiglass, box, tensiometer etc) is measured during the experiment.

3.5 Plexiglas ®, squared-grid and Styrodur ® Grid

We mount a Plexiglas (or a Styrodur®) at the base of the sample in order to limit water evaporation and also infiltration, and to keep the sample as well (Figure 2-5 a,b). The plexiglass is glued (using hot glue gun) to the metal box.

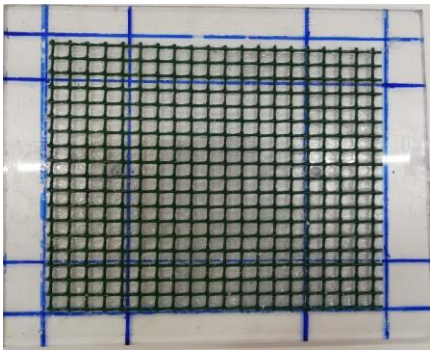

a) Squared-grid fixed on Plexiglas

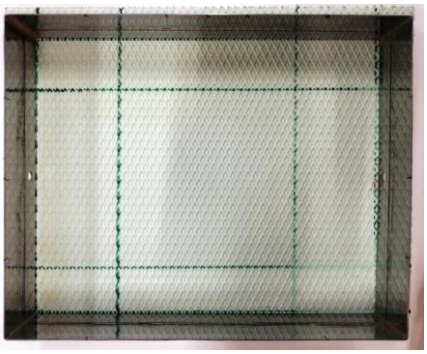

b) Diamond grid on Styrodur®

Figure 2-5 Two types of friction grid in the form of a) square and b) diamond

Based from pre-tests (and literature), cracks can initiate (from disturbed sample) only if there is a kind of friction (increase the soil adhesion) at the bottom of the specimen. Therefore, friction is added in the interfacial between the soil sample and the Plexiglas (in each treatment). This is a grid in form of square (1 mm height, 1 cm length). The grid is glued firmly to the plexiglass to avoid detachment during the experiment. Other type of grid is also utilised in order to find out the possible effect of different type of friction. The friction is in the form of diamond (form, Styrodur®) and is used only for samples from the undisturbed samples. This second type of grid does not require the use of plexiglass.

4. Process of sample saturation

The samples are saturated for 24h before the commencement of the experimentation (Figure 2-6 a,b). For the preparation, solid grid (with peace of cloths) is place under the sample to allow water (distilled water) to pass through the soil by capillarity. To assure the saturation of all pores (from the smallest to the largest pores), the thin

sample (1.6 cm) is immerged into water until 4-5mm of the sample emerges from the surface. The idea is to fill all pores and avoid water to get inside the sample from the top and entrap air in some pores. This is also the reason to take 24 h to saturate one sample. The sample is fully saturated when the soil surface starts to shine. However, the experiment should not last more than 24 h due to probable soil structural breakdown. For instance, intact sample should not show too much change in volume during saturation when the sample is taken at field capacity (from the field) as it is the case of the present study. Based on experiment, the soil structure breakdown is observed from excessive swelling of the sample.

The disturbed sample requires different mode of saturation. The DS sample is dried at 40 °C (this keeps its carbon composition), crushed and sieved at 2mm. The sample is mixed with 45-50 % of water (volume percentage). The slurry is poured uniformly into the metal box 25x20x1.6 cm. There is no need for further compaction due to the fact that the mixture (paste) fit the chosen thickness (1.6 cm) without compaction. This is due to the fact that the moisture is still below the liquid limit of silt-loam soil (>55 %) (Atique and Sanchez, 2011).

i) Sample saturation

j) Sample starts to saturate (shiny)

Figure 2-6 Method used for a) sample saturation until the soil presents b) shiny surface

5. General process during the experimental set-up

The first step consists of preparing the samples and the tensiometers. The balance is set to zero and all sensors are connected to theirs respecting loggers (CR800 or Arduino) or connected directly to the computer (PC) via port USB (such as Balance and Arduino). The chamber needs to be pre-heated prior the onset of the experiment. It is time to put the sample on the balance, check the initial weight, adjust the position of the sample to be right under the camera and in horizontal position. After that, the tensiometer (+ tube) is fixed to the sample, to the box and to the chamber (Figure 2-7). Any vibration can be seen from the reading of the balance. The light is on and the camera starts taking picture every 30 minutes. Verification is done every day to check if everything is going well (no shortcut, every sensor is reading, etc).

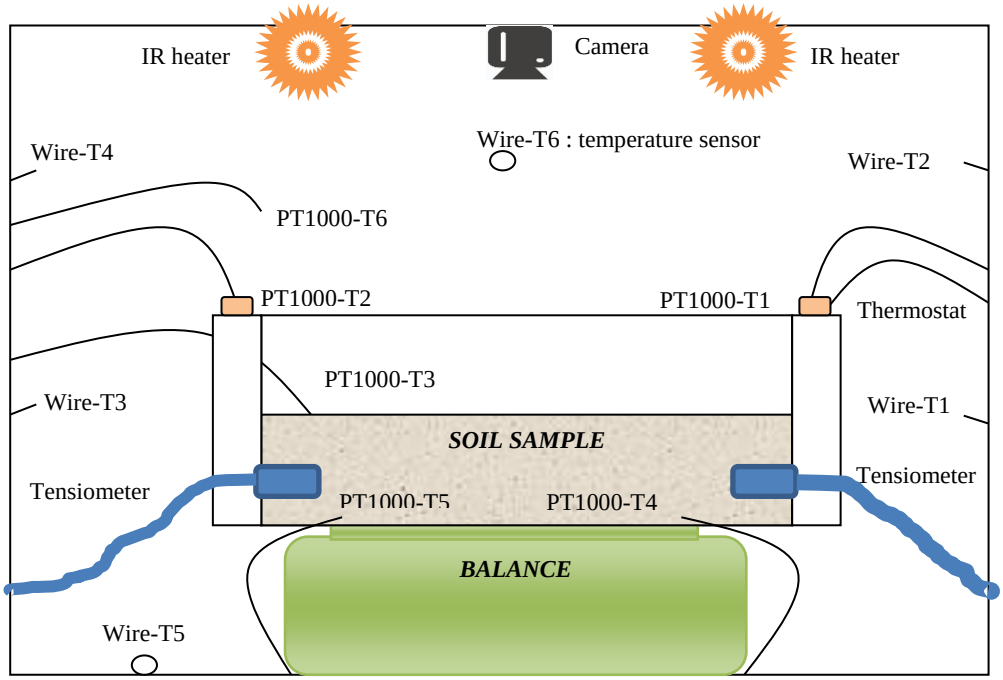

a) Scheme of the inside chamber showing the position of each device and sensors

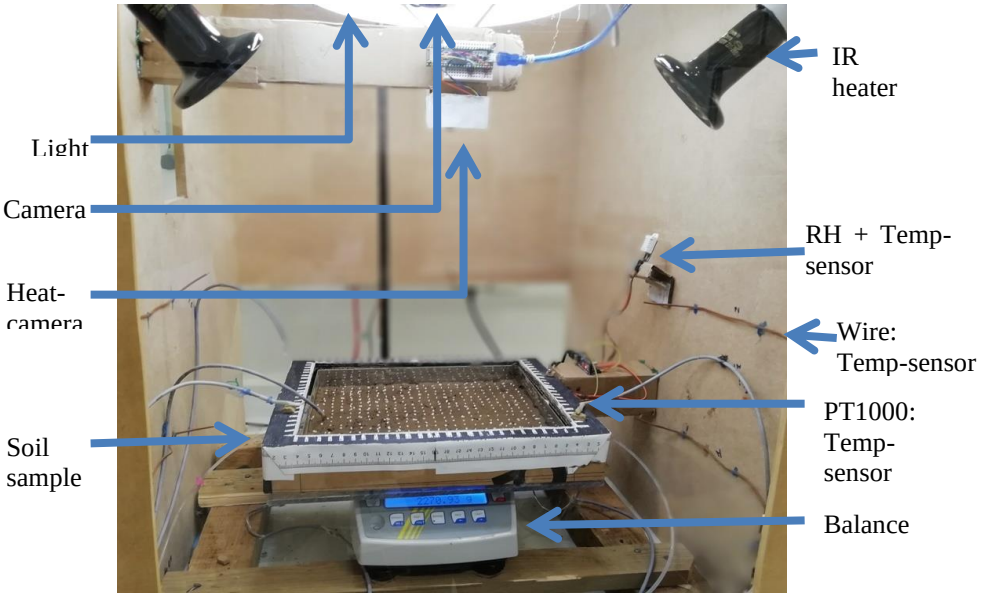

b) Real image from the chamber showing the position of each device and sensors

Figure 2-7 Overview of the experimental chamber with all devices and sensors

6. Image collection and processing

6.1 Image geometry correction and ROI selection

The images are collected from the camera and stored in the computer. Each image has its own number and time. The data is therefore arranged according to their identity in each treatment. In one series (in one treatment), all images are taken with the same disposition (position of the sample vis-à-vis the camera, the possible tilt of the camera objective etc). Therefore, the image presents similar default. Therefore, “perspective correction” embedded into GIMP software addresses the issue of image distortion. This consists of fitting each image in a rectangle (20 x 25 cm) corresponding to the real size of the sample. Only one image per treatment (called reference image) is corrected by this process. The remaining pictures are corrected automatically with the help of the reference images using the feature extraction plug-in (called "Extract Block Matching Correspondences”) associated with transform plug-in ("Landmark Correspondences") of ImageJ software. ImageJ takes more than 400 points from the corrected image (or reference image) to correct the remaining images in the same treatment using script (Macro on ImageJ).

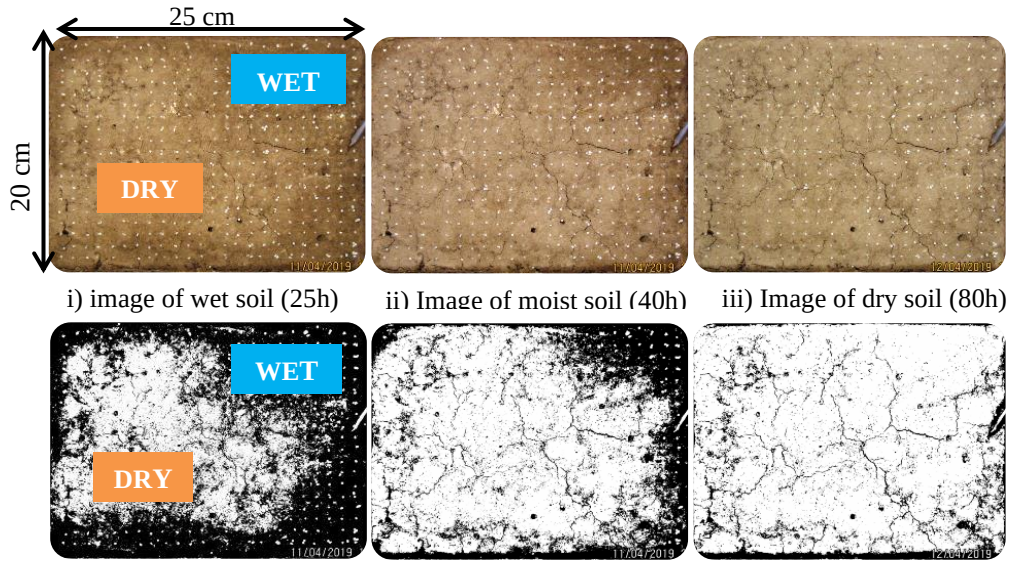

i) image of wet soil (25h) ii) Image of moist soil (40h) iii) Image of dry soil (80h)

**The black pixels indicated the wetter part of the sample*

iv) Binary image of wet soil v) Binary image of moist soil vi) Noisy image of dry soil

a) Difficulty during direct crack extraction due to spatial humidity difference on sample

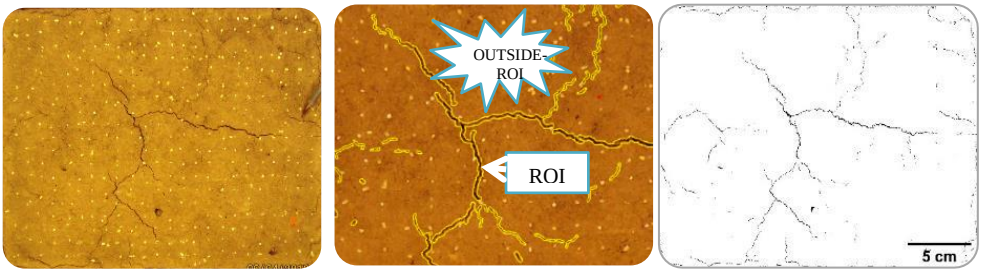

i) Coloured image of cracked soil | ii) Cracks delineated by ROI (yellow) | iii) Extracted cracks from ROI (binary)

**The black pixels indicated the wetter part of the sample*

b) Crack extraction using ROI (region of interest) during image analysis

Figure 2- 8 Comparison of two crack extraction procedures in which the first method (a) analysed the entire image while the second one (b) operated only on a delimited ROI (Region of interest). Note the background noises created by the moisture difference for the first method and an almost clean binary image for the second method.

Generally, more than 400 images were treated per sample. The common technique for crack extraction is the use of median filter associated with the rolling back algorithm or reference filter (Auvray et al., 2014; Lakshmikantha et al., 2009). This consists of creating a "background" image (without cracks), and deducting the crack image from subtraction of the background image with the original images.

However, when applying this method in this study, we obtain noisy images (background) especially when the soil is wet (Figure 2- 8a). This is due to high moisture spatial variation in the undisturbed samples (RTRI and CTRO). Therefore, following the idea of Auvray *et al.* (2014) on extracting cracks through median filtering, ROI (Region Of Interest) that outlines fully developed cracks (taken at the end of the experiment) is created for each sample. ROI is achieved by drawing lines in the middle of the cracks and extending them symmetrically to a buffer of 50 pixels (0.4 cm) wide for primary cracks (and for many cracks in disturbed sample) while 10 pixels (~0.1 cm) wide for secondary cracks onward. The ROI is applied to each sample sequenced images (from crack initiation to full development). Image processing and crack extraction are performed from the created ROI images using ImageJ (Figure 2- 8b) and PCAS (Particles Pores Cracks Analysis System) software.

6.2 Image processing on ROI sequenced-images

The image processing consists of treating the images through series of semi-automated steps using PCAS package including: pre-processing techniques, mathematical operations and geometrical transformations (Figure 2- 9a) (Zeng et al., 2019). Figure 2- 9b summarises the image processing in six steps as illustrated by Zeng *et al.* (2019) which is inspired by many other authors (Tang et al., 2008; Lakshmikantha et al., 2009; Atique and Sanchez, 2011; Shit et al., 2015). The first

step converts the RGB images into black (cracks) and white (background) (Figure 2-9b-iii; Figure 2- 9*b-i*, *ii*) using Otsu auto-threshold segmentation method. The second step removes the impurities (dots, outliers) from the background (Figure 2- 9b-*iii*). The skeletonization during the third step reduces the crack pattern to median lines (Figure 2- 9b-*vi*). The last step identified cracks characteristics and clods (Figure 2-9b-*v*, *vi*).

The image analysis is mainly done automatically except for the ROI drawing as explained before. The image analysis is partly done with ImageJ and PCAS. The drawback using PCAS is that the PCAS software analyses the image one by one and the process itself takes many slow steps. It takes time to analyse all images; therefore, we decide to reduce the number of analysed images using this software (20-30 images per treatment). The data on weight (from balance), on suction (from tensiometer), and on cracks (from image analysis) are combined based on their respective time and arranged in one excel file together using principally macros in VBA (Visual Basic for Applications) language. Macros do automate repetitive data-processing functions and can even generate graphs. The data arrangement made statistical analysis easier. This is the reason why we mainly use statistical analysis using Ex-Stat 2020 ® despite some other analysis that we conduct using R ® and Matlab ®.

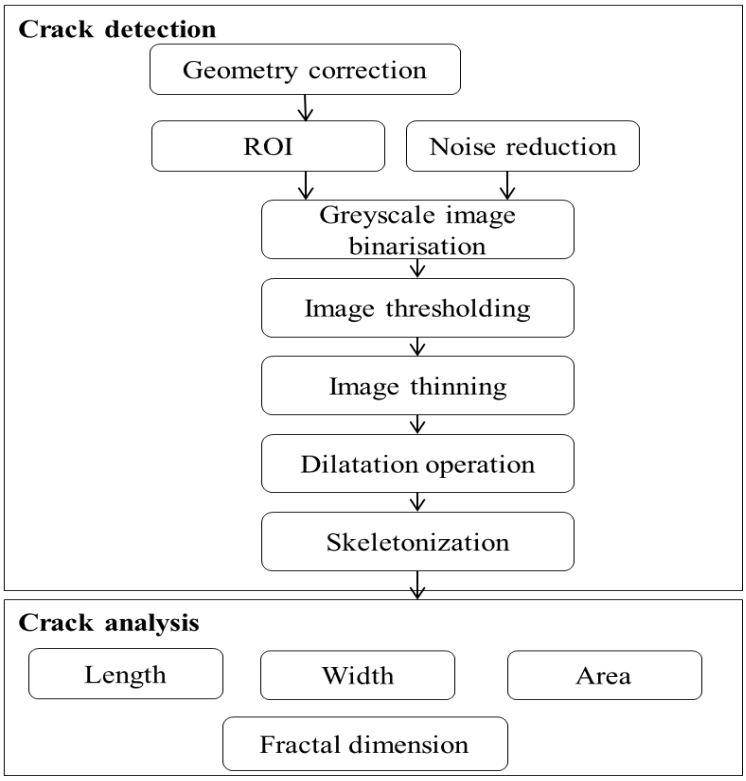

a) Flowchart of the image analysis

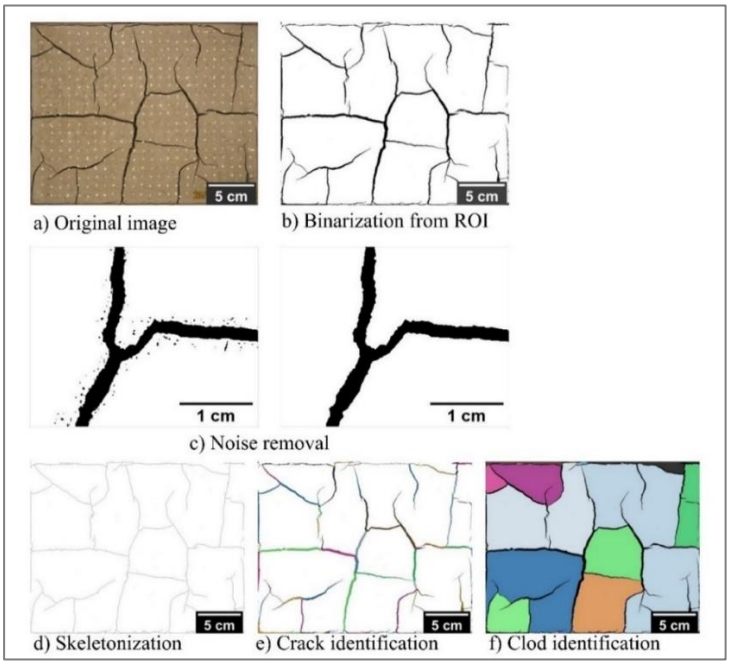

b) Image processing and analysis

Figure 2- 9 Main procedure for image analysis represented in flowchart (a) and diagram of image processing showing the original image (a), the binary (b), skeletonized (d) as well as identified crack (e)/clod (f) images. Data outputted from ImageJ and PCAS software. (*Source: Tang et al. (2008),and Shit et al. (2015))*

6.3 Crack geometrical parameters

6.3.1 Crack area, CIF, crack length, width, fractal dimension and probability entropy

All geometrical parameters of crack patterns in this study were acquired from the PCAS package. The area of crack, the crack length, width, were estimated from size of black pixels of the binary image (Le Roux et al., 2013). The surface crack ratio or CIF (crack intensity factor) is one of the parameters that was used to evaluate the evolution of crack with time. The Crack Intensity Factor (CIF) defines the percentage of the crack surface areas over the total surface area of the specimen (20*25 = 500 cm^2). It was measured from photographs of the sample surface and processed using digital image processing technique elaborated by Tang et al. (2008), Le Roux et al. (2013), Wan et al. (2019). Cracks were thinned to single pixel thickness (line) along the medial axis osf the centre of skeleton object (Figure 2- 10a). The sum of those lines constituted the total crack length. The thinning procedure came from the process of skeletonization (Figure 2- 10 b). Crack width was calculated from the average distance (Feret diameter) of random lines starting from boundary pixels and crossing the medial axis (Lomeling et al., 2016).

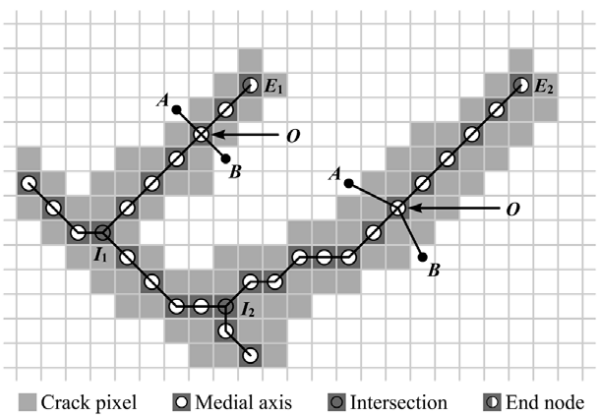

a) measuring crack length from node distance

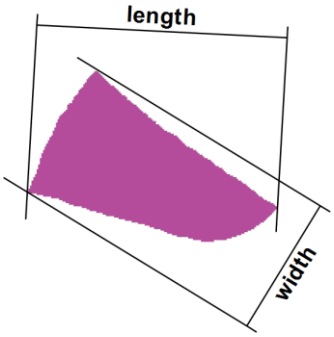

b) measuring crack width using ferret diameter

Figure 2- 10 Process of measuring crack length and crack width using Feret diameter and distance between nodes during skeletonization. (Source: *Liu et al., 2013; Sezer et al., 2008*)

6.3.2 Fractal dimension (Fd)

Fractal dimension is an important parameter of fractal geometry that finds significant applications in various fields including image processing. Fractal geometry is a mathematical concept which helps characterising the irregular form of object found in nature. It informs about the extent of fractal boundary at various scale. Fractal comes from a Latin word "frangere" means "to break". A fractal is a never-ending pattern. Fractals are infinitely complex patterns that are self-similar across different scales. It can take into consideration the object turtuousity, roughness, dissimilarities etc. The overall assessment of fractal dimension of digital image lays on the box counting method which is incorporated in the PCAS package (Figure 2- 11). The cracked images are subdivided into many boxes of increasing size (r). The box containing cracks is counted as N(r). The fractal dimension is then calculated from the slope of linear relationship between the logarithms of N(r) over the logarithm of r (Mihashi et al., 2006).

The general formula for fractal dimension in the box counting method is as follow:

$$Fd = \frac{\mathrm{Log}(N(r))}{Log(\frac{1}{r})} \quad (1)$$

Where: Fd: fractal dimension; r: Size of the considered area; N(r): box containing cracks

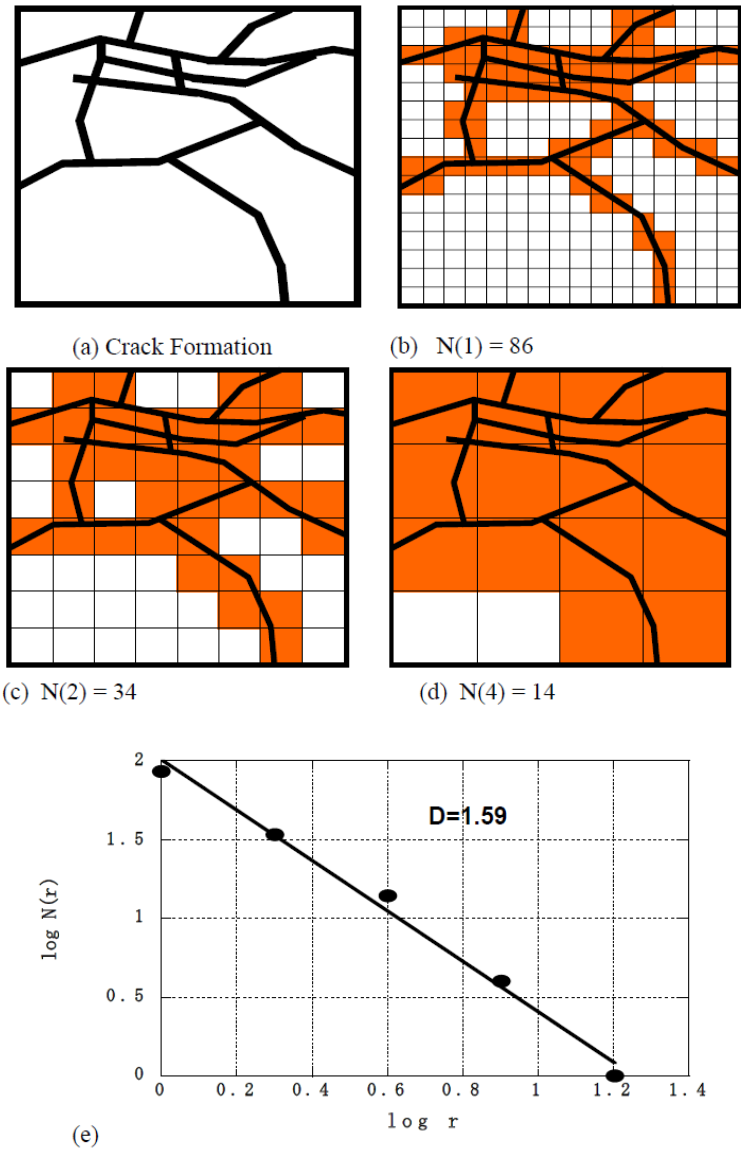

Figure 2- 11 Description of the processes to measure the fractal dimension of cracking image (a), at different size (b,c,d) and plotted on logarithmic graph (e) (Mihashi et al., 2006).

Based on the above formula, it is observed that wider (and large) cracks will occupy more pixels; and therefore, it will present greater Fd than narrower (thinner) cracks. It implies that that fractal dimension portrays also some aspect of crack area, width etc. Moreover, cracks of different pattern (occupying different number of pixels) but

in similar (chosen) area have different Fd is therefore affected by crack density and distribution (Mihashi et al., 2006).

6.3.3 Probability entropy (H)

Entropy is a measure of uncertainty quantifying the similarities and differences of two objects, groups or events. It portrays the complexity/randomness or irregularity/disorder of the system dynamics. The greater the randomness, higher is the entropy. In the case of analysing crack events, Entropy quantifies the similarity or difference in the distribution of black (cracks) and white (background) pixels in a given area. Entropy is measured between 0 and 1. Lower entropy indicates lower probability of crack occurrence and strong difference (in numbers) between white and black pixels. Inversely, higher entropy (close to one) indicates higher probability, a high level of disorder (meaning low level of purity), and close similarity or small difference (black and white pixels). Therefore, uniform distributions have maximum uncertainty (or surprise). The plot of entropy function applied on only two possible outcomes (Bernoulli trials) from events shows a maximum entropy value at the middle of the probability distribution (i.e., uniform probability distribution as the case of fair coins: 50 % tails, 50 % tails) (Figure 2- 12).

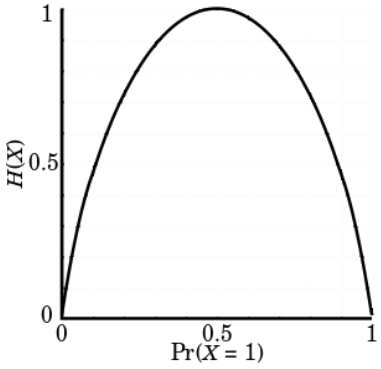

Figure 2- 12 Shannon entropy in relation to the probability of occurrence on Bernoulli trials (only two possible outcomes). This is used most frequently in computational science and imagery. (Source: https://www.analyticsvidhya.com/blog/2020/11/entropy-a-key-concept-for-all-data-science-beginners/)

The formula of Shannon 1948 is widely used for calculating the probability Entropy

$$H = -\sum p(x_i)\log\left[p(x_i)\right] \quad (2)$$

Where: xi are the possible outcomes while p(xi) is the probability of the outcomes xi

7. Pre-test for determining the optimum sample thickness

Despite the fact that we use one type of soil thickness, it is worth to mention the reason for the choice of the soil thickness used in this study. We have selected a thickness of 1.6 cm during our research experiment because of the result from the pre-test. In fact, this thickness was the minimum size that allows us to insert a tensiometer in the soil. Moreover, we observe that thinner samples are more fragile (delicate) and difficult to handle (operate with). As illustrated in Figure 2- 13, by applying friction (grid 1) at the base of the sample crack length increased by 3-4 (from 18 to 60 cm) while crack width is almost two times (300 µm to 700 µm). When reducing the sample thickness from 4 cm to 2 cm, the amount of cracks (area, length etc) increases exponentially whereas crack width remained almost constant (Figure 2- 13). The sample thickness of 2cm is therefore enough to get numerous cracks on the sample (on DS) surface according to the pre-test. This thickness is also used by various researchers according to the work of (Tang et al., 2021). However, since the study assesses both disturbed and undisturbed samples; we decided to reduce the thickness as much as possible till 1.6 cm.

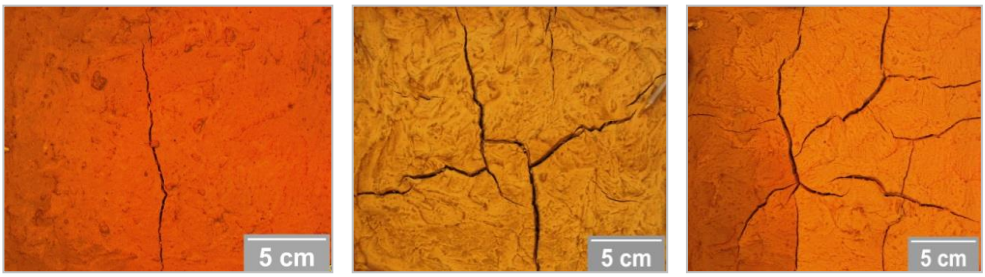

a) 4cm thick + No-grid (Less friction)

b) 4cm thick + grid (Squared)

c) 2cm thick + grid (Squared)

Figure 2- 13 Effect of soil thickness and grid on crack intensity from pre-test experiment

CHAPTER 3

Experimental and Numerical Investigation of the Drying of an Agricultural Soil

The content of this chapter has been published in the journal E-UNSAT 2020: Njaka Ralaizafisoloarivony, *Kien* Tran, *Aurore* Degre, *Benoît* Mercatoris, *Angélique* Leonard, *Dominique* Toye, and *Robert* Charlier. *E-UNSAT 2020,* E3S Web of Conferences 195, 01034 (2020). https://doi.org/10.1051/e3sconf/202019501034.

Remark: For better understanding and reading of the article, different corresponding unit from geomechanics (in bracket) to unit used in Agricultural science is given below:

Label	**Geomechanics unit**	**Agronomy unit**
Evaporation	Kg/m^2	cm^3/day
Water flux	$Kg/m^2.s$	cm/day
Mass heat transfer coefficient α	m/s	m/s
Coefficient β	$W/m^2.K$	cm/day.°C
Water density	Kg/m^3	g/cm^3
Water dynamic viscosity	Pa.s	g/cm.s
Water permeability	m^2	cm/day
Inverse air pressure	cm-1	Pa^{-1} (or mbar)
Liquid water specific heat	J/Kg.K	cal/g.°C
Medium thermal conductivity	$Wm^{-1}.K-1$	cal. $°C^{-1}.cm^{-1}.day^{-1}$
Water evaporation latent heat	J/Kg	cal/g
Bulk and shear modulus	Pa	Pa

Prelude explaining the importance of this chapter in relation to the study's objectives:

From large review of literature, it was revealed that there is no unique (specific) procedure for crack analysis whether in engineering or agricultural science. Therefore, this study tries to implement various experimental set-ups in order to find out the best methodology which can respond adequately the study's objective. One of the primary questions that needed to be answered was the question about the drying kinetics of the Luvisol. There is no specific literature analysing the drying of the Luvisol, yet this is the main soil type that is used throughout the study. Moreover, understanding the drying of the Luvisol will answer partly the second objective of the thesis which is the correlation between cracks and soil hydraulic properties (including water content and water evaporation).

Most of the previous experiment on drying were conducted at the department of Chemistry (at the University of Liège) conducted mainly by the team of Prof. Angélique Léonard. They perform their experiment through small drying chamber with controlled temperature and relative humidity. This kind of set-up cannot fit our study due to the fact that we use big samples (> 10cm) and we intend to observe the sample surface using camera. Or, the chamber is locked and cannot be modified to fit other devices. For that matter, we thought of using HYPROP ® device which is mainly used to asses water retention of agricultural soil. The device is accurate enough to monitor soil water modification (water content, suction and water evaporation) with time. Moreover, the set-up is not disturbed even if we install camera to monitor the sample surface. It is however important to mention that the device is sensitive to vibration; therefore, the process of camera snapshotting should be done automatically without human intervention. This was done correctly thanks to the software development kit (SDK) on Cannon® camera.

This study is therefore an overview of the drying process (and evaporation) of Luvisol using HYPROP device. The general procedure as well as the data analysis are following the standard methodology used in engineering science. This explains the use of different formulation, equation and variables proper for engineers. This is because the study was intended to target engineering community specifically the soil mechanical group. However, this study is also a shift (bridge) toward agronomical study since we use agricultural soil and device used in agronomy. In order to find out the adequacy, accuracy and the reproducibility of the experiment as broadly used in engineering study; predicting model was performed considering the thermo, hydro-mechanical behaviour of the sample. The predictive model used the finite element code LAGAMINE developed at the University of Liege.

By summary, this study is therefore a kind of validation of the study methodology as well as an open room (bridge) for further experimental study in agricultural science.

Abstract

Due to climate change, soil desiccating became a serious concern in the agricultural area of Belgium. Knowing soil evaporation kinetic can help to elucidate and predict: the soil moisture regime, soil water retention and soil water content. Those parameters are vital for water use efficiency and sustainable agriculture. This research investigated the mechanism of soil evaporation using both laboratory experiment and numerical simulation. Soil samples (Luvisol) were collected from the agricultural field in Gembloux-Belgium, and tested in a small drying chamber. Sensors measured the chamber temperature and humidity, while digital camera monitored the soil surface throughout the experiment. HYPROP device recorded the water change, soil suction, and soil water retention curve. During three evaporation experiments, four periods were observed rather than three as commonly recorded in the theory of drying. The modelling considered thermo-hydro-mechanical framework for predicting the drying process of Luvisol. The model used the finite element code LAGAMINE created at the University of Liege. The software aims at assessing the mechanism of water transport between soil and atmosphere. The results of the simulation showed major domination of Darcean flow during desiccating, while some short vapour diffusion occurred only after the soil surface began to de-saturate.

1. Introduction

The process of evaporation is quite complicated in agricultural soil since it is conditioned by the soil characteristics (textures, structure, etc.), soil management (tillage, covered crop, etc.), and the environmental condition (precipitation, temperature, etc.). The increase of the world temperatures raised the soil evaporation rate, leading to severe crop water stress and considerable yield loss. In Belgium, several dry spells (no rainfall) were recorded over the course of the 21st century (Bernstein et al., 2007). Understanding the kinetic of evaporation of the Luvisol (soil of Belgium) will help to find appropriate method to enhance water use efficiency and alleviate the effect of climate change on plant water stress.

Based on previous studies, three distinct periods of evaporation occurred during the process of drying (Léonard et al., 2005). The first period is a Constant Rate Period (CRP) during which the evaporation flux is at its highest and constant. When the soil water supply decreases, there is prompt drop of the soil evaporation called "critical-moisture content", indicating the start of the first Falling Rate Period (FRP 1) (Keey and Suzuki, 1974; Coumans, 2000). The soil surface starts to dry drastically till the third period called second Falling Rate Period (FRP 2). The evaporation is very low due to strong interacting forces at the soil liquid-solid interface. Despite wide knowledge of the process, it is not well understood if the soil water evaporation is mainly due to liquid transport by capillary or by gas diffusion transport. Moreover, the soil characteristics and its behaviour will play huge roles in this mechanism (Kutilek, 1996; Peng and Horn, 2007).

In general, there is a complex soil hydro-thermo-mechanical behaviour. Any change in soil temperature, shrinkage, porosity, etc. affects the soil water evaporation.

Those in turn impact the water suction, water content, contaminant transport, available water for plant etc. (Simaůnek et al., 2003; Gupta et al., 2006). Previous numerical estimation model assessed the drying mechanism at pore level (ex: Pore network Model). They were limited to isothermal condition and non-deformable sample due to the need for high speed computer (Le Bray and Prat, 1999). Continuum models were commonly used for evaporation test (Wakao et al., 1968; Prat, 1991). Gerard et al. (2010) coupled hydro-thermal conditions to simulate convective drying of a silt soil. Prime et al. (2014) and An et al. (2018) used the same method for limestone and sand, respectively. The mechanical parameter was also added to the model in order to properly describe the shrinkage of the sampled material (Gallipoli et al., 2003; Hubert et al., 2018). This study used agricultural soil and considered water flow (hydro-), temperature (thermo-) and soil shrinkage (mechanical) to model the kinetic of evaporation.

2. Materials and Methods

2.1 Sampling

Three samples of soils were taken from 0-10 cm depth from an agricultural site in Gembloux-Belgium. The soil was a Cutanic Luvisol based on FAO soil classification (WRB, 2014) and contained about 70 % silt, 20 % clay and 10 % sand. The bulk density and specific gravity of the undisturbed soil were 1.38 g cm^{-3} and 2.65 g cm^{-3} respectively. The same soil was oven dried (at 40°C for one week), crushed, sieved at 2mm, and gradually compressed (dry) on three core rings (5 cm height x 8 cm diameter) to form the original bulk density. Those three disturbed samples were used during the study.

2.2 Device preparation and analysis

Drying experiment was conducted in a drying chamber using HYPROP device (UMS GmbH, Munich, Germany). The device was very accurate for continuous measurement of water evaporation, matrix suction (from 0-100 kPa, 2 % accuracy) and soil water content. The samples were saturated for 24h and inserted on the HYPROP package. The soil surface was exposed to a free evaporation. Precision balance (0.01 g) monitored the soil weight (Figure 3-1). Temperature and relative humidity were measured with Platinum resistance thermometer (0.1 °C accuracy) and DHT22 sensors (2-5 % accuracy), respectively. A Canon digital camera (12 Mpixel, 5 % accuracy), placed 0.5 m above the sample, monitored the soil shrinkage. All data was recorded every one min except for the camera (30 min). The HYPROP package came with hydraulic models to fit the data including: Mualem, Van Genuchten, Durner models, etc. For the evaporation prediction, the model used was the LAGAMINE code (Collin et al., 2002) with Finite Element Method. It predicted the process of moisture transfer between the soil surface and the ambient.

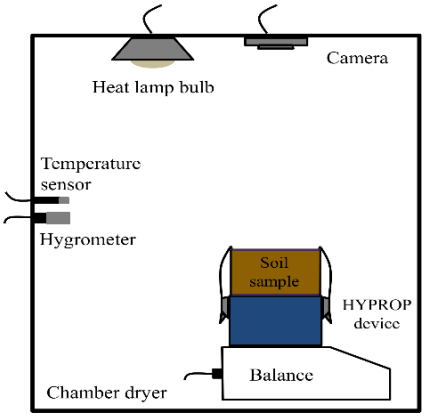

Figure 3-1. Drying chamber of the experiment

3. Experimental results

3.1 Soil water evaporation evolution

The evaporation rate was observed through the water loss per surface unit and over time:

$$\bar{q} = -\frac{1}{A}\frac{dm}{dt} \quad (1)$$

Where: m [kg] and A [m^2] were the mass and surface area, respectively.
Figure 3-2 showed the soil evaporation rate over time. All three tests presented high fluctuation during the first hour of the experiment, but depicted rather similar trend for the rest of it.

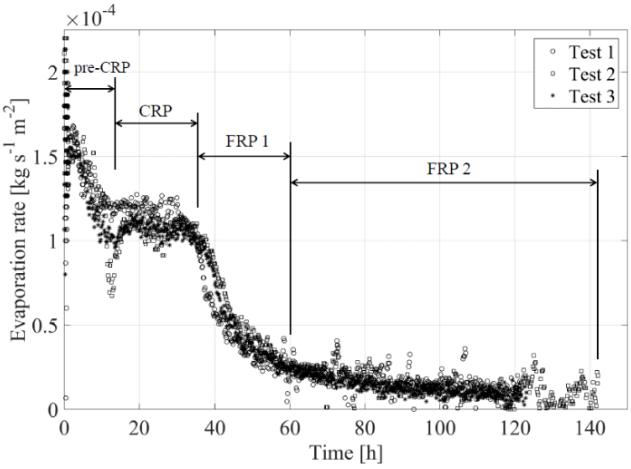

Figure 3-2. Change of evaporation rate with time

Four distinct periods of evaporation were observed. Figure 3-2 presented a pre-CRP period during the first 15 h which was characterised by high evaporation rate attaining 1.2 x 10^{-4} kg $s^{-1}m^{-2}$. This was due to the excess of water in the beginning and the pre-heating of the chamber. The second period CRP occurred when the evaporation attained around 10^{-4} kg $s^{-1}m^{-2}$. The CRP lasted for about 20 h, passed through a "critical-moisture content", then continued to the third period (FRP1) when the evaporation rate declined. The sample surface experienced a rapid drying. The beginning of the last period FRP2 was observed as soon as the evaporation rate arrived at its lowest.

3.2 Soil temperature evolution

Figure 3-3 showed the temperature above and below the samples (illustration of test 3).

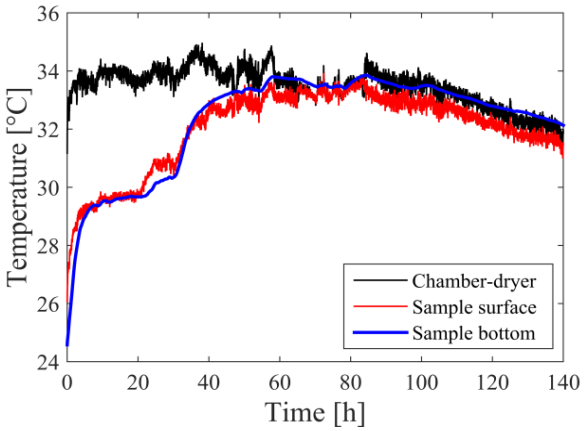

Figure 3-3. Soil temperature evolution with time (test 3)

During the pre-CRP, the bottom and the surface temperatures increased at the same rate. Temperatures were almost constant throughout the CRP periods. Since the evaporation rate was constant, the result indicated that the applied heat was compensated proportionately by the heat consumed to produce vapour. When there is not enough water vapour during FRP, the soil temperature raised to reach the ambient temperature. Similar result was found by Kowalski (2003). He observed that the stagnant temperature during CRP was the wet-bulb temperature obtained from the relation proposed by Stull (2011). Based on the relation, the calculated wet-bulb temperatures of our samples were 19.1, 19.7 and 21.3 °C, respectively.

3.3 Shrinkage

The shrinkage was observed from sequenced images taken from fixed camera. ImageJ software converted the coloured image into gray 8-bit and in binary images. The expansion of the black pixels of the binary images represented the soil shrinkage

(Nandan et al., 2019). The shrinkage was expressed in percentage of the areas of black pixels over the sample total surface.

Figure 3-4 showed that the soil surfaces were reduced by 6.7 %, 5.1 %, and 6.2 %, for the three samples. The shrinkage took place during the pre-CRP. More than 70% of the shrinkage occurred during the time the degree of saturation was quite high (> 0.75).

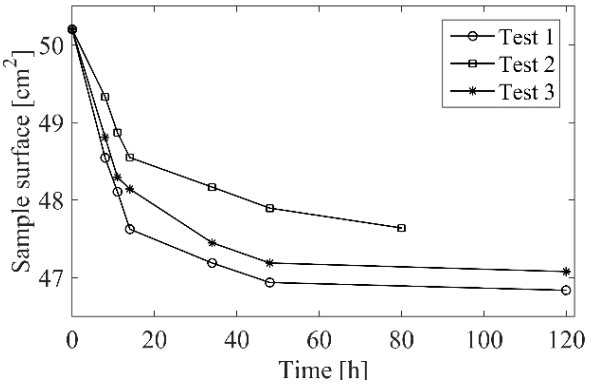

Figure 3-4. Soil surface shrinkage with time

4. Coupled thermo-hydro-mechanical model

4.1 Mechanical model

Soil mechanical properties (i.e. stiffness modulus) were related to soil moisture content (Fredlund et al., 1977; Edil and Motan, 1979; Sawangsuriya et al., 2009). The results showed an increase of soil (stiffness) modulus with matric suction. The relationship shrinkage degree of saturation was nonlinear; therefore, we choose a nonlinear elastic mechanical model. Bishop's effective stress was used.

$$\sigma'_{ij} = \sigma_{ij} - p_g\delta_{ij} + S_r(p_g - p_w)\delta_{ij} \quad (2)$$

Where: σ'_{ij} effective stress tensor, σ_{ij} total stress tensor, S_r degree of saturation, δ_{ij} Kronecker's tensor, p_w and p_g water and gas pressure.

In order to reproduce the nonlinear behaviour of the soil, equation 6 related the stiffness modulis to the suction $p_c = p_g - p_w$

$$\sigma'_{ij} = D^e_{ijkl}\varepsilon_{ij} \quad (3)$$

$$D^e_{ijkl} = 2G\delta_{ik}\delta_{jl} + (K - \frac{2}{3}G)\delta_{ij}\delta_{kl} \quad (4)$$

$$G = \frac{3(1-2\nu)}{2(1+\nu)}K \tag{5}$$

$$K = \frac{K_0}{3(1-2\nu)}\{(k_1 - 1)[1 - exp(-k_2 p_c)] + 1\} \tag{6}$$

Where: D^{e}_{ijkl} global elastic tensor, ε_{ij} elastic strain, K and G bulk and shear moduli, ν Poisson's ratio of the porous medium, K_0 initial value of the bulk modulus, k_1 and k_2 are fitting parameters, p_c suction.

4.2 Hydraulic model

The fluid transport was predicted by a biphasic flow model as follow. The advective fluxes of liquid and gas were determined by Darcy's law. We assumed that the media were non-reactive material, so that water and gas flow depended on the degree of saturation (S_r) only. S_r was determined from the water stored in porous medium and the suction p_c, and calculated from the dual porosity model of Durner (1994).

$$q_w = -\frac{k_w}{\mu_w}(\nabla p_w + \rho_w g) \tag{7}$$

$$q_g = -\frac{k_g}{\mu_g}(\nabla p_g + \rho_g g) \tag{8}$$

$$S_r = S_{res} + (S_{sat} - S_{res})\{w_1 \underbrace{[1 + (\alpha_1 p_c)^{-n_1}]^{m_1}}_{S_{e1}} + w_2 \underbrace{[1 + (\alpha_2 p_c)^{-n_2}]^{m_2}}_{S_{e2}}\} \tag{9}$$

Where: q_w and q_g mass fluxes of liquid and gas, ρ_w and ρ_g water and gas density, g acceleration due to gravity, k_w and k_g water and gas permeability, μ_w and μ_g dynamic viscosities water and gas, $w_{1,2}$ weighing factors, $\alpha_{1,2}$ inverse of air entry pressure, S_{sat} and S_{res} water maximal saturation and the water residual saturation, $S_{e1,2}$ effective saturation, $m_{1,2}$ and $n_{1,2}$ model parameters, $m_{1,2} = 1/n_{1,2}$.

Adopting this water retention with the formulation proposed by Mualem (1976), we obtained the hydraulic function k_w. The diffusive flux followed the Fick's law.

$$k_w = K_w \frac{(w_1 S_{e1} + w_2 S_{e2})^l \{w_1 \alpha_1 \left[1 - \left(1 - S_{e1}^{\frac{1}{m_1}}\right)^{m_1}\right] +}{(w_1 \alpha_1 + w_2 \alpha_2)^2}$$

$$\frac{w_2\alpha_2\left[1-\left(1-S_{e2}^{\frac{1}{m_2}}\right)^{m_2}\right]\}^2}{(w_1\alpha_1+w_2\alpha_2)^2} \tag{10}$$

$$i_v = -D_v\,\tau\varnothing(1-S_r)\nabla_{\rho v} \tag{11}$$

$$RH = \frac{\rho_v}{\rho_{v,sat}} = exp\left(\frac{-p_c M_v}{\rho_w\, RT}\right) \tag{12}$$

$$\rho_{v,sat} = \{1994.4\, exp[-0.06374(T-273) + 0.1634\, x\, 10^{-3}\ (T-273)^2]\}^{-1} \tag{13}$$

Where: K_w saturated water permeability, l pore connectivity, i_v diffusive flux by Fick's law, D_v diffusion coefficient of vapour into dry air, τ and $\varnothing$ tortuosity and porosity, $\rho_v$vapour density, RH relative humidity, M_v molecular mass of the water vapour, R gas constant, T temperature in Kelvin, $\rho_{v,sat}$ saturated vapour concentration.

4.3 Heat transfer

The heat transfer in porous media was governed by three mechanisms of transfer: - the heat conduction (Fourier's law), - the convective heat transfer (related to the flow of liquid, air and water vapour), - and an additional heat flux associated with the latent heat (Le Bray and Prat, 1999).

$$V_T = -\Gamma_m\nabla T + \underbrace{[c_{p,w}\rho_w q_w + c_{p,a}\rho_a q_g + c_{p,w}(\rho_a q_g + i_v)](T-T_0)}_{convection} + \underbrace{(\rho_v q_g + i_v)L}_{latent} \tag{14}$$

Where: $c_{p,w}/c_{p,a}/\ c_{p,v}$ water/air/vapour specific heats, ρ_a air density, i_v diffusive flux of water vapour, T_0 initial temperature, L water evaporation latent heat.

4.4 Thermo-hydraulic boundary conditions

The simulation was performed on 2D-axisymetric cylindrical soil subdivided in 20 x 50 mesh elements. The boundary considered the transfer between the thin layers of soil surface and the ambient (Figure 3-5). The sample was saturated and only the upper soil surface allowed water to pass. The vapour flow and the heat transfer were due to vapour density difference and temperature difference between the ambient and the soil surface (Nasrallah and Perre, 1988). The radiant flux from the lamp-bulb and the air to the soil surface was estimated by the Stefan-Boltzmann equation.

$$\bar{q} = \alpha(\rho_{v,surf} - \rho_{v,air}) \tag{15}$$

$$\bar{f} = L\bar{q} - \beta\left(T_{air} - T_{surf}\right) - R_n \tag{16}$$

$$R_n = \varepsilon_s \sigma A\left(T_{air}^4 - T_{surf}^4\right) + R_{lamp} \tag{17}$$

Where: $\bar{q}$ vapour flow, α mass transfer coefficient, A surface area, $\rho_{v,surf}$ and $\rho_{v,air}$ vapour density soil surface and ambient, $\bar{f}$ heat flux, β coefficient, T_{air} and T_{surf} temperature of soil ambiant and surface, R_n net radiant from Stefan-Botlzmann law, ε_s soil and bulb emissivity, σ constant of Stefan-Boltzmann, R_{lamp} flux term of lamp-bulb.

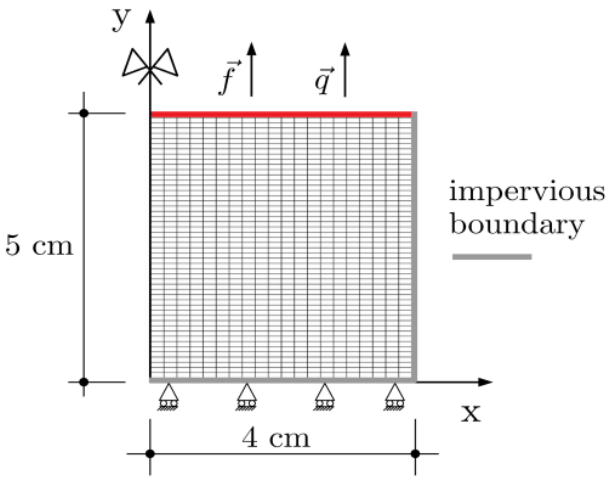

Figure 3-5. Boundary conditions of the model

5. Numerical results and analysis

5.1 Parameters used in the simulation model

Table 3-1, 3-2, 3-3 and 3-4 present all hydraulic, thermal, and mechanicals parameters used in the models. The model parameters were obtained from the experiments (Figure 3-3,Figure 3-4) and the HYPROP results. The predictive model was compared to the results from test 3 (Figure 3-6 to 11).

Table 3-1 Mass and heat transfer coefficients from experiments

	$\alpha[ms^{-1}]$	$\beta[Wm^{-2}K^{-1}]$
Test 1	0.0055	122.6
Test 2	0.0050	78.6
Test 3	0.0048	84.8

Table 3-2 Parameters of the hydraulic model

$\rho_w[kgm^{-3}]$	Liquid water density	1000
$\mu_w[Pa{\cdot}s]$	Water dynamic viscosity	10^{-3}
$K_w[m^2]$	Water permeability	$1.8\ 10^{-12}$
$\alpha_1[cm^{-1}]$	Inverse of air entry pressure (macro-pores)	0.1
$\alpha_2[cm^{-1}]$	Inverse of air entry pressure (macro-pores)	0.025
m_1[-]	Durner model parameter	0.23
m_2[-]	Durner model parameter	0.41
S_{res}[-]	Residual water saturation	0.004

Table 3-3 Parameters of the thermal model

$c_{p,w}[Jkg^{-1}K^{-1}]$	Liquid water specific heat	4180
$c_{p,v}[Jkg^{-1}K^{-1}]$	Water vapour specific heat	1800
$c_{p,\alpha}[Jkg^{-1}K^{-1}]$	Air specific heat	1000
$\Gamma_m[Wm^{-1}K^{-1}]$	Medium thermal conductivity	0.9
$L[Jkg^{-1}]$	Water evaporation latent heat	2500

Table 3-4 Parameters of the mechanical model

$\rho s[kgm^{-3}]$	Solid density	2650
∅[-]	Porosity	0.52
K_0[Pa]	Bulk modulus	10^5
G_0[Pa]	Shear modulus	$4\ 10^{-6}$
ν[-]	Poisson's ratio	0.25

5.2 Soil shrinkage

The non-linear elasticity law allowed predicting the soil stiffness and gave good agreement with the result with $R^2 = 0.996$ (Figure 3-6). The shrinkage model presented in equation 6 fitted well the experimental result with soil bulk modulus $k_1 = 1.2\ 10^4$ and $k_2 = 5\ 10^{-8}$.

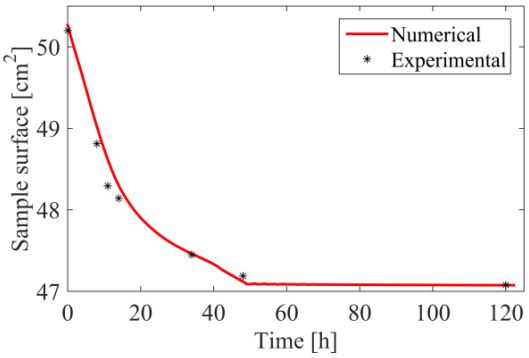

Figure 3-6. Experimental and numerical surface shrinkage

5.3 Kinetics of evaporation

The numerical result of evaporation with degree of saturation and with time fit well with the experimental data except for the first period. The estimated evaporation rate of CRP coincided with the data. The high evaporation of the first period could not be reproduced due to the fact that the mass transfer coefficient between the surface and the ambient was obtained from the average evaporation rate in the CRP period. Therefore, it was not possible to get a coefficient value higher that during the CRP (Section 4.4). However, the CRP period lasted longer and there was overestimation of evaporation during FRP period (Figure 3-7). In order to deal with the problem, high evaporation rate was introduced to the pre-CRP period (i.e., saturated state Sr ~0.8), and then the prediction curve fit well the experimental data ($R^2 > 0.9$) (Figure 3-8).

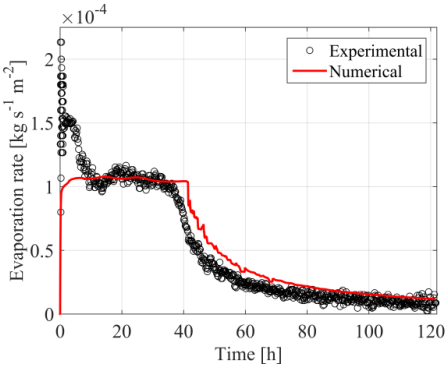

Figure 3-7. Experimental and prediction of soil evaporation rate

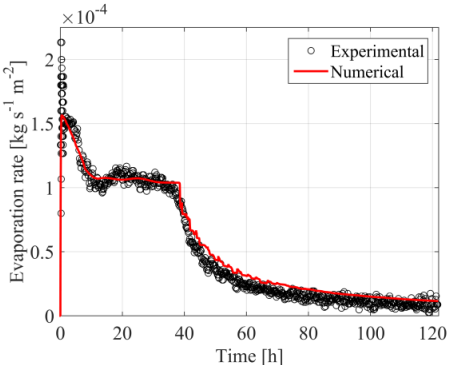

Figure 3-8. Improved numerical prediction of soil evaporation rate

5.4 Soil temperature

The model managed to predict the temperature variation during the experiment. Temperature started from 28°C to the plateau of 32°C which was the wet-bulb temperature (Figure 3-9). The temperature increased during the period FRP and then reached the ambient temperature.

5.5 Water transfer

The moisture transport during drying can be investigated based on Coussy (Coussy and Brisard Volume, 2009) theory. It indicated that material with permeability below 10^{-19} m^2 presented mainly Darcean advective water transport. Water was in liquid form and very negligible vapour diffusion. Therefore, the Luvisol was dominated by advective flow as its intrinsic permeability was of magnitude of 10^{-12} m^2. Moreover, Figure 3-10 showed that moisture was mostly removed by Darcean advective flow. Figure 3-11 portrayed the humidity distribution in the sample. The entire sample has 100% relative humidity during saturation. There was formation of evaporation front (dry-and-wet front) when the soil starts to de-saturate. The front moved to bottom as the soil kept on drying.

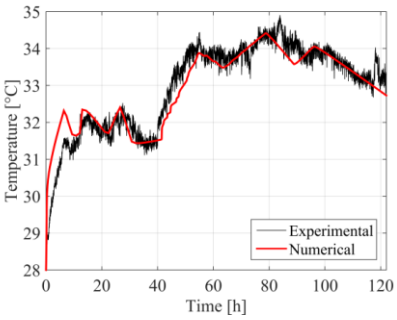

Figure 3-9. Experimental and predicted soil surface temperature

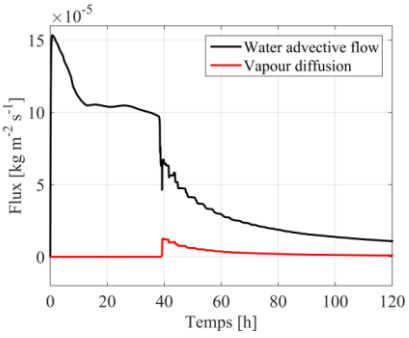

Figure 3-10. Temporal evolution of water and vapour flow at the soil surface

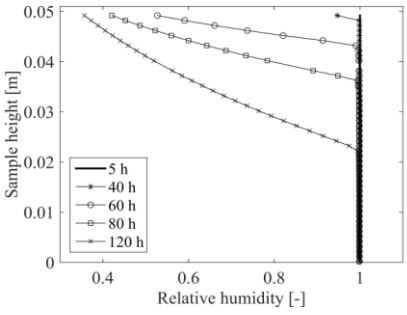

Figure 3-11. Relative humidity profile along the sample with times

6. Conclusion

The study showed the process of evaporation of Luvisol in experimental and numerical approaches. Four evaporation periods were identified instead of three during the laboratory test. The soil temperature followed the Krischer's curve; however, the wet-bulb temperature was higher due to the applied heat (>30 °C). The fully coupled thermal-hydraulic-mechanical model managed to reproduce the soil surface shrinkage, the temperature variation and the soil evaporation processes especially when correction was added during the start of evaporation. The moisture transfer mechanism of the agricultural Luvisol involved mainly Darcean advective flow. Vapour diffusion contributed a little during the entire process of evaporation. The evaporation front move from the soil surface to the bottom as the soil continued to dry.

What is important from the article and how this is important for the study's objective?

This article intends to give an overview of the kinetic drying of a Luvisol. This is according to the broader methodology in the mechanical engineering using devices (HYPROP ®) and chamber (laboratory environment) specially used in agronomy.

The overall result is similar to what is observed from the mechanical engineering. The thermo, hydro-mechanical model could fit the output data without adding external factors (due to change of devices themselves). For instance, the evaporation periods found in this study are already reported before (in engineering research) except that this study reports 4 periods instead of 3. This could come from the difference in terms of sample characteristics (size, and initial water content).

Therefore, the study results prove that it is feasible to continue the project using the current methodology. There is also possibility of expanding the experiment by adding devices such as: camera, sensors, tensiometer, etc. The results give also an insight on the possible improvement for the future experiment. We observe from the results the effect of the fluctuating environmental condition (temperature and relative humidity) on the sample's water evaporation. This condition could be the reason for different value of the parameter Beta (β: convective transfer coefficient) in this study. This is because the sample was exposed to a room condition. This condition can change despite the use of heater to heat the sample surface. For instance, to accommodate the camera and other device, the upper part of the chamber was not hermetically protected from the room condition. This could also be the reason (origin) for the difference in sample shrinkage with time in Figure 2-4. All these problems are tackled by covering perfectly the small chamber. The inside chamber is therefore isolated from the laboratory environment. In order to monitor the experiment, one part of the chamber is covered with transparent glass. This part is covered from outside (-in) by black curtain to avoid light to enter the chamber.

In conclusion, this experiment helps us to monitor the feasibility of the drying experiment using apparatus used in the agronomical science. This helps as well to improve the methodology based from the results output. In all, this study is crucial for the entire study.

Since there is no possible change concerning this article; some of the questions addressed concerning this article is briefly answered here in this paragraph: For instance, some omitted number is observed in page 55. Instead of K_1 and K_2, it is written (by mistake) K_1 and $K_{1.}$ The different value of the coefficient beta (β: heat transfer coefficient) (Page 55) may come from the environmental condition.

CHAPTER 4

A first insight on the interaction between desiccation cracking and water transfer in a Luvisol of Belgium

The content of this chapter has been published in the Soil Systems-MDPI 2021: Ralaizafisoloarivony, N.; Degré, A.; Mercatoris, B.; Léonard, A.; Toye, D.; Charlier, R. A First Insight on the Interaction between Desiccation Cracking and Water Transfer in a Luvisol of Belgium. Soil Syst. 2021, 5, 64. https://doi.org/10.3390/soilsystems5040064

The importance of this chapter in relation to the study's objectives:

This paper responds to the third objective of this thesis which intends to find out the interaction between crack formation and soil hydraulic properties. The paper is subdivided into 5 parts starting from the:

- Abstract which summarises the result output.

- Introduction highlights the most relevant literature associated with the study objective. This section is highly compiled in terms of length and content. Therefore, part of the literature has been added in chapter 5 (of this thesis) to elucidate some missing information

- Material and methods: describe the overall technique used during the experiment. This part is in complementarity with the methodology shown in the previous chapter 2. The previous chapter (chapter 2) highlights the details procedure which is not given in this chapter. It includes sample extraction, sample preparation and storage, experiment set-up, details procedure on data/image collection and analysis. However, this chapter 5 gives the overviews of the entire methodology as well as the laboratory procedures and various equations (Bulk density, evaporation, pore distribution…) which are not specified in chapter 2.

- Results and discussion: this section mentions the kinetic of drying of the Luvisol. The result from this chapter is in complementarity with the results in Chapter 3. This chapter shows the overall interaction between the crack development and the soil water characteristics such as water content, water evaporation and water suction. The interaction is shown by plotting the raw data (cracks, and soil water per time) on the same graph or by observing the progression of cracks versus soil water, or evaporation versus water content (known as Krisher's curve). The soil water retention curve (SWRC) permits to observe soil pore/crack size distribution, the crack variation against suction (by extrapolating the suction), and the crack evolution along with the SWRC. The results respond to the research question mentioned in the introduction (Chapter 1) concerning the interaction between soil cracking and soil hydraulic properties on Agricultural soil.

- Conclusion: The conclusion summarises the most underlying results. Small perspective has been proposed for further study.

In summary, this section intends to give the most important information of the thesis which is the interaction between cracks and soil hydrology. The section is highly reduced. Therefore, further explanation and discussion is given in the next chapter 5.

Abstract

The present paper presents the interactions between water retention/evaporation and cracking during desiccation of intact and disturbed Luvisol of Belgium. Disturbed (DS) and undisturbed samples (NDS: reduced-tillage-residue-in (RTRI) and conventional-tillage-residue-out (CTRO)) were collected from agricultural field in Gembloux-Belgium. The drying experiment took place in controlled laboratory conditions at 25 °C. Moisture content, soil suction and surface cracks were monitored with precision balance, tensiometer and digital camera, respectively. Image processing and analysis were performed using PCAS ® and ImageJ ® software. The results showed that crack formation initiated at stronger negative suction and lower water content (Wc) in DS>>CTRO>RTRI. Suction and crack's propagation were positively correlated until 300 kPa for DS, and far beyond the wilting point for NDS. For NDS, cracking accelerated after reaching the critical water content (~20 % Wc) which arrived at the end of the plateau of evaporation (40 h after crack initiation). The Krisher's curve revealed that the soil pore size > 50 µm and likely cracks are important parameters for soil permeability. Soil structure and soil fibre content could influence the crack formation dynamic during drying. The agricultural tillage management as well influences crack propagation. As retention and conductivity functions are affected by cracks, it is likely that the fluids movements in the soil will also be affected by cracks following a desiccation period (i.e., when cracked soil is rewetted).

Keywords: Fracture; moisture content; evaporation; soil water retention; drying

1. Introduction

Crack propagation is an important natural phenomenon in agricultural field, especially in fine grained soils as in the Luvisol of Belgium (Gentile et al., 2009; Stoops et al., 2020). Cracks may act as bypass for water and solutes, lower the soil water content and increase its matric suction (Shepidchenko et al., 2020). Factors affecting cracks are numerous and complex (mineralogy, temperature, moisture, thickness, other boundary conditions) (Lakshmikantha et al., 2009; Zeng et al., 2019). However, it is commonly observed that the process of crack initiation and propagation is water dependent (Tang et al., 2010). Cracks form when the tensile strength of the soil is reached during desiccation (Zeng et al., 2019).

Soil physical (structure, porosity, aggregates) and chemical properties (pH, organic carbon , cations, anions) are supposed to influence the crack formation/propagation (Merlin et al., 2016). These parameters are essentially affected by agricultural practices. Tillage and residue management influence the soil porosity and fibber/organic matter content and therefore affect water and gas movement (Aguilar Torres et al., 2004). For instance, the additional of organic matter and biochar were found decreasing crack formation (Aguilar Torres et al., 2004; Lu et al., 2021).

Tillage also influences the soil structural heterogeneity and the soil compressibility which can affect the crack formation and propagation (Tang et al., 2008; Weninger et al., 2019). In fact, soil heterogeneity could affect the distribution of water creating

weak area during shrinking (Peron et al., 2009; Tang et al., 2011). Moreover, tillage smashes soil aggregates, modifies structure which might lead to soil compaction and change the soil permeability (Merlin et al., 2016; Zhang et al., 2017). However, there is still some gaps in understanding the interaction between cracks and soil hydraulic properties under varied agricultural practices. It was Lakshmikantha et al. (2009) and Tang et al. Tang et al. (2008) who were among the pioneers analysing cracks and soil water properties. Later studies found some link between crack maximum width and water permeability (Mihashi et al., 2006; Shepidchenko et al., 2020).

Some authors reported that under saturated surface conditions, the evaporation depended only on the vapor pressure difference between the atmosphere and the sample surface (excluding cracks) (Léonard, 2002; Kowalski, 2012). Others mentioned the possible effect of macropores (and cracks) as they assure the water connectivity between the saturated and partially air-filled soil (called drying front) (Hubert et al., 2018b).

Even if previous researchers found that cracks enlarge the soil porosity, increase the soil permeability and reduce the air entry value (AEV: which is the minimum suction at which air starts to enter largest pores) (Al-Dakheeli et al., 2018), it is still hard to include cracks in soil water retention curve (SWRC) and permeability due to their geometric complexity. Moreover, cracks are changing in configuration and in size during soil desiccation (Mihashi et al., 2006). This requests researchers to include a dynamical analysis of cracks in parallel to soil hydrodynamical assessment (Al-Dakheeli et al., 2018). However, due to crack complexity (in form, size, configuration and distribution), crack analysis is often neglected in regards to soil hydrology (research) especially as far as agricultural science is concerned (WRB, 2014; Merlin et al., 2016).

Therefore, this study will assess the dynamics of soil cracking, and soil hydrology during drying in a controlled experiment for one single soil (Luvisoil) under 3 contrasted treatments (two types of samples under different management systems, and one type of disturbed/mixed samples). Each treatment has three replicates. The purpose of using remolded sample is to question the impact of agricultural soil structure. Furthermore, many cracking studies utilized disturbed sample to represent agricultural soil (Tang et al., 2008; Lakshmikantha et al., 2009; Tang et al., 2010). Therefore, we want to assess the difference between disturbed and undisturbed samples. The study will also evaluate the potential interaction between soil cracking and soil hydrology, and discuss the observed differences among treatment.

2. Materials and Methods

2.1 Sample collection and preparation

We collected nine topsoil (0-15 cm) samples composed of 3 Reduced-tillage-residue-in (RTRI), 3 Conventional-tillage-residue-out (CTRO), and 3 Disturbed soils (DS) (composite remoulded sieved samples from RTRI and CTRO). The remoulded sample are interesting as they erase the tillage history and so give a reference for comparing results. The RTRI and CTRO plots are 15 m X 45 m each and are located

two meters apart. The samples were collected from agricultural field in Gembloux, Wallonia, Belgium. The crop rotation in the study area is composed of cover crop (rapeseed: *Brassica napus L.*, mustard: *Brassica nigra L.*, oats: *Avena sativa L.*, and peas: *Pisum sativum L.*), maize (*Zea mays*), winter wheat (*Triticum aestivum L.*), and sugar beet (*Beta vulgaris L.*). The preceding crop was sugar beet.

The samples were prepared from a rectangle steel box of 25 cm length x 20 cm width x 1.6 cm height or soil thickness (Figure 4-1). The thickness was chosen in order to enhance the drying induced cracking process according to literature and pre-testing experiment (Lomeling et al., 2016; Zeng et al., 2019). The undisturbed samples (NDS = RTRI and CTRO) were saturated with distilled water (from bottom by capillary rise) for 24 h before the commencement of the experimentation. In order to assure pore saturation, the water is levelled (until) to 4-5 mm below the sample surface. The initial water content obtained in NDS was between 45-50 %. This value was obtained from the mass difference between saturated sample and oven dried (105 °C 24 h) samples converted into volume, divided by the total volume of the wet sample. The soils from DS were subjected to crushing, oven drying at 40 °C, sieving at 2 mm diameter and moulding at 45-50 % of water content (as NDS). At this moisture percentage, the DS samples obtained a bulk density similar to the NDS samples without need for further soil compaction. The slurry is uniformly poured into metal box the same size as used for intact soil. The overall sample is slightly shaken to fill the box evenly and remove some trapped air in the sample. The specimen is covered and settled for 2 h prior the drying experiment.

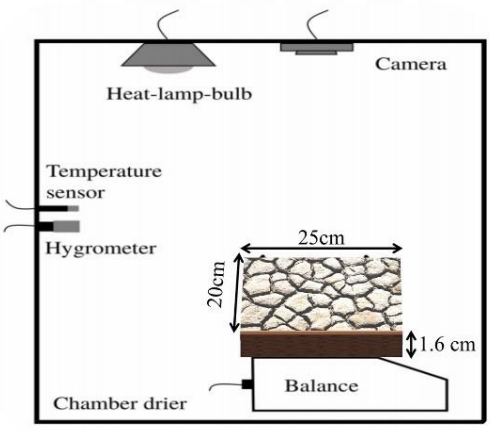

(**a**) Design of the drying chamber composed of soil sample, camera, balance, heating bulb, and sensors

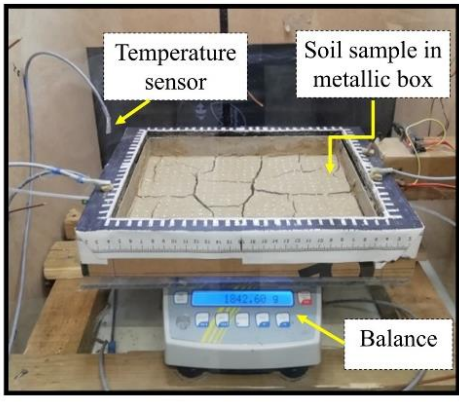

(**b**) Real photo of the inside chamber showing cracked sample in metallic box

Figure 4-1 Overview of the experimental chamber set-up illustrating (a) tools: camera, balance, heating bulb, and sensors, and (b) soil sample + metallic box

2.2 Sample physical/chemical characteristic and fibre (roots, stubble, straw) analysis

Intact soils were collected from core rings near the sampling location (in three replicates) in order to measure the soil bulk density and porosity. The formula of bulk density and porosity is given below:

$$BD = \boldsymbol{m_s/V} \quad (1)$$

$$\boldsymbol{\rho_s} = \boldsymbol{\rho_m V_m + \rho_{om} V_{om}} \quad (2)$$

$$\Phi = (\mathbf{1} - BD/\boldsymbol{\rho_s}) \quad (3)$$

Where: BD, ρs: soil bulk density and particle density (g.cm^{-3}), Φ: soil porosity, ms: mass of oven dried (at 105°C for 24 h) soil (g), V: volume of core cylinder (cm^3), ρm: mineral density (2.65 g.cm^{-3}), ρom: organic matter density (0.8 g.cm^{-3}), Vm, Vom: volume fraction of mineral and organic matter (%)

Clay, silt and sand fractions were quantified using pipette method (ISO 11464, 2006). The organic carbon, humus content and pH of each treatment were measured according to the standard procedure (ISO 10694, 1995; ISO 10390, 2005). pH-meter measured the soil pH at a soil/water ratio of 1:5. The total carbon (TC) was calculated from the quantity of CO_2 coming from burning sample. The total organic carbon (TOC) required a pre-removal of carbonic mineral (by HCl 2N) before burning the sample.

Based on literature, this soil is classified as a Cutanic Luvisol (WRB, 2014), composed mainly of silt (80±2 %), clay (15±1,5 %) and sand (5±2 %). The C:N ratio is between 10 and 12 (C content of 20-35 g per kg soil) (Degrune et al., 2017), and the bulk density is around 1.3-1.4 g.cm^{-3}. After the experiment, crop straw, stubble, and roots were sieved (2 mm) from soil, spread on white paper, scanned by camera, and quantified using image analysis.

2.3 Drying and chamber preparation

The experiment took place at Gembloux-Agro-Bio-Tech laboratory. Drying was conducted in a small chamber heated with lamp bulb (Exoterra® ceramic heat emitter at 30 °C). We pre-heated the chamber prior to the experimental set-up as proposed by Tran et al. (2019). Precision balance monitored the change in sample weight every 15 minutes. Water tensiometer, pressure transducers (0-400/500 kPa) connected to CR800 datalogger (programmable device by Campbell Scientific ® controlling sensors) measured the soil water suction. They were inserted in horizontal position (4 cm inside the sample) in the middle width section of the metallic box. The top surface of the sample was exposed to a free evaporation and monitored by 12 Mp Canon ® camera (Canon Powershot SX 520 HS ®) which took a picture every 30 min. We installed a Plexiglas ® at the base of each sample to hold the specimen and to avoid an evaporation from its basal. Friction in squared-form grid (1mm height, 1cm length) was added in the interfacial between the soil and the Plexiglas ®. The experiment lasted for 7-10 days. About 330 to 480 pictures were taken for each sample.

2.4 Determination of moisture content, evaporation, soil water retention curve and pore size distribution during drying

2.4.1 Krischer curve

The moisture content was calculated from the weight difference between the soil at a given time and the oven dried soil (oven drying at 105 °C for 24h after 7-10 days of experimentation). The soil evaporation portrayed the rate of water dissipation through the sample area per second (and converted in cm.day^{-1}) (Song and Cui, 2020). The representative curves and their parameters in the result section were averaged from the three replicates. Krischer curve treated the drying rate q (cm.day^{-1}) as a function of the water content (θ) adjusted with the initial water content (θo) of 0.5. The drying rate formulation is given below:

$$q = \frac{Soil\ mass\ (t) - Soil\ mass\ (t-1)}{A * \Delta t} \quad (4)$$

Where: q: drying rate (cm.day^{-1}), Soil mass (t,t-1): change of soil mass (during 10min) transformed into water volume (cm^3) using water density, A: sample surface area (cm^2), Δt: time interval between two measurements (day).

The maximal drying rates (qmax) and the critical water contents (Wcrit) were deduced from the graph of drying curve versus time. The critical water content corresponds to the time of curve deflection after the plateau of maximum drying rates (Gerard et al., 2015).

2.4.2 Soil water retention curve (SWRC)

The SWRC represents the volumetric water content (θ) against water suction (in kPa). The volumetric water content is obtained from the weight difference between the wet and oven dry soil (105 °C for 24 h) converted into volume (water volume (cm^3) = water mass (g) / water density (1 g/cm^{-3})) and over the total volume of the wet sample (800 cm^3 = 25 cm x 20 cm x1.6 cm). In the calculation of SWRC, the effective saturation is often used according to the following equation:

$$S_e = \frac{\theta - \theta_r}{\theta_s - \theta_r} \quad (5)$$

Where: Se is the effective saturation, θ: is the water content at time t, θs is the saturated water content and θr is the residual water content (i.e., water remaining in dry soil). Residual water content is the remaining water content at high tension obtained when the gradient d(volumetric water content)/dh (i.e., h: suction) becomes zero. In calculation, residual water content is considered to be zero.

The non-linear equation of van Genuchten (1980) and the one of Durner (1994) fitted the monomodal and bimodal pore structure, respectively. The bimodal function of Durner (1994) is a combination of two VG models, which considers macropore (first modal) and micropore (second modal). The fitting curves were calculated using the SWRC-fit package developed by Seki (2007). The double model is given below:

$$S_e = w_1 \left[\frac{1}{1 + (\alpha_1 h)^{n1}}\right]^{m1} + w_2 \left[\frac{1}{1 + (\alpha_2 h)^{n2}}\right]^{m2} \quad (6)$$

Where: α (cm^{-1}), *n1, n2, m1, m2* are empirical parameters and *m* is calculated by $m = 1-1/n$; *w1, w2 are weighing factor. w2 is set to zero f*or monomodal curve making the second part of the Se formula equal to zero.

The three SWRC curves representing each treatment were obtain by averaging the volumetric water content and the water suction of the three replicates. The measured water suction was unfortunately limited to 400-500 kPa due to classical water-filled tensiometer cavitation. For instance, we utilized a ceramic cylinder (0.5 cm diameter and 2.5 cm long) connected to pressure transducer (BLPR2-IM-040606 ® of World Precision Instrument ®) by plastic tube filled with degassed water. The degassing procedure used vacuum instruments (glass chamber + pump) for 72 hours. This problem (of missing data) was addressed by extrapolating the water suction (in the range 400 -15 000 kPa) from available water content data (between 0-500 kPa) using the fitted-SWRC models (monomodal and bimodal). The quality of the fit is presented in Appendix D and Appendix C.

2.4.3 Pore size distribution (PSD)

The water retention curves were converted into PSD . The cumulative pore volume fraction of the i^{th} fraction (if we divide the SWRC in *n* fractions) is equal to the ratio of the measured water content to the saturated water content (which is equal to Se at i^{th} fraction):

$$S_{ei} = \sum_{j=0}^{j=i} v_i \; ; \; i \; = \; 1, 2, \dots, n \tag{7}$$

Where Sei is the effective saturation (Se) at i^{th} fraction, *v*i is the volume fraction at i^{th} fraction, n is the total number of fraction (i.e., number of portions of SWRC).

The corresponding pore diameters di (at i^{th} fraction) is converted from the water matric suction using the Jurin's law which is simplified in the equation of (Chang and Cheng, 2018):

$$h_i = \frac{3000}{d_i} \tag{8}$$

The curve of pore size distribution (PSD) was obtained by pairing the cumulative pore volume fractions in equation 8 and the calculated pore diameter from equation 7 (Weninger et al., 2019). The obtained PSD was classified in 3 classes for statistical comparison. Pore diameters below 50 µm were classified as storage/residual/binding pores; those between 50 and 500 µm were transmissive pores; and >500 µm were fissures (Weninger et al., 2019).

2.5 Image processing and analysis

Prior to image processing, the images were corrected (tilt correction, geometry correction, etc) using GIMP ® software. The image processing followed five main steps as proposed by Lakshmikantha et al. (2009), Tang et al. (2008), Le Roux et al., (2013) and Li et al. (2016a) using ImageJ ® and PCAS ® packages. The first steps converted the RGB image into grey images, then into black (cracks) and white (background) pixels. This binarization process was based on the Otsu's thresholding

technique. The second step removed all the impurities and noises (dots; outliers) from the images using series of techniques (filter, smooth, sharp, erode, dilate, noise removal, thickening). The skeletonization process during the third step transformed the binary image into skeleton (or thinned medial axis) images. The remaining steps (4 to 5) consisted in identifying cracks, and measuring their width and length (Figure 4-2).

Crack width and the crack length were estimated from the black pixels of the binary image using PCAS software (Le Roux et al., 2013). The sum of medial axis (crack branches) between nodes gave the total crack length. Crack width was estimated from the Ferret diameter of fractal images. Feret diameter is defined as the orthogonal distance between two parallel tangents (Inan Sezer et al., 2008). Crack width was calculated from the average width of each fractal image.

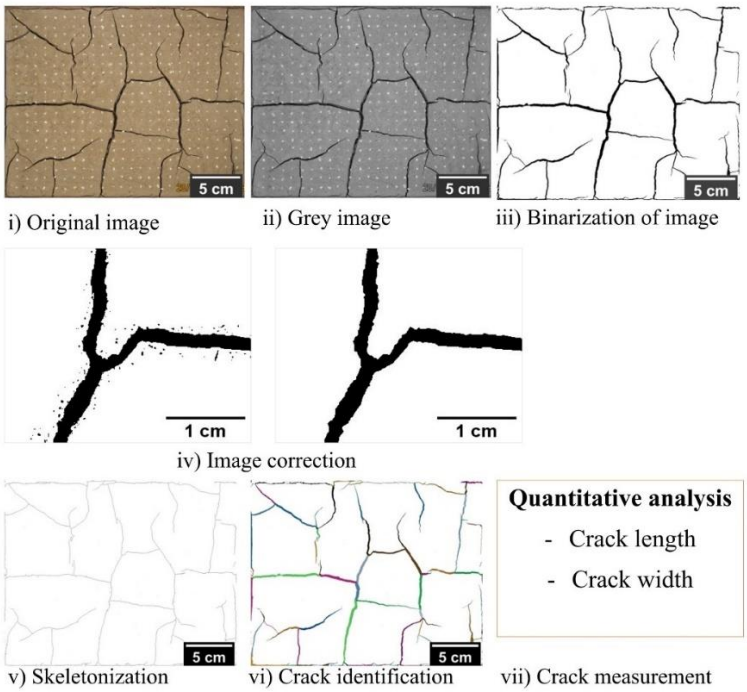

Figure 4-2 Image processing and analysis

2.6 Statistical analysis

All graphs represent the averaged data from three replicates per treatment (i.e., each treatment has three replicates). The relationship between the evaporation rates/water content/water suction and crack length were analysed using Pearson correlation. The strength of the relationship was assessed statistically with linear regression. The parameters of the Krisher's curve and the SWRC (mono and bimodal curve) were

compared statistically among treatment (RTRI, CTRO and DS). Repeated measures ANOVA with mixed models (restricted maximum likelihood (REML) + compound symmetry) from XLSTAT software analysed the pore distribution class between treatments. All statistical analyses were performed at a confidence level of 95 %. The RMSE (root mean square error) and R^2 (determination coefficient) of the extrapolated water suction (from SWRC) versus observed data were also calculated.

3. Results and discussion

3.1 Soil physical and fibre characteristics

Table 4-1 presents the soil physical and chemical characteristics. The results show significant differences in bulk density and total porosity between reduced tillage-residue-in (RTRI) and the other treatments (CTRO and DS) at 95% confidence level. Note that the difference in terms of soil mineralogy is assumed to be low since all samples were coming from neighbouring plots. Fibres were removed from DS during the process of sieving. Fibres from RTRI were slightly shorter (in individual length), narrower in width and lighter (almost decomposed) in weight compared to CTRO (Figure 4-3).

Table 4-1 Soil physical characteristics and fibre content from each sample.

Category	RTRI	CTRO	DS
BD, $g.cm^{-3}$	1.39±0.02b	1.5±0.02a*	1.56±0.02a*
Porosity	0.46±0.01a*	0.42±0.01b	0.40±0.01b
pH	7,78±0,16	7,28±0,14	8,3±0,21
Clay, %	15.93±0.16	15.13±0.16	15.95±0.14
Silt, %	78.62±0.18	79.48±0.18	78.98±0.15
Sand, %	5.44±0.09	5.38±0.09	5.07±0.08
Fibre total area, cm2	25.99±8.63	27.85±10.69	0.00±0.00
Fibre total length, cm	169.17±76.15	110.55±55.26	0.00±0.00
Fibre average width, cm	0.16±0.03	0.22±0.06	0.00±0.00
Fibre weight, g	0.87±0.1	1.02±0.09	0.00±0.00
Fibre percentage, mg.g-1 soil	0.71±0.1	0.89±0.06	0.00±0.00

* *BD: bulk density, a,b,c: significance difference at 5% error (* p>0.01, ** p< 0.01), RTRI: reduced tillage residue-in, CTRO: conventional tillage residue-out, DS: disturbed sample, N/A: no data. Note: Values represent means ± standard error of the mean (n = 9). The soil porosity is calculated from the bulk density considering the amount of soil organic matter. Fibre includes all fresh organic matter (roots, straw, stubbles) extracted from the undisturbed samples*

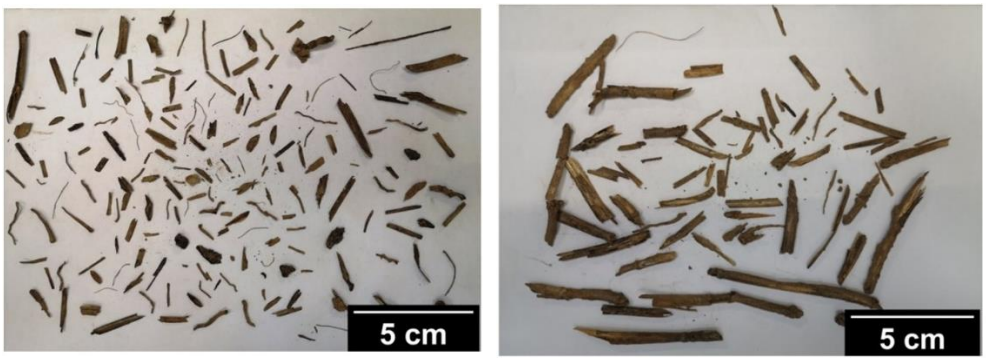

(**a**) RTRI-1 (**b**) CTRO-1

** RTRI: reduced tillage residue-in, CTRO: conventional tillage residue-out*

Figure 4-3 Representative fibres (crop stubble/roots) collected from undisturbed samples (case of RTRI-1 and CTRO-1). Note the many small and almost decomposed roots from RTRI and the few large fresh stems (cereal) for CTRO.

The total length of fibres was greater in RTRI than CTRO (Table 4-1). It is important to mention that some roots and part of straws (5-10 cm) were also remaining in the field for CTRO. However, all residue (roots + above ground biomass) were left for RTRI. CTRO presented long (individual size) and almost intact organic matter mainly composed of aboveground biomass (straws). Roots were fewer compared to RTRI. The crop stubble/roots area was almost similar for both treatments; however, in RTRI fibres were many/small and in CTRO they were few/big (Figure 4-3)**.**

3.2 Comparative curves of water evaporation, water content and water suction in undisturbed (RTRI and CTRO) and disturbed sample (DS)

The average curve of water evaporation (with time and against degree of saturation) in each treatment is shown in Figure 4-4 a,b. We observe two distinct periods. During the first evaporation period (before 40 h and 40 % of $\theta/\theta o$), the curve is at its steady and maximum stage (qmax in Appendix A). The undisturbed samples (RTRI and CTRO) present the highest water evaporation rate (>150 and 120 $cm.day^{-1}$, respectively) compared to disturbed soils (DS) (< 100 $cm.day^{-1}$). The deflexion of the evaporation curve (40-50 h) corresponds to the start of the second period. During this second period, DS takes time (> 100 h) to attain its minimum evaporation rate (compared to NDS ~100 h).

Figure 4-4 c shows initial water content of about 45-50 % for all treatments. The water content decreases linearly before attaining its stabilisation line. The deflexion of the curve indicates that the critical water content (Wcrit) is reached after 40-50 h (about 40% of standardized water content in Krisher's curve Figure 4-4 b). Appendix

A shows that the critical water content (Wcrit) is around 0.2 for NDS while almost unseen for DS since DS curve was linear. All these indicators emphasize that water removal is more restricted in DS than NDS. Water loss induces an increase in water suction as shown in Figure 4-4 c. The suction (in kPa) increases exponentially at around 60-80 h which was 20-40 h after the critical water content.

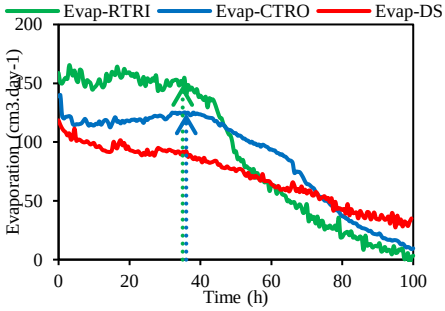

(**a**) Soil water evaporation with time between undisturbed (RTRI and CTRO) and disturbed samples (DS).

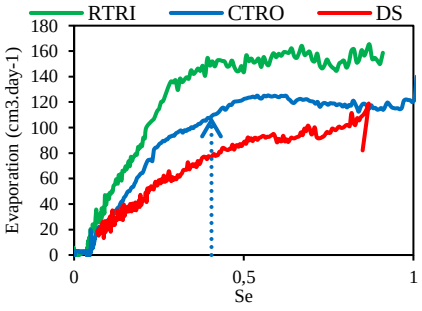

(**b**) Krisher's curve showing the interaction between evaporation and degree of saturation. The arrow indicates the critical water content (Wcrit)

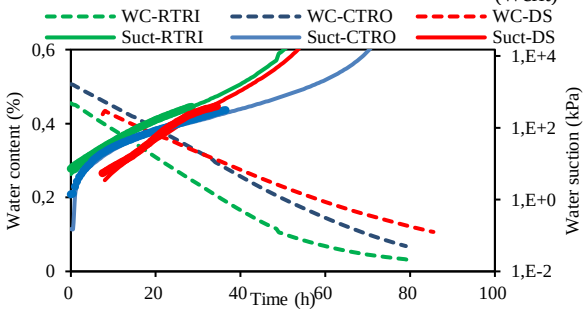

c) Water content and extrapolated (line)/observed (dots) water suction change with time between RTRI, CTRO and DS

** Evap- RTRI/CTRO/DS: Water evaporation for RTRI/CTRO/DS; Wc- RTRI/CTRO/DS: Water content for RTRI/CTRO/DS; Suct- RTRI/CTRO/DS: Water suction (kPa) for RTRI/CTRO/DS; RTRI: reduced tillage residue-in, CTRO: conventional tillage residue-out, DS: disturbed sample*

Figure 4-4 Evaluation of the progression with time of water evaporation, water content and water suction for each treatment. Note the deflexion of the evaporation curve from around the critical water content. The critical water content is also obtained from the average of three replicates as the treatment's curves (RTRI, CTRO, and DS).

3.3 Crack length and width between disturbed/undisturbed sample

Figure 4-5 presents the progress of (a) average crack length and (b) crack width with time. The maximum crack length (observed at 80 h after crack initiation) was two to three times longer in DS (~230 cm) than in NDS (70-100 cm). For NDS, crack

length increases slowly during the first 30 h-40 h of crack initiation. Later, it progresses slightly faster (from 20-80 cm in the next 40 h) and linearly. However, DS starts with first strong increase after the first 18 h (growth from 0 to 140 cm in <10 h), then a slower rise (~100 cm in the next 40 h) before reaching a stagnation period (~80 h). Small differences can be observed between RTRI (~100 cm) and CTRO (~70 cm) in terms of total crack length. Concerning crack width, for NDS, the average crack width decreased linearly (from 600 to 400 µm) before reaching a plateau of stagnating phase (around 40-50 h in Figure 4-5 b). The decrease indicates the formation of thinner cracks during crack progression. However, for DS the average crack width increased promptly (up to 750 µm) after the first 18 h (i.e., formation of wider cracks) before decreasing slowly and linearly (i.e., formation of thinner cracks).

Figure 4-6 depicts cracks obtained from image analysis 10-20 h, 30-40 h and 80 h after crack initiation. The results show that DS forms 90° (T-pattern) and 120° (Y-pattern) crack-junctions while undisturbed sample (NDS) forms only Y-pattern cracks (Figure 4-6). Wang et al. (2018) describes T (90°) junction as the results of coalescence of two cracks while Y (120°) junction as some extension of cracks. The T-junctions are mainly observed between primary cracks (first main cracks) in DS which ended by forming a clod (polygonal looping cracks). The Y-junction (in DS) comes later when the secondary and tertiary cracks are forming. This is the period during which the soil is slightly dry and the crack propagation is more difficult. Therefore, the formation of (only) Y-junctions in NDS evokes the difficulty of spreading cracks in undisturbed samples (compared to DS).

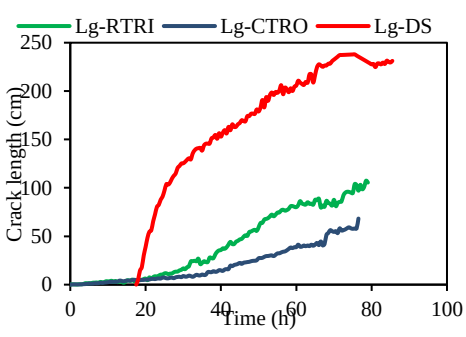

(**a**) Crack length progression with time for undisturbed samples (RTRI and CTRO) and disturbed sample (DS)

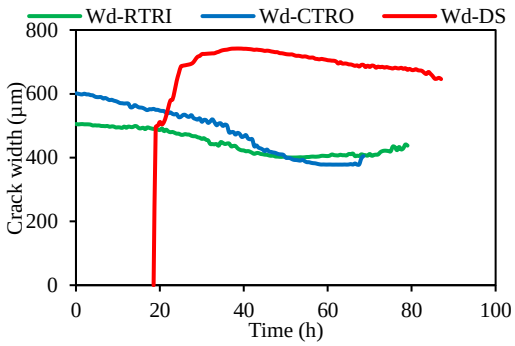

(**b**) Crack width progression with time for undisturbed samples (RTRI and CTRO) and disturbed sample (DS)

** Lg-RTRI/CTRO/DS: Crack length for RTRI/CTRO/DS; Wd-RTRI/CTRO/DS for RTRI/CTRO/DS, RTRI: reduced tillage residue-in, CTRO: conventional tillage residue-out, DS: disturbed sample, NDS = RTRI and CTRO.*

Figure 4-5 Evaluation of crack progression presented in width and length for disturbed (DS) and undisturbed samples (NDS). The data was obtained from average of three replicates. Note the great crack size and fast crack increase in DS compared to CTRO and RTRI. The decrease in crack width indicates the formation on thinner cracks

during drying. Note that crack width represents the average crack width (at time t) while crack length is the total crack length from a sample.

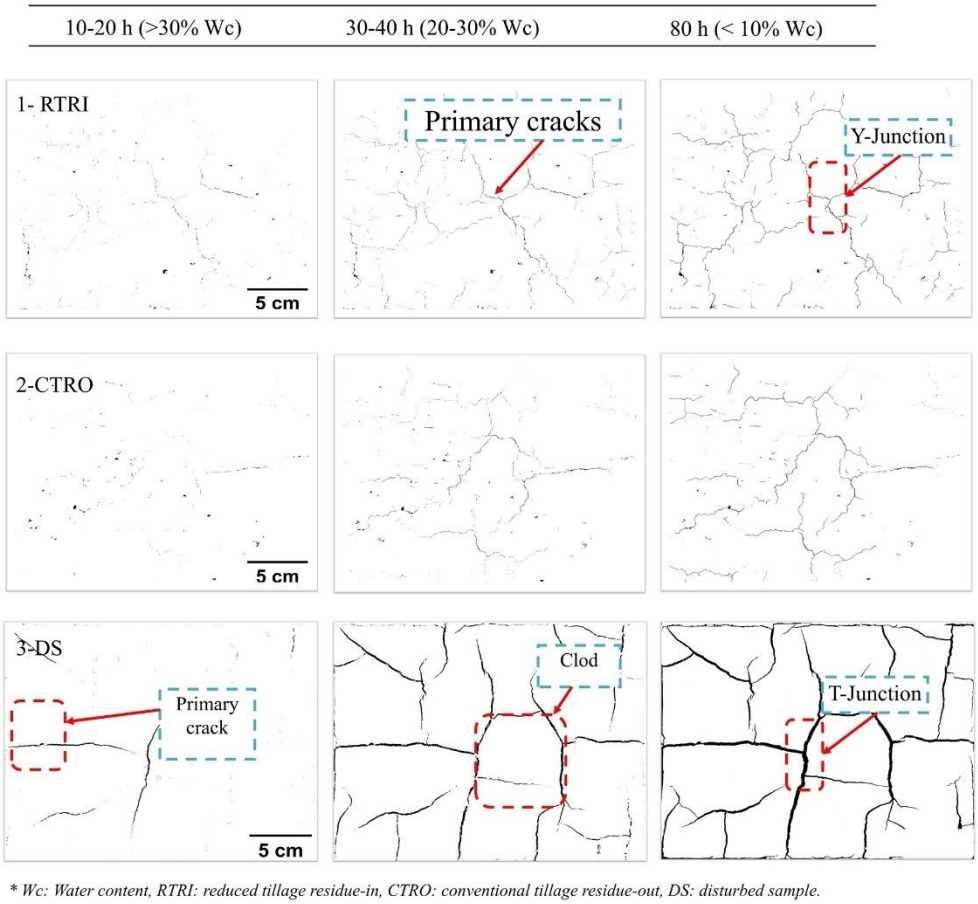

** Wc: Water content, RTRI: reduced tillage residue-in, CTRO: conventional tillage residue-out, DS: disturbed sample.*

Figure 4-6 Crack development between 10-20 h after crack initiation, 30-40 h and 80 h for RTRI, CTRO and DS. Note the formation of Y-junction cracks (cracks intersect at 120°) for RTRI and CTRO while T-junction cracks (cracks intersect at 90°) and clod (looping cracks) for DS.

3.4 How does drying drive the cracking?

Figure 4-7 a presents the growth of crack length with suction. Figure 4-7 a shows a clear increase of crack length with suction up to 300 kPa for DS, and beyond the wilting point (> 1 500 kPa for NDS (undisturbed samples)), indicating a strong link between the suction (which is a driving force) and the progressive cracking. Drying of soils induces shrinkage. However, in our experiments, shrinkage is restrained on one hand by the drying gradient along the sample thickness, and on the other hand by

the basal friction (grid) installed at the base of the samples. This shrinkage restriction provokes soil cracking. In the field, the drying gradient over thickness is probably the main reason of cracking (Zhu et al., 2020). Moreover, soil heterogeneity may also contribute to cracking (Tang et al., 2008). Mechanical analysis of cracking is out of scope of this paper.

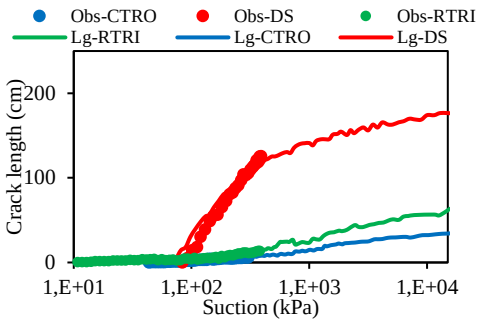

(**a**) Crack length as a function of the suction. The big dots and lines represent the observed and extrapolated data, respectively.

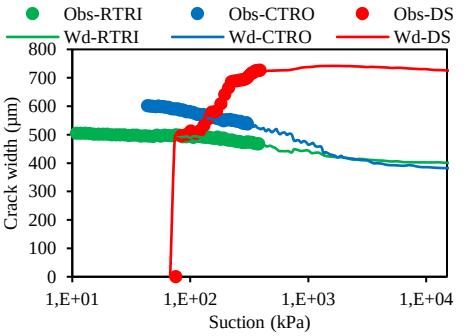

(**b**) Crack width as a function of suction. The big dots (Obs-) and line represent the observed and extrapolated data, respectively.

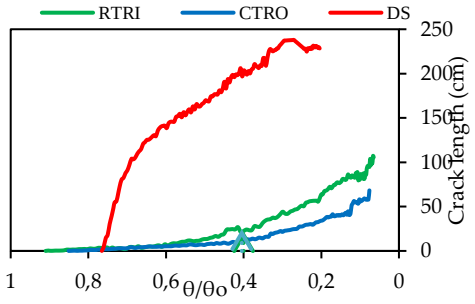

(**c**) Crack length progression with normalised water content (θ/θo) for DS and NDS. Where θ is the volumetric water content at time (t) and θo the initial water content. The arrow points the critical water content for NDS.

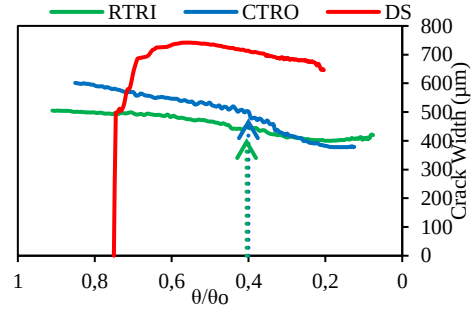

(**d**) Crack width progression with normalized water content (θ/θo) for DS and NDS. Where θ is the volumetric water content at time (t) and θo the initial water content. The arrow points the critical water content for NDS.

Figure 4-7 Progression of average crack length and width in function of water suction (expressed in kPa) and degree of saturation. The degree of saturation indicates the ratio between the water content (at time t) over the initial saturated water content. The arrow indicates the critical water content measured from the Krisher's curve (Figure 4-4 b).

Through the concepts of effective stress (Terzaghi, 1943; Bishop, 1960), an increase of suction implies an increase of tensile stress state, and so strain appear which is in fact a shrinkage. The disturbed sample is more sensitive to an increasing suction than

the non-disturbed samples (slope 4 E-2 vs slopes 3 E-3 and 2 E-3 cm.kPa^{-1}). Among the non-disturbed samples, the treatment (tillage associated with residue management) effect induces less differences. Cracks in RTRI is about 50% longer than in CTRO. Crack width (Figure 4-7 b) of structured samples (CTRO and RTRI) are not clearly evolving with suction, while it evolves monotonically for disturbed samples (DS). This may be related to the amount of fibres (straw, stubbles, roots) which were removed from DS before the experiment (Table 1). Figure 4-7 c,d shows that the crack (length and width) change with water content is comparable to the one observed with suction (Figure 4-7 a,b). It is clear from Figure 4-7 c,d that the crack formation starts to gain in amplitude when the NDS reach their critical water content. The critical water content is about 20 % for undisturbed sample (NDS) (Appendix A). This implies that the Wcrit (critical water content) is also critical for crack propagation.

3.5 How could cracks modify the water transfer?

3.5.1 Porosimetry curve related to sample structure and its change with cracking

Figure 4-8 a shows porosimetric curves for all samples tested. These curves are obtained based on the tensiometers measurements (until 400-500 kPa) and on the average of water content (based on sample weighting). Based on this methodology, the knowledge of pore distribution above 3 µm is much stronger than for pores lower than 3 µm. This limit refers to the cavitation of the tensiometers. Below this pore size, we rely on extrapolation of the SWRC.

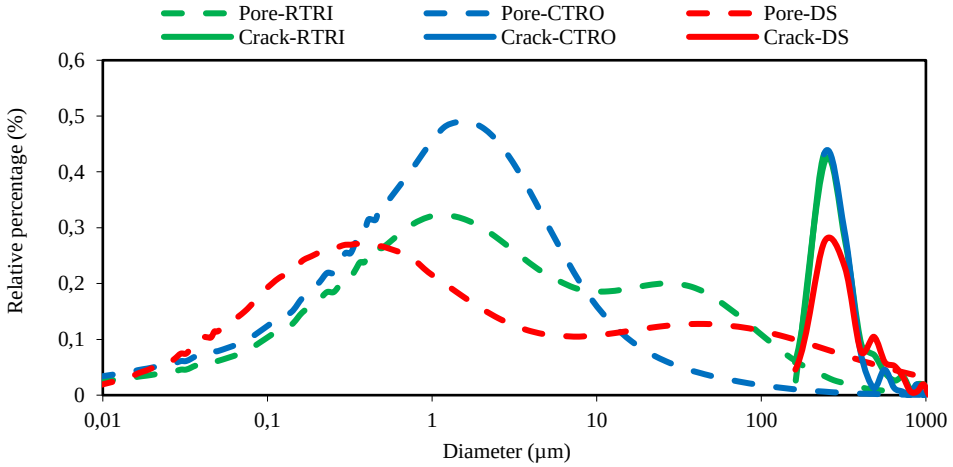

** Crack-RTRI/CTRO/DS: distribution of crack width in RTRI/CTRO/DS, Pore-RTRI/CTRO/DS: distribution of pores from SWRC in RTRI/CTRO/DS. RTRI: reduced tillage residue-in, CTRO: conventional tillage residue-out, DS: disturbed sample.*

(a) Pore size distribution obtained from mono/bimodal fitting curve and relative frequency of crack width distribution for undisturbed (NDS) and disturbed (DS) samples. The x-axis is set in logarithmic scale

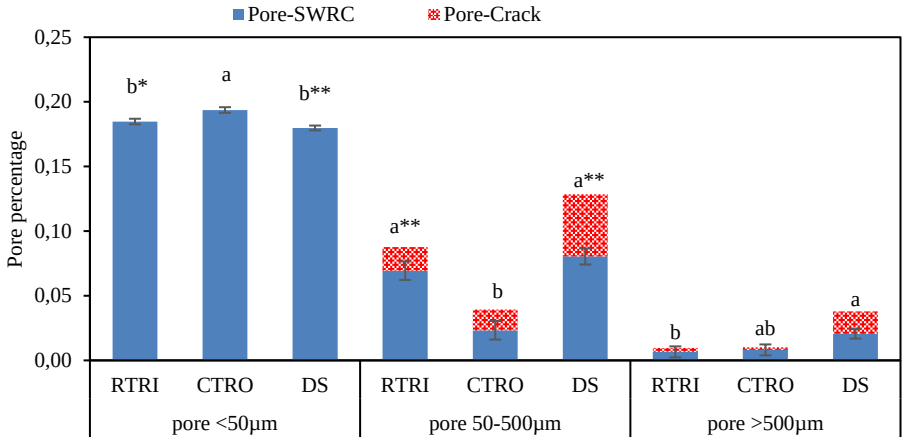

**Pore-SWRC: pore obtained from the SWRC (real data), Pore-Crack: pore obtained from the crack width distribution (at full expansion around 80h after crack initiation), RTRI: reduced tillage residue-in, CTRO: conventional tillage residue-out, DS: disturbed sample. a,b,c: significance difference at 5% error (* p>0.01, ** p< 0.01), RTRI: reduced tillage residue-in, CTRO: conventional tillage residue-out, DS: disturbed sample.*

(**b**) Histogram comparing pore percentage distributed in three pore classes between treatments (RTRI, CTRO and DS). The histogram painted in blue indicates pores obtained (from SWRC) from real observation data limited at 400 – 500 kPa. The graph (in blue) showed the standard error and the significance difference at 5% statistical error. Note that the percentage of pore below 50 µm is divided by 5 for better observation of the data. The red histogram shows the pores added from cracking. It was classified based on final crack width distribution (i.e., at 80 h after crack initiation). It is noted that the total percentage of crack is around 3 % for DS and 0.9 % for RTRI and CTRO.

Figure 4-8 Comparison between a) pore size distribution (PSD) taken from SWRC and crack width frequency distribution obtained from image analysis and b) pore percentage distributed in three pore classes. Note the bimodality (two pics) of the curves from RTRI and DS while monomodal (one pic) curve for CTRO. Note also the significant pore percentage between 50-500µm for DS and RTRI.

Figure 4-8 a show only one pore family for CTRO samples with a peak at 3 µm diameter. RTRI samples show 2 pores families, the most frequent one around 3 µm, the second around 30µm. In disturbed samples DS, the 1st pores family has a lower radius around 0.5 µm, while the second family has a larger and more dispersed radius around 50 µm. The preceding analysis doesn't consider the cracks. Crack width in CTRO and RTRI vary slightly between 200 and 600 µm (Figure 4-7 d). They create a kind of 3rd pores family, one order larger, but with a different shape. This family appears relatively late in RTRI and CTRO samples and doesn't interact with the

tensiometers which have cavitated at that time. Cracks in DS have about the same width but appear earlier.

3.5.2 Water transfer during crack formation and its impact on SWRC

During the 1st evaporation period, the samples remain saturated and permeability concerns primarily the larger and saturated pores (Hubert et al., 2018b). The CRP (Constant Rate Period from Krisher's curve in Figure 4-4 b) is upheld as long as there are liquid connections between the drying front and the evaporating surface (Yiotis et al., 2006). The length of the plateau and the magnitude of the evaporation depends on the macropores. Cracks are not present at that time. RTRI presents a longer plateau (it ends at $\theta/\theta o = 40$ %) than CTRO (it ends at $\theta/\theta o = 50$ %) (Figure 4-4 b). This is logical if one considers the porosimetry curve: RTRI has a significant family of pores around 30 microns, which doesn't appear for CTRO samples. As permeability is mostly driven by the larger pores, the RTRI permeability should then be larger than the CTRO one (Figure 4-8 a,b). Interestingly, only about 20 % of crack length has developed at the plateau end for each tillage case (Figure 4-4 b; Figure 4-7 c). So, cracks should not disturb much this 1st phase.

Disturbed samples (DS) don't show any clear plateau. The evaporation rate is lower from the experiment beginning. Following, it could be considered that the initial permeability is lower. This is supported by the pore size distribution (Figure 4-8 a,b) which indicates that DS presents fewer large pores than CTRO and RTRI. Low permeability induces short hydraulic connection layer making difficult to extract water from the soil (Hubert et al., 2018b). While cracks develop earlier and much intensively in DS, this should not increase significantly its permeability during the first half of the tests. If permeability is significantly enhanced by cracking, it will not appear clearly during a drying test, because the increase arrives too late. However, it could possibly much affect a wetting phase following a drying one.

During the second period of evaporation (Figure 4-4 a,b) known as the Falling Rate Period (FRP), crack appears (crack initiates for DS) and develops faster (for all samples) (Figure 4-7 c). This period starts when the evaporation curve decreases. The film of water linking the surface and the sample is interrupted. During this period, the surface is no longer saturated and the wetting front (layer of saturated moisture) sinks deep inside the sample. The drying of the soil decreases its overall permeability. Moreover, the evaporation is mainly coming from vapour rather than liquid transport inside the soil (Hubert et al., 2018b). The water transfer becomes more and more difficult explaining the abrupt drop of the evaporation curve. This creates dry surface and induces crack formation (Figure 4-7 c,d). We observe from the result that the evaporation curve dropped faster (stepper slope) on undisturbed sample (NDS) than DS.

During this drying experiment, the soil water retention curve (SWRC) of all the samples has evolved with the soil structure due to crack formation. It is added evidence of the importance of structure dynamic in soil hydrodynamic behaviour. Figure 4-8 a,b and Figure 4-9 a,b present the SWRC for all treatment associated with crack formation.

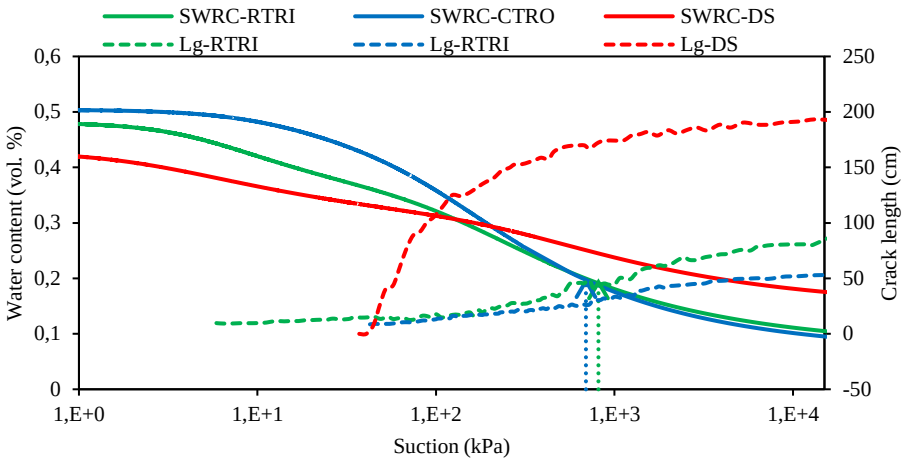

** SWRC-RTRI/CTRO/DS: Soil water retention curve for RTRI/CTRO/DS, Lg-RTRI/CTRO/DS: crack length for RTRI/CTRO/DS. RTRI: reduced tillage residue-in, CTRO: conventional tillage residue-out, DS: disturbed sample.*

(**a**) Observation of crack length propagation inside the soil water retention curve (SWRC). The arrows indicate the suction corresponding to the critical water content for undisturbed samples. Note the earlier crack initiation for RTRI compared to CTRO and DS. Note also the fast crack increase for DS in short suction interval.

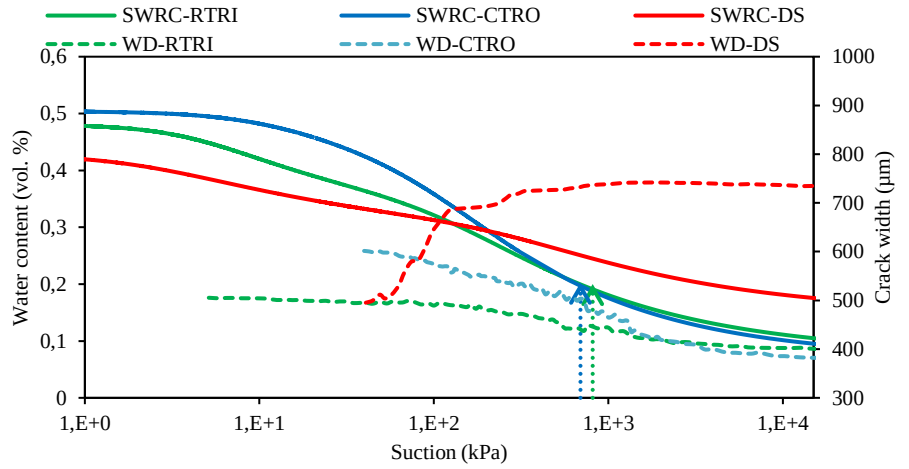

** SWRC-RTRI/CTRO/DS: Soil water retention curve for RTRI/CTRO/DS, Wd-RTRI/CTRO/DS: crack width for RTRI/CTRO/DS. RTRI: reduced tillage residue-in, CTRO: conventional tillage residue-out, DS: disturbed sample.*

(**b**) Observation of crack width propagation inside the soil water retention curve (SWRC). The arrows indicate the suction corresponding to the critical water content for undisturbed samples. Note the earlier crack initiation for RTRI compared to CTRO and DS. Note also the fast crack increase for DS in short suction interval.

Figure 4-9 Graph showing the crack initiation and development in the SWRC for disturbed and undisturbed sample. Note the early crack initiation in RTRI and the fast rise of cracks in DS. The arrow indicates the critical water for the NDS.

We observed that cracks initiate when the water content decreases significantly during a drying process. Until then, the SWRC are not influenced by the cracking. However, at the drying end, crack have appeared and the SWRC are influenced by cracks, for the low suction range. Cracks arrive at lower suction for RTRI (~7 kPa in the SWRC) compared to CTRO and DS. However, despite the fact that cracks come late in the SWRC (~50 kPa) for DS, they (cracks) attained large size quicker (0-152 cm from 50 - 300 kPa) than NDS. In the contrary, for CTRO, cracks start at higher suction (> 10 kPa) and remain very low at strong suction (< 50 cm length until 1000 kPa). Therefore, this treatment (CTRO) could not influence its retention curve (SWRC).

Figure 4-8 b shows the increase of pores due to cracking (value taken at the end of the experiment). The results show that crack affects strongly pores between 50 µm-500 µm followed by pores > 500 µm. Pores additional in DS is more important compared to NDS (RTRI and CTRO). Between pore 50-500 µm, crack raises the pore percentage by 20 % in RTRI, 40 % in CTRO and 37 % in DS. Concerning pores > 500 µm, we notice an increase of 30 % in RTRI, 20% in CTRO and more than 45% in DS. Therefore, during wetting of a dry sample, cracks should probably modify the hydration process.

Conclusions

Cracks formation during soil desiccation appears to be strongly linked to the soil structure (that is highly affected by remolding for disturbed samples (DS)), and to a lesser extent, to the agricultural management system. We assume that the difference between disturbed and undisturbed reside on their structural characteristics despite no specific soil structural analysis in this study. Using disturbed and undisturbed soil samples, we observed that:

1) The crack initiation and development are driven differently (among treatment) by the water suction. Crack initiation required stronger negative suction and lower water content in DS compared to NDS. Concerning the undisturbed samples, crack started at slightly weaker (lower) suction (< 100 kPa) in RTRI than in CTRO.

2) For the undisturbed samples (NDS), the soil structure was assumed to restrict further expansion during stronger suction. DS could swell and shrink greatly producing thicker and longer cracks. This could be triggered by the lack of sample structure and removal of frictional elements (sand, roots, fibre). Crack expands faster

(in NDS) when the critical water content was reached and the evaporation starts to drop (end of constant evaporation rate period: CRP).

3) Soil water permeability is commonly related to soil pore size distribution. RTRI and DS contained significantly higher macropore (> 50 µm) than CTRO. The rate and the duration of CRP (in RTRI compared to CTRO) was related to large pores (> 50µm) and possible earlier forming cracks (at < 100 kPa). This explained the lower evaporation rate in DS despite its high cracking length.

4) Crack seems not affecting the SWRC during the first drying since they arrive late (>100 kPa) in the curve (for CTRO and DS). However, the shrinkage observed bring structural changed inside the sample even at lower suction. After the first drying, cracks changed the pore size distribution of the sample. Surely, this should affect the subsequent wettings and dryings.

The output of this study revealed that soil disturbance (DS) changed the soil cracking pattern while decreasing the rate of evaporation and probably reducing the soil permeability. Therefore, care should be taken when analysing cracks through remoulded samples. Moreover, despite the small difference among undisturbed samples, RTRI presented slightly higher cracks, higher evaporation and higher macropores than CTRO. Further study should include other agricultural practices (for example use of biochar or sticking mucilage, etc.) under laboratory and/or field conditions.

What is important from the article and how this is important for the study's objective?

This chapter is one of the crucial parts of the thesis which responds huge portions of the study's objective. This chapter includes information concerning cracks and their interaction with soil hydrology. However, the methodology is not highly detailed; therefore, chapter 2 was added to bring missing information as far as the technical details are concerned. Questions concerning the methodology that used to assess crack formation on Luvisol is also detailed. Therefore, the experiment can be easily reproduced based on the information from those two chapters.

The output of this study revealed critical points not only for this chapter (and the thesis) but also for the coming chapter 6. First of all, it has been observed that crack progression is highly influenced by the soil disturbance and by the soil structure. This responds partly to the question about the effect of the soil agricultural practices (tillage and disturbance) on cracks. The second important information, is the interacting effect between cracks and soil hydraulic properties. On one hand, crack formation is influenced by the soil water content, the change in soil suction, and the rate of water evaporation. On the other hand, it proves also that any method that manages to control soil water content or evaporation could avoid crack formation. Moreover, the porosity created during the crack formation/expansion affects the overall porosity (especially macropore > 50µm) of the soil and likely the SWRC. This SWRC is an important indicator in agronomy since it gives the soil water content at field capacity, wilting point, and the water available for crops.

The results show as well that cracks can be a very important issue if water (or rainfall) is scarce or highly fluctuating in some area. This is because cracking soils will further deplete the soil water storage in shorter period. This brings the importance of the coming chapter (Chapter 6) which tries to find a sustainable (organic) alternative to deal with cracks. However, as explained above, since this chapter is highly compressed and compiled, Chapter 5 has been added to fill some missing information.

In summary, this chapter 4 is very crucial for the thesis because all other chapters are trying to whether prepare for this chapter (for example Chapter 1, 3, 4 and 5), or solve some issues (in Chapter 6 and 7) that are exposed from this chapter.

Finally, since there is no possible change concerning this article; some of the questions addressed for this article is briefly answered in this paragraph. For instance, the preceding crop is mentioned in page 66 because it may have some effect on the cracking result. We did not use the porosimetry analysis (in the methodology) because the porosimeter only use small size which could ignore cracks and other pores.

CHAPTER 5

Complementary discussion to the manuscript in chapter 4

1. Image analysis and processing are keys for crack analysis

Chapter 4 of this dissertation discusses the main process of image treatment and analysis and the quality of the study output. The quality of the output data confirms that the newly improved methodology (ROI) is adequate and reliable as far as crack analysis is concerned. The methodology was based on assemblage of various common techniques (correction, thresholding, skeletonization, crack identification) associated with a new one (ROI). Other studies which used sophisticated machines gave almost the same range of crack magnitude. The data output gives accurate data trends with very small variation (error). The advantage of the new methodology could be explained by the focus of the analysis within a small frame of delimited probabilistic area. The analysis is therefore simplified since the majority of the background (along with its noises) is removed by the process. The pixels distinction (classification) through image segmentation and thresholding could be performed accurately. Therefore, the noise reduction permits improving the overall crack determination together with its characteristics (length, width, area etc). However, we observed from the analysis that noises are still present and difficult to remove 2-3 h after crack initiation (especially for the undisturbed samples) due to the fact that the background remains important compared to the cracks. This observation highlights some important parameters (conditions) which need to be considered to efficiently apply this new methodology: the rate of crack formation, crack final size, the chosen size of the ROI and also the moment during which the methodology is applied. For example, fast growing cracks (as DS) could be easily extractible (discernible) from digital images starting from their initiation compared to thin slow forming cracks. Therefore, thin forming cracks requires adjustment of the chosen ROI especially at the onset of crack formation since crack ratio is too small (at that period) compared to the background. The size of the sample and the required accuracy should also be taken into account.

2. Challenge in cracks analysis

Until now, quantifying crack development from its initiation to its maximum spread seemed difficult due to crack complexity (shape, size, not straight, no parallel boundaries, many looping branches). It is still hard to measure some visible fine cracks (< 0,2 mm) because they are often removed during the process of segmentation (Figure 5-1). Those finer cracks were commonly observed in undisturbed soil (RTRI and CTRO) but existed as well in DS. This could reduce the crack length estimation but also underestimate the number/size of clods (looping cracks) (Figure 4-6). The recent image processing/analysis techniques do not address some challenges such as the background noise found on undisturbed soil (RTRI, CTRO) (Figure 2- 8b). Therefore, the method applied on intact agricultural soil required advanced image processing technique. This study proposed a method (crack delimitation with ROI) to overcome that limitation in which the processing analysis was studied case per case. Difficulty occurred also when the soil was completely dry because there was no more

distinction in colour between the cracks and the background. Tang *et al.* (2012) reported this issue in their research. The current study addressed this problem by using a ring-light-bulb which created a shadow along opening (cracks). The image analysis was performed automatically with the PCAS and ImageJ packages.

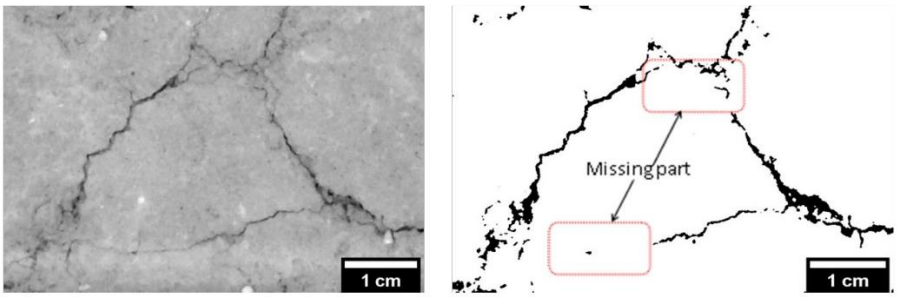

(a) Crack in grey image (RTRI-3) (b) Binary image with missing section

Figure 5-1 Figure representing on the left, (a) a grey image of looping cracks (clod) (crack); on the right, (b) a binary image showing omitted part of the cracks after image processing.

3. Parameters for crack identification

3.1 Parameters for crack identification

Many crack parameters have been investigated by various authors to describe the complexity of crack configuration. Crack description starts from basic interpretation of observable features such as length, width, depth. Determining the crack width is still problematic since it is variable along the length (i.e., no constant width). Previous studies took the average value from many sections manually. The use of digital images permit measuring crack width based (on average value from) on the maximum thickness of fractal image (Feret diameter). More complex features (crack probability etc) could be recorded nowadays due to the advance of computer programming; however, this study collected the simplest form of crack to conduct the experiment (area, length and width). The chosen parameters are enough to show vivid difference between the considered treatment. For instance, the undisturbed samples (NDS) are found presenting shorter and thinner cracks compared to DS.

We collected other parameters used in many literatures and correlate them with the one considered in this study. Table 5-1 presents the correlation coefficient (or the R^2 value) between crack parameters. Based on the result from the correlation matrix, there is strong positive relationship ($R^2 > 70$ %) between the crack intensity factor and area, perimeter, length, and width. The area and perimeters are highly correlated with length and width ($R^2 > 94\%$). It indicates that both length and width increase simultaneously during the drying experiment. The result shows further that the crack perimeter and length increase with decreasing form factor. It suggests that during the process of crack formation and development, cracks become more and more elliptical.

Finally, only form factor has high relationship with the fractal dimension. Similarly, Liu *et al*. (2011) stated that among crack geometric parameters, fractal dimension was used to describe the variation of form factor. Lot of research is interested in fractal dimension. This is because of this parameter provides a mathematical framework to quantify the irregular shapes of cracks found in nature, such as soil crack patterns (Baer et al., 2009). Fractal dimension was also used in models to characterize solute transport (Rieu and Sposito, 1991). Recently, researchers found that fractal dimension can be important for investigating soil hydraulic properties (Lakshmikantha et al. (2009). Therefore, part of this discussion (section) is reporting part of the study which investigates (in the next section) the possible correlation between fractal dimension and soil hydraulic properties. (Lakshmikantha et al., 2018).

Table 5-1 Correlation matrix of cracks parameters

Variables	CIF	Area	Perimeter	Length	Width	Fractal dim.	Form factor
CIF	***1.00***	**0.77**	**0.77**	**0.74**	**0.72**	0.49	-0.44
Area	**0.77**	***1.00***	**0.97**	**0.95**	**0.94**	0.38	-0.55
Perimeter	**0.77**	**0.97**	***1.00***	**0.99**	**0.93**	0.47	**-0.70**
Length	**0.74**	**0.95**	**0.99**	***1.00***	**0.90**	0.48	**-0.74**
Width	**0.72**	**0.94**	**0.93**	**0.90**	***1.00***	0.23	-0.46
Fractal dim.	0.49	0.38	0.47	0.48	0.23	***1.00***	**-0.64**
Form factor	-0.44	-0.55	**-0.70**	**-0.74**	-0.46	**-0.64**	***1.00***

3.2 Fractal dimension

Fractal dimension is one of the parameters which is studied just after the conventional parameters (length, width, area, etc). Since cracks are in the form of lines, curves, zigzag etc their value oscillates around 1 dimension (a straight line) and rarely 2 when the lines fill a full area (e.g., circle, triangle, rectangle) (cf. appendix: Fractal dimension). For instance, Figure 5-2a compares the fractal dimension (Fd) between RTRI, CTRO and DS. It is worth to note that the Fd value was calculated from the average of 3 to 4 samples in RTRI, CTRO and DS. The highest fractal dimension is observed in DS followed by RTRI and CTRO. The Fd starts (Period A) from 1.0, 1.1 and 1.3 for CTRO, RTRI and DS, respectively. The fractal dimension is almost stagnant throughout the experiment for DS except the first 2 h during which increasing Fd is observed. This period corresponds to the increase of water suction. This is obvious since crack development along with its structural complexity are also increasing with water suction.

The water suction increases therefore with fractal dimension for both DS and undisturbed samples despite the weak correlation coefficient as given in Table 5-1. Fd is fairly higher than that of undisturbed samples during all periods (Figure 5-2a). The Fd attains 1.29, 1.27 and 1.34 for RTRI, CTRO and DS, respectively (Figure 5-2 a). Lomeling et al. (2016) found that Fd value of 1.0 during the beginning of the

experiment indicated the homogeneity (linear) of crack pattern compared to a value of 2.0 which described more heterogeneous (complex pattern) cracks, especially after cracks were widening. Therefore, the increase of Fd during the experiment shows that cracks gradually become heterogeneous (complex) with time except for DS which portrays cracks with similar pattern.

The conventional tillage and reduced tillage present closely similar Fd. For those treatment, the curve of Fd presents two distinct periods which corresponds inversely to the progress of water content curve (Figure 5-2b). The highest crack development in NDS coincided with the highest Fd. The output of this study stress the close relationship between fractal dimension and soil water properties as also reported by other authors Tang et al. (2008) and Lakshmikantha et al. (2009). However, concerning the water evaporation and fractal dimension, the correlation is not very strong especially for DS (Figure 5-2c). Fractal dimension increases linearly with time during the stage 1 and 2/3rd of stage 2 of evaporation. The maximum Fd is achieved 10h prior the minimum evaporation (stage 3).

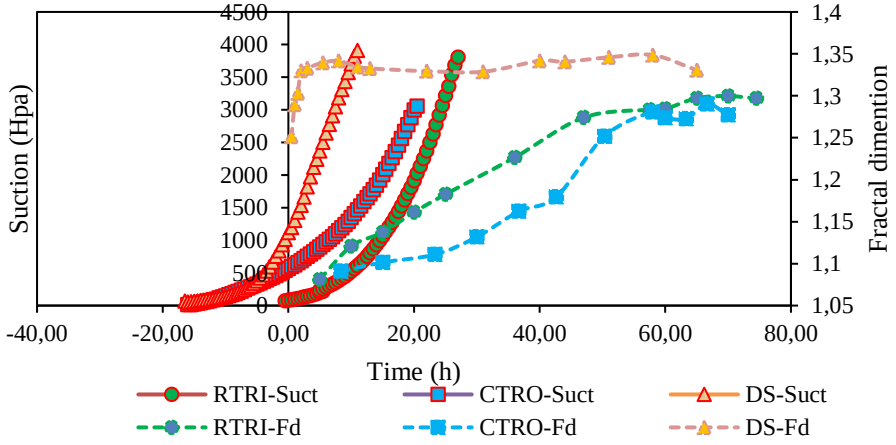

(a) Fractal dimension and water suction with time

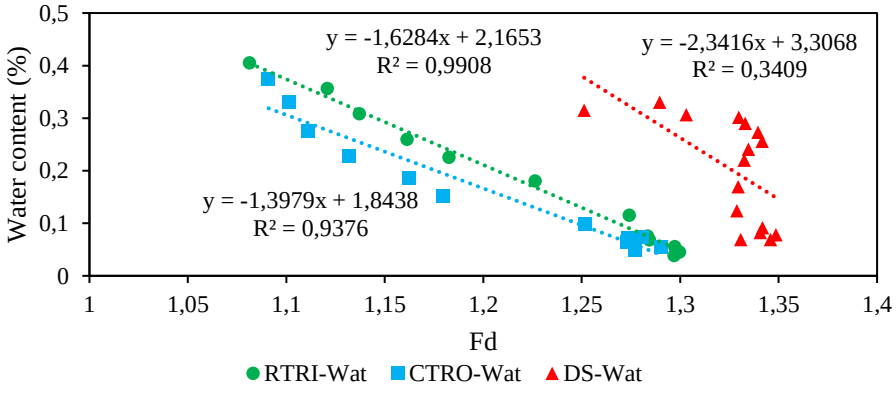

(b) Correlation between fractal dimension and water content

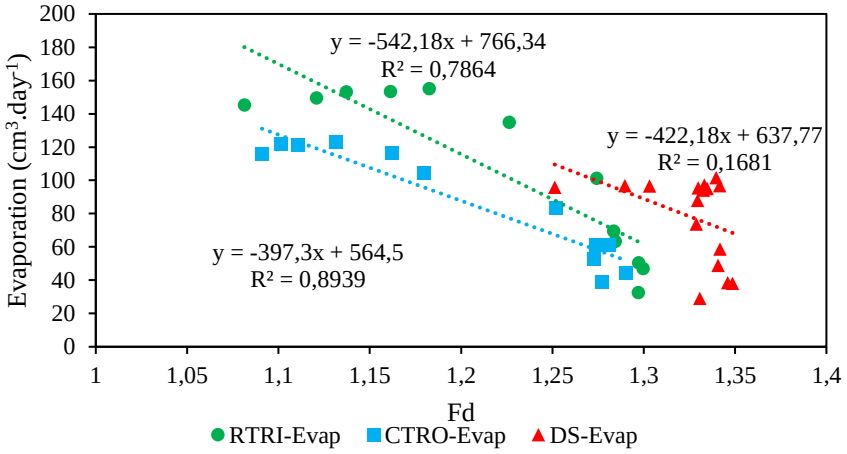

(c) Correlation between fractal dimension and water evaporation

Figure 5-2 Evolution of fractal dimension along with water suction, water content and soil water evaporation

3.3 Alternative to crack description using Nedler's logistic curve (1961)

Cracks initiation and progression can be described from their geometrical characteristics (as in the previous sections) but also from the characteristics (trend) of the cracking curves. The geometrical characteristics (length, width, area etc) have their own advantages such as accurate information about the cracks at time t or their evolution. The problem occurs when researcher tries to compare different curves of different shape and characteristics. For instance, in this study it is hard to make a comparison between treatments since the magnitude of the cracks change significantly in time. This is the reason why we have to dissect the curve in three parts (3 periods A, B and C) and the comparison was made within each period. This is the main advantage of describing the curve based on its shape and fitted with a known model (with parameters). For instance, the shape of the cracking curve shows an S-like trend which can be fitted with the Nedler's logistic curve (1961). This logistic curve is widely used to depict the crack expansion in function of the soil shrinkage and bulk density. However, in this study, it is chosen to fit the curve of crack development (CIF) with time which is in the shape of S or sigmoid format (Figure 5-3). The equation helps to determine and define each step and periods during crack expansion: a first stage A of low crack development followed by a second stage B of fast-growing crack area and a third stage C of almost no increase of crack. Details about the data is shown in Figure 5-3 and Figure 5-4. The logistic curve is able to illustrate the three stages found on undisturbed sample (RTRI and CTRO) and the two stages for the disturbed one (Figure 5-4). Due to high variation of the crack intensity factor represented by the parameter *(b)*, the standard error is very high, resulting in a non-significance difference (in terms of CIF) among treatment. The logistic curve is also

able to depict the slight difference in terms of the slope of the curve using the parameter *(c)* (Figure 5-4). According to the value of *(c)*, the logistic curve predicts that the disturbed sample attains its maximum crack size in very short time compared to conventional and reduced tillage. Based on the information collected from Table 5-2 ; the Root Mean Square Error (RMSE) of the fitting curve (compared to the crack progression) is quite low for almost all samples (~0.01). This indicates the performance of the predicting curve (Zhu et al., 2020). Therefore, this fitting curve can be used to predict the trend of a cracking curve but also to compare statistically each curve based on the parameters of the fitting curve.

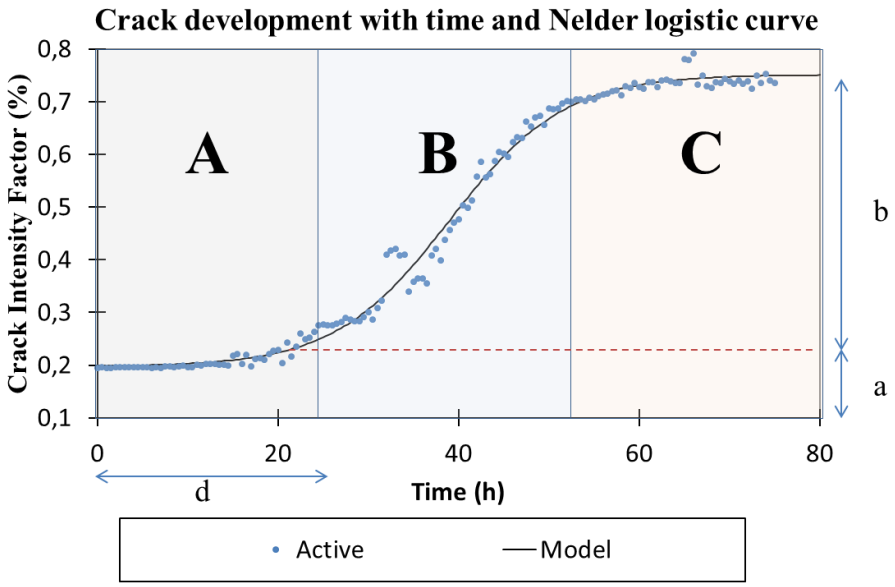

Figure 5-3 Crack development curve explained with Nelder logistic curve parameters (case of reduced tillage RTRI-1). The red line indicates the limit of the parameter (b) which describes the crack development during phase B and C. The parameter (a) shows the amplitude of cracks during the first phase A. Parameter (d) shows the extent of period A.

The equation of the Nelder logistic curve was written as follow:

$$K = a + \frac{b}{1+e^{-c(t-d)}} \quad (1)$$

Where: k: CIF, a: intercept, b:graph amplitude, c:inverse of slope, t: time, and d:extent before crack starts

Table 5- 2 Model performance parameters for each treatment

Treatment	DF*	R^2	RMSE
RTRI-1	154	0,98	0,030
RTRI -2	146	0,99	0,020
RTRI -3	140	0,99	0,015
CTRO -1	131	0,99	0,011
CTRO -2	149	0,99	0,016
CTRO -3	131	0,95	0,012
DS -1	132	0,95	0,210
DS -2	159	0,97	0,153
DS -3	139	0,96	0,144

**DF: degree of freedom, R^2: coefficient of determination, RMSE: root mean square error*

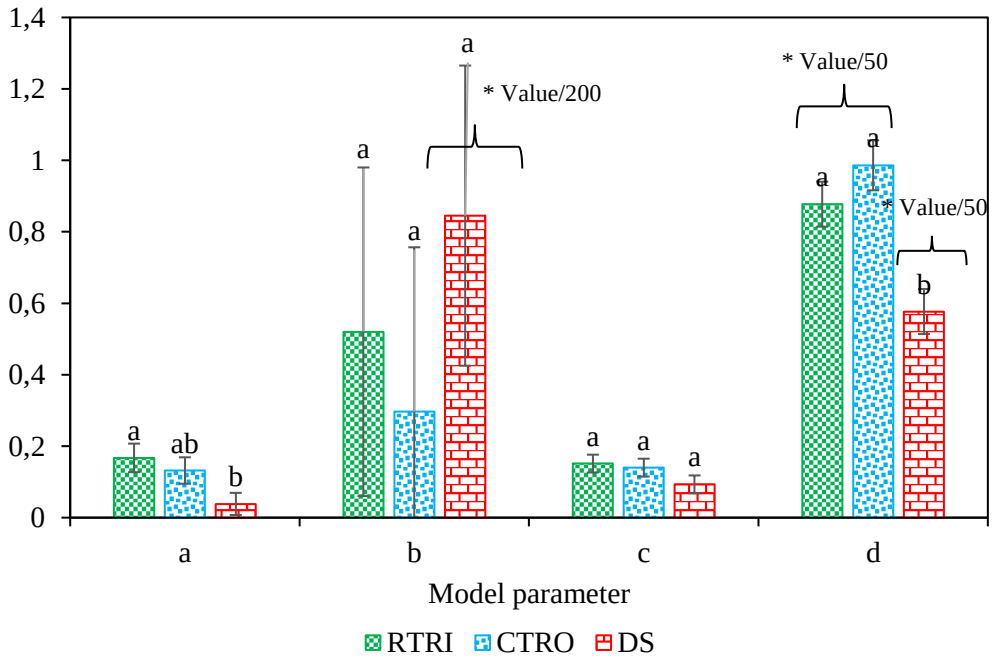

** Value/x means that the original value was divided by number x in order to fit to the graph*

Figure 5-4 Nelder's logistic curve parameters describing crack evolution with time

4. Mechanism of crack initiation and propagation

The new methodology allows to make vivid evidence of great distinction between disturbed and undisturbed samples; and also, between RTRI and CTRO. It was seen during crack initiation and also during crack progression.

4.1 Crack initiation

The crack initiation is highly associated with the water content and water suction. To initiate cracks, DS required very strong negative water potential (-800 hPa) and low water content (30 %) compared to the undisturbed sample CTRO (-500 hPa; 40 % WC) and RTRI (-70 hPa; 45 % Wc) (Figure 5-5). In this study, we consider two types of undisturbed samples (CTRO, RTRI) and disturbed samples (DS) which shared almost the same mineralogical composition. However, they undergone different treatment; therefore, they should present (probably) different characteristics especially in terms of structural pattern. It can be ascribed to soil porosity, soil aggregation and the presence of cracks (and/or micro-cracks) in the soil making the opening very easy at low pressure (Naveed et al., 2018; Zhu et al., 2020). The pre-opening could be the result of wet-drying cycle or other physical and biological activities. Certainly, presence of micro-crack in soil accelerated crack formation and increased the magnitude of crack in soil (Kumar and Arora (2015). The study shows therefore that crack initiation is not only intricately linked with water content and suction, according to the theory of Tang *et al.* (2008); but also, with the soil characteristics (structure, porosity, fibre, etc) (Cf. Chapter 4).

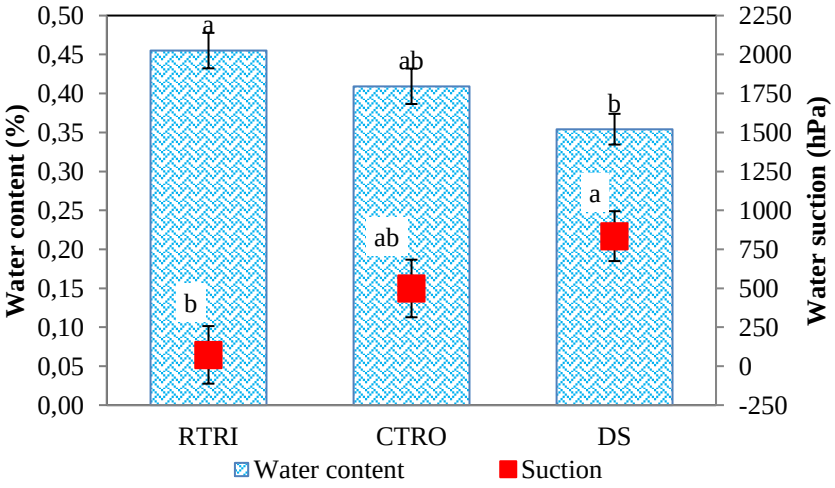

Figure 5-5 Water content and soil water suction during crack initiation

4.2 Where do cracks initiate?

Concerning the location of crack initiation, huge distinction has been detected between disturbed and undisturbed sample. The disturbed samples (DS) are highly affected by the form of the frictional-grid at the base of the samples. For instance, for the case of DS with rectangle grid, cracks start from the edge and almost from the middle-edge of rectangle box. Other studies are slightly in line with this finding such as the observation of Vo *et al.* (2017) who reported that the weak area (where crack starts) is located in the centre of clod or away from the primary crack. It is however important to stipulate that this type of crack is widely reported in geotechnical or engineering study who deals with disturbed samples or moulded specimen (bentonite, pure clay etc) (Nahlawi & Kodikara, 2006, Tang *et al.*, 2011). The reason for this is due to concentration of the stress on a specific area of the surface (which can also be the weak area) as reported by Zeng et al. (2019). In the contrary, DS with diamond grid presents random position of crack initiation which mainly occurs arbitrarily inside the box. This stipulates a well distribution of the weak areas (points) and probably the shrinkage stress. For undisturbed samples, crack initiates almost randomly for RTRI and more or less axial for CTRO.

Crack initiation along vertical section remains a real debate amongst researchers. Further observation from this study reveals that cracks are clearly observed at the base of the samples (all samples) but in smaller size and shorter in length (Figure 5-6a,b). This indicates that crack starts from the sample surface and develops toward the bottom. Therefore, it is evident from the results that for disturbed samples, only the grid come against the shrinkage. During the pre- test (Figure 2- 13), we could observe that at a certain size and thickness (10 x 14 x 4 cm) there is no crack formation on disturbed samples. In the opposite, for NDS, the frictional-grid affects the process of shrinkage together with the soil structure. Therefore, crack initiates randomly at the sample surface (which dries first). The crack initiation is random due to small soil structure difference at laboratory scale including small difference in: density, pore, aggregates, micro-cracks etc. All these results emphasize the importance role of soil structure as mentioned above and also the possible contribution of fibre in the samples.

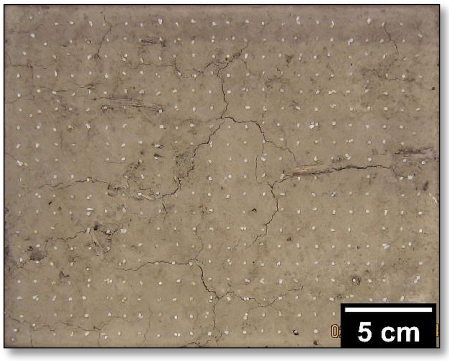

a)-Cracks from sample surface (CTRO)

b)-Cracks appearance at the bottom of the sample

c)-Cracks from disturbed sample-1

d)-Cracks from disturbed sample-2

Figure 5-6 Illustration of crack distribution at the sample surface and at the bottom.

4.3 Crack propagation

The propagation of cracks is also very different between disturbed and undisturbed samples. The overall results evoke a slow initial crack propagation for undisturbed sample (RTRI, CTRO) until it reaches a threshold where it expands abruptly in length, width, and area (CIF). The slow crack propagation could be related to the presence of closed micro-cracks (due to re-wetting) which could be opened easily at low suction as elaborated before. However, the crack propagation remains slow (stagnant) for a while probably as a results of soil structural limitation specifically, due to aggregate stability, soil arrangement (due to fauna and flora, microbiological activity, and mechanical action), different physical/chemical bounds (cutans, fibre, clay-humus, H-bound, ionic/covalent bounds, etc) (Bronick and Lal, 2004; Yost et al., 2014; Ye et al., 2020). The crack expansion waits for the time where the suction surpasses the soil structural strength. However, DS passes directly through the fast propagation period B and attains its maximum crack size in a very short time. This emphasizes the importance of soil structural strength and stability in soil cracking. For instance, DS should be homogenous (similar porosity all over the sample section) and deprived of elaborated structure. This renders an almost homogenous soil shrinkage (iso-deformation/compression shrinkage) which could not break until soil stress exceed the soil strength as mentioned by Zeng *et al.* (2019). This finding demonstrates that crack output from disturbed sample cannot be extrapolated to assess crack formation in undisturbed agricultural soil. These results expose the importance of conserving soil physical properties during research experiment. The change in soil structure even at short period as the case of CTRO has a tremendous effect on crack progression.

A part from the fact that the timing of the propagation is very short in DS compared to NDS. The cracking process continues with the formation of wide and long primary crack followed by short and narrow secondary/tertiary cracks. This study reveals that the form of the interfacial friction also affects significantly the progression of cracks. With squared-grid friction, the new forming crack tends to be perpendicular to the primary forming cracks (Tang et al., 2010).The secondary cracks forms also almost

perpendicular to the primary cracks. This could be due to maximum stress release criterion as indicated by Lachenbruch (1962) because the internal stress is released in the existing cracks, and the next crack will form perpendicular to it where the maximum tensile stress is located. Other studies of Peron *et al.* (2009) and Corte and Higashi (1960) reported a crack intersection from 90-150 °C due to the concept of energy minimization process. For diamond grid, cracks propagate in a branchy-forms. Generally, for DS, crack increases in width as well as in length starting from the crack initiation. This increase in width is important until 20 h after crack initiation. The overall results from DS demonstrate that the crack propagation is highly influenced by the form of the friction-grids especially for primary and secondary cracks.

In the contrary, for NDS, the progression of crack is almost random especially for RTRI while quite orthogonal to the primary cracks for CTRO. This shows that grid may have an effect on the crack; however, there are also other factors which play major roles on crack's expansion. We expected that well-structured samples as RTRI deviate the crack orientation from orthogonal plan (form of the grid); however, CTRO remains more or less influenced by the grid. The influence of the micro-cracks in the soil explains as well the random propagation (not in x-y direction) of crack in RTRI compared to other treatment (Figure 5-7). For instance, CTRO and DS take almost the x-direction and/or y-direction. Probably the crack distribution on the surface would have an effect on the size of crack width. For instance, despite the fact that the width of the primary cracks is not increasing very much for NDS; CTRO present slight thicker crack than RTRI. We tend to think that the more crack propagation detaches from x and y-axes (orthogonal pattern), the thinner the cracks become. This observation is also valid for DS. For instance, under squared-form friction, the forming cracks propagate toward the x-y axes; while in diamond friction, cracks propagation is non-orthogonal. Simultaneously, crack width is slightly thicker in orthogonal cracks (squared friction) than non-orthogonal cracks (diamond friction).

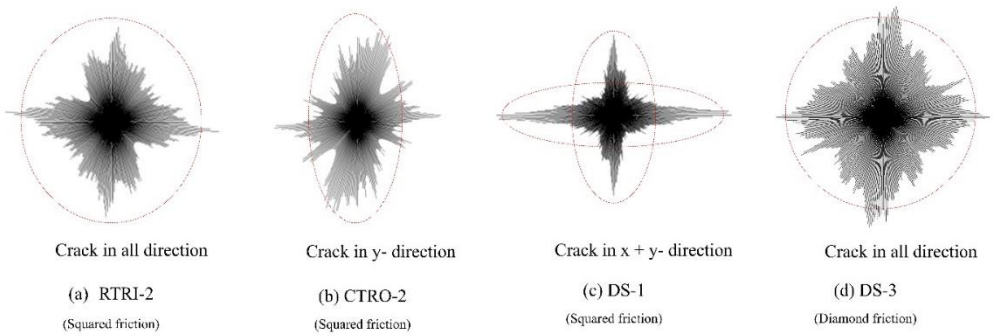

Figure 5-7 Illustration of crack direction in the samples at full crack expansion

4.4 Quantity and quality of fibres on crack formation and propagation

The output of this study shows that undisturbed samples present reduced crack formation and propagation. Despite the fact that soil structure is the main (evoked) reason for the crack restriction, it is however possible to invoke the effect of fibre embedded in soil. In agricultural soil the connection between soil and roots can be assured by the presence of many fine roots for RTRI and few big and fresh straw for CTRO. Due to the presence of those fibres, soil is less prone to shrinkage and resisted to compressive force according to Valadez-Gonzalez *et al.*, (2009) and Khattak and Alrashidi (2006). Previous study found that presence of fibres render soil stronger, more ductile, less swell/shrinkage, and has increase fracture energy of soil (Hejazi et al., 2012; Jayanthi and Singh, 2016). The presence of fibres could reinforce soil against cracks as reported by researchers such as (Alwahab and Alqedra, 1995; Harianto *et al.*, 2008). In this study by comparing sample with and without fibre, the difference is not only found on the number of cracks but also on the crack width, crack direction, the origin of cracks, crack connection and crack depth. All this indicates that fibre could restrain further crack propagation after crack initiation (Consoli et al., 2010). It is evident that the amount (size, volume) and the quality (fresh, straight, strength) of fibre is important for reducing cracks. In this study fibre account for 0.7-0.9 mg/g of the soil total weight (Chapter 3: paper 2, Table 3-1). Other researchers found that the optimum fiber content was 0.3 % in clay in order to optimise the crack (Qiang et al., 2014). Chaduvula *et al.* (2017) advocated to use of 0.5 % fiber content with 15mm length to get the maximum crack reduction on clay soil in barrier systems. Therefore, there is no doubt about the effect of fiber inclusion (in soil) on cracks. This is explained from increasing of soil tensile strength, transfer of stress, and additional bi nding of particles (Liu et al., 2020).

4.5 Effect of soil structure on crack formation

As reported in the results section of Chapter 4, soil structure plays a major role in crack formation and propagation. We observe a limited crack formation and progression in soil with conserved structure (NDS) compared to disturbed structure (DS). One of the plausible reasons for this is the structural stability during shrinkage. For instance, during drying, soil particles are dragged together due to capillary tension, forcing the soil pores to shrink. The structural arrangement and the degree of connectivity between the soil particles assure the mechanical stability of the soil despite the increasing pressure (suction). The soil shrinkage can be reflected in the cracking curve. As the shrinkage curve can be used to determine the structure of pore space according to Braudeau *et al.* (2004), Cornelis *et al.* (2006), Schäffer *et al.* (2013); therefore, the cracking curve could give also this information. We observed from the results that the slope of the cracking curve is less steep in the undisturbed sample (structural sample) compared to unstructured disturbed sample. This shows the strength of interaggregate bonds which assure the soil hydrostructural stability. Hydrostructural stability is defined as the “ability of soil to withstand internal stresses caused by decreasing water potentials during drying” (Schäffer et al., 2008). In the

contrary, disturbed sample shows steeper slopes showing the breaking of interaggregate bonds and weak hydrostructural stability.

The second reason for the structural effect on crack dynamics is the presence of different pore spaces which do not shrink at the same level. We could observe that the undisturbed sample especially RTRI presents bimodal curve of microporosity and macro-porosity. Macropores are considered as a structural porosity in some researches (Schäffer et al., 2013). Water contained in the macropores drained easily and replaced by air while the micropores remain saturated until attaining the air-entry point. This explains the sigmoidal shape (S) of structured soil as reported by Schäffer et al. (2013). This sigmoidal shape is indeed observed with undisturbed sample in this study. In the contrary, structureless soils (clay paste, slurry) break their macropore explaining the linear shrinkage (in 1:1 ratio) with water depletion until air-entry point is attained as reported by Boivin *et al.* (2006) and Mallory *et al.* (2011) . This study unveils therefore that structured soil is stable and it is less affected by shrinkage and produce limited number of cracks.

Third, the soil structural may bring differences in terms of soil density distribution within the soil samples. This difference in density creates a modification in shrinkage characteristics at aggregate level. Weak area absorbs more water but shrinks stronger (and faster) than dense (stiff) area. This explains as well the formation of cracks during soil saturation as the case of RTRI. In the contrary, the soil disturbance destroys the soil structure, rendering homogenous samples (pores and density). By consequence, all part of the sample is weak, absorbing water and shrinking faster. However, due to the structural (density) similarity in DS, there is no specific weak area to initiate cracks. Therefore, cracks only initiate when the stress (due to increasing suction) exceeds the general soil strength. This explains as well the delay (and huge size) in crack formation for DS. Along with this soil stiffness, the soil structure associated with structural distribution of roots can be an important element for limiting crack formation in NDS specifically RTRI. This comes from the fact that roots are incorporated tightly with the soil general structure (aggregates, porosity, etc). Roots makes soil less compressive (limiting swelling/shrinking) according to Valadez-Gonzalez *et al.* (2009) and Hejazi *et al.* (2012).

4.6 Effect of sample thickness interacting with other parameters on crack formation

This study chooses a thickness of 1.6 cm in order to obtain sufficient number of cracks and also to be able to insert the tensiometers into the sample during the study experiments. The correlation (or equation) between thickness and cracks proposed by Zeng et al. (2019) concludes that the horizontal tensile stress σ is inversely proportional to the sample thickness. This simple relationship seems explaining adequately the crack formation on DS since it considers the sample as homogenous. However, other factors should be associated with the soil thickness for undisturbed and heterogenous sample. For instance, we observe that at the same thickness as DS, the cracks on undisturbed soil (RTRI and CTRO) were not strong enough to split the soil surface to form clods. This indicates that the tensile stress is not sufficient to open crack. Therefore, the chosen soil thickness is (becomes) too large for impacting cracks

propagation on NDS. This suggests the use of thinner soil sample (for undisturbed soil) with thickness below 1.6 cm (used in the current experiment) in order to obtain additional cracks and clods. The results prove that soil structural stability (as in undisturbed sample and specifically for RTRI) is very important in crack formation and propagation, and this parameter should be considered in the equation relating soil thickness and cracks. As illustrated in the previous section, soil with high structural stability (as NDS) is both affected by the friction and also by the strength of the structure itself (which opposes the crack expansion). This explains the low crack formation and absence of clods in NDS.

The relation (equation) soil thickness-cracks should consider other factors such as soil density which was found reducing crack formation by researchers. For instance, the shear resistance (strength) of soil is a result of interlocking of particles and possibly cementation or bonding at particle contacts strength (Poulos, 1971). Therefore, reduction of soil porosity (or density; i.e., packing of soil particles) would reduce the soil shrinkage and affect therefore the formation of cracks. Last but not least, the presence of fibre in the agricultural soil should also be considered in the equation since fibre reinforce the soil (increase soil strength) against crack formation and development. As we observed during the experiment, NDS contain certain number of fibres constituted of fresh and slight decomposed straw, stubbles, and roots. This fibre contents could make an important distinction between disturbed and undisturbed in this study. Not only the quantity but also the fiber structure associated with the sample thickness should also play a major role in crack formation. However, the effect of fiber structure (root distribution, extension etc) cannot be assessed in thin sample. Therefore, thicker samples would give more distinction between RTRI and CTRO.

4.7 Interfacial friction and soil structure in relation to soil desiccation cracking

During the process of soil desiccation, the friction between the bottom of the sample and the base of the box comes against the soil shrinkage and provokes the crack initiation and propagation. As elaborated before, the presence of friction increases significantly the crack formation and propagation indicating that (horizontal direction) the interfacial friction plays an important role on desiccation cracking. The higher the interfacial friction, the higher the force that holds the soil particles (i.e., to resist the constrained forces). The intensity of crack propagation is therefore related to the strength of the friction (Vo et al., 2017; Zeng et al., 2019). According to Zeng et al. (2019), when the interfacial friction is high, the crack initiation time is delayed. Moreover, crack may start at a period of low soil water content and high-water suction. This scenario (effect of interfacial friction on cracks) seems corroborated with the result from the DS where the soil structure has been destroyed. We can notice from DS that the interfacial friction in squared form developed rectangular cracks while diamond friction engendered polygonal-like cracks. Concerning the intact soils, the effect of interfacial friction is highly reduced due to its soil structure as explained above (Xu et al., 2018). Moreover, the stress is evenly distributed to the soil surface.

All these conditions result to a less crack area, length, width, etc as illustrated in the previous chapter.

5. Hydraulic properties associated with soil cracking

The crack formation and expansion cannot stand alone without considering water suction, water storage and permeability. We could notice that the general process of soil desiccation includes complex interaction of water evaporation, shrinkage and soil cracking. Apparently, water evaporation at pore level tends to intensify the soil suction, increasing the stress in soil and triggering shrinkage. Overwhelming stress (i.e., surpassing the soil strength) provokes crack initiation and propagation. There is therefore great interaction between crack progression, shrinkage and soil hydraulic properties (water content, evaporation, suction,).

5.1 Soil evaporation evolution in different treatment

Theoretically, it is well known that the desiccation process is characterised by water loss from soil pores which is qualified as water (moisture) evaporation. The parameters involving in soil evaporation is still under debate among researchers. However, this study stipulates that soil under different management (tillage and residue and disturbance) presents different scenarios as far as soil evaporation is concerned. In fact, the output of the study gives some important information concerning the different phase of evaporation. The three evaporation periods are well presented in undisturbed samples while DS shows almost no constant rate period. This result is observed both from the evaporation curve and also the Krisher's curve. It is always important to notice that it could be linked to the initial water content (45-50 %).

As many authors reported that during the constant rate period (CRP) the magnitude of the evaporation rate is mainly governed by the external condition of the samples specifically the temperature and the relative humidity of the ambient. This implies that water evaporates as a result of vapor pressure difference between the ambient (air inside the experimental box) and the sample surface. However, we found that by exposing the treatment at the same condition, RTRI presents longer plateau than CTRO and almost no CRP for DS. Therefore, there should be more parameters which were not always considered in studying cracks. We noticed from literature (Hubert et al., 2018b) that the rate of evaporation is maintained as long as water network is connected to the evaporating surface. This implies that the surface layer can be no longer saturated forming a drying front. According to Hubert *et al.* (2018) this drying front, which is the interface between the saturated and partially air-filled (unsaturated) area, depends on the pore size distribution (PSD). It is obvious that the front can go deep for porous sample as the case of RTRI. However, based from the result output (in Chapter 4 Figure 4-8 b) there is no great difference between DS and RTRI in terms of PSD. We assume therefore that pores are more connected in RTRI due to soil aggregation as compared to DS. Interconnected pores allow water to move and evaporate much easier than isolated pores. This distance in which the liquid could reach the surface is called hydraulic connection layer (Hubert et al., 2018b). High

permeable sample with connected pores presents therefore longer hydraulic connection layer than its own thickness creating uniform saturation front (Lehmann et al., 2008). This makes an easy water flow through the porous system to the surface.

Therefore, based on the evaporation curve associated with the pore size distribution and connection, DS presents low permeability compared to CTRO and RTRI which affect the rate of evaporation and the length of the CRP. Therefore, soil disturbance (which can be assimilated to the state of soil after tillage) reduces the capacity of water to move freely in the soil and evaporate to the atmosphere. Reduced tillage allows water permeability due to abundance of macropores compared to conventional tillage.

5.2 Cracks formation in relation to water evaporation

Relating cracks and water evaporation is complex (Figure 5- 8). Crack initiation occurs at a certain moment of water evaporation as soil continues to dry. Locating the critical water content is important to comprehend water evaporation-cracking process (Tang et al., 2021). This is defined as the amount of soil water content at which crack initiates. This moment should fall within the three typical stages of water evaporation: (1) constant rate stage; (2) falling rate stage; and (3) residual rate stage (Tang et al., 2011b) (Figure 5- 8).

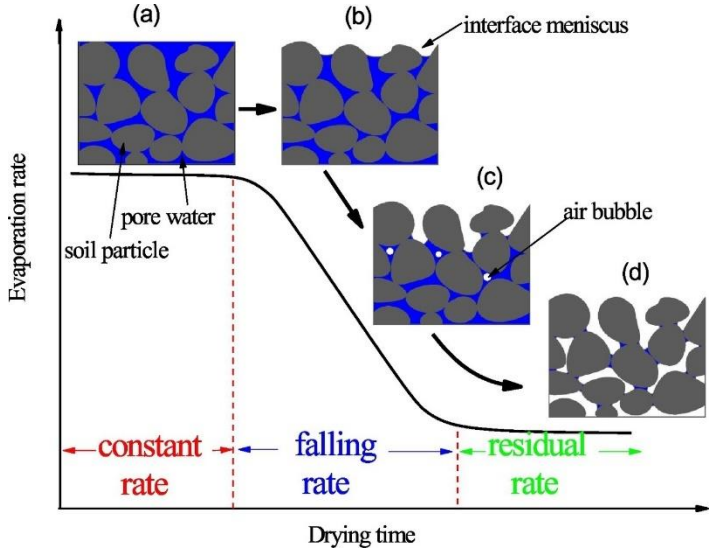

Figure 5- 8 Evolution of evaporation rate with time (Tang et al., 2021)

Researchers indicate that the critical water content at the onset of cracks vary considerably from one set of experience to another due to many parameters. This raises the possibility of variable Wcritic for different soil samples under similar environmental condition. The output of the study reveals that the critical water content is attained during the CRP during which the soil is water saturated. This period corresponds however to the moment where air enters into the soil media making the transition from saturated to unsaturated state and from constant rate period of

evaporation into falling period. Based on the study output, the Wcritic is low in DS compared to CTRO and RTRI. This indicates that Wcritic seems decreasing with increasing of soil disturbance. For information, DS is more disturbed than CTRO and RTRI. Therefore, critical water content could also be influenced by the soil physical properties (structure, pore distribution, pore structure etc). Tang *et al.* (2010) added that Wcrit is influenced by soil thickness, temperature, and contact between soil particles.

Crack progression falls during the second period of evaporation (Falling rate period). This period is very important for water evaporation since the soil surface is no longer saturated and the water transport inside the sample is in the form of gas state. This reduces significantly the water movement in soil. Therefore, the crack progression has limited effect on water evaporation form this period. This condition made the negative correlation between water evaporation and water content in this study. In fact, the crack progression is far stronger than the progression of evaporation. Moreover, the soil water content is also reducing during the desiccation, making the water evaporation more difficult. Therefore, further investigation relating cracks-evaporation should therefore fix one of the parameters such as water content. This could not be conducted during this study due to the study objective.

5.3 Desiccation cracking and soil water suction

As mentioned in other studies, the onset of cracks portrays the presence of tensile stress inside the soil which is dominated primarily by suction. What is new from this study is that suction does not have the same degree of importance in the treatment. As mentioned in Figure 5-5, DS requires strong suction followed by CTRO. In the contrary, we can spot that RTRI needs only 70 kPa to initiate cracks. We observed (in RTRI) that there was no significant change in soil volume (i.e., shrinkage) at crack initiation. This indicates that water suction is not very important for crack initiation in RTRI, however it plays major role in crack progression. No volume change emphasizes the strength and the stability of the structure.

By developing deeper, suction is very crucial for crack initiation in DS; however, its cracks propagation required less energy due its lack of soil structural, weak bondage between soil particles, and no fibres. This explains why crack develops rapidly just after the crack initiation as compared to the NDS. Most of the suction value reported in literature is in the range of the critical suction for CTRO and DS i.e. suction >100kPa (Peron et al., 2009; Tang *et al.*, 2010). This close similarity of CTRO and DS in terms of water suction requirement (for crack propagation) explains their similarity in soil structure due to disturbance and tillage.

5.4 Desiccation cracking and soil volume shrinkage

As shown in Figure 4-5 , this study displays that disturbed samples (DS) present strong volume shrinkage even before the crack initiation compared to the undisturbed samples (Figure 5-9**Erreur ! Source du renvoi introuvable.**a,b, c). This is strong evidence of an important role of soil structure and fibre removal in the crack formation. It is clear that this result is very similar to crack formation in paddling soil, verstisols, landfill liners and nuclear waste disposals where there is high soil

disturbance in clayey soil (Chen *et al.*, 2017 ;Zheng *et al.*, 2018; Kan *et al.*, 2020; Vail *et al.*, 2020). Cracking is not only driven by the quantity of clay particle (which is around 10-15% in this study) but also the type of clay in combination with the general structural pattern of the soil. The work of (Parvin et al., 2017; Smet et al., 2018) in the surrounding area (of the field of study) shows the general structure of the soil (up to micro/nano scale) and the type of clay which is dominated by Smectite (montmorillonite) and illite. Those types of clay material present strong hydrophilicity (ex: montmorillonite) (Murray, 1991) in which water can be stored abundantly in between the clay layers (Vogel et al., 2005).

According to some researchers the majority of the crack development (80%) occurs during the first normal shrinkage and only few in the residual shrinkage (Tang et al., 2011a). Cracks grow faster until they reach the air entry point. They attain their maximum size during shrinkage limit. Despite the fact that soil shrinkage is not very detailed in this study, all these information show evidence of soil shrinkage and crack propagation in DS. As reported by Tang et al. (2011b) there is a strong relationship between crack and void ratio projection (or volume shrinkage). Moreover, cracks can be a good indicator for soil shrinkage and vice-versa (Tang et al., 2011a).

However, for undisturbed sample, it seems that crack formation is not entirely linked to the void ratio and soil shrinkage. There is strong effect of soil structure against soil shrinkage and at the same time some facilitation (predisposition) of crack initiation due to presence of micro-cracks, aggregates and other parameters. Therefore, there is need for adaptation of the curves relating soil cracking and soil shrinkage for NDS. In fact, the soil cracking characteristic is in concave-form in NDS rather than convex (in DS).

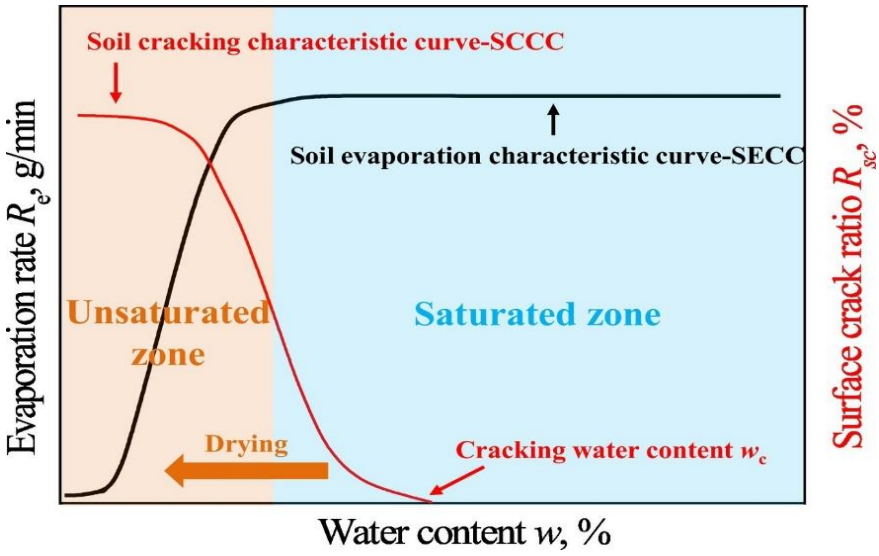

(a) Evolution of surface crack ratio and evaporation rate with water content during drying based on observation of Tang et al. (2021)

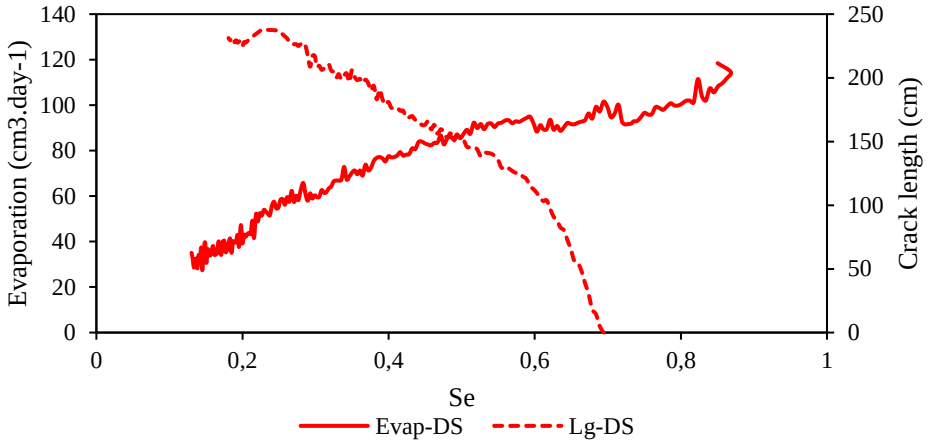

(b) Evolution of surface crack ratio and evaporation rate with water content during drying for DS

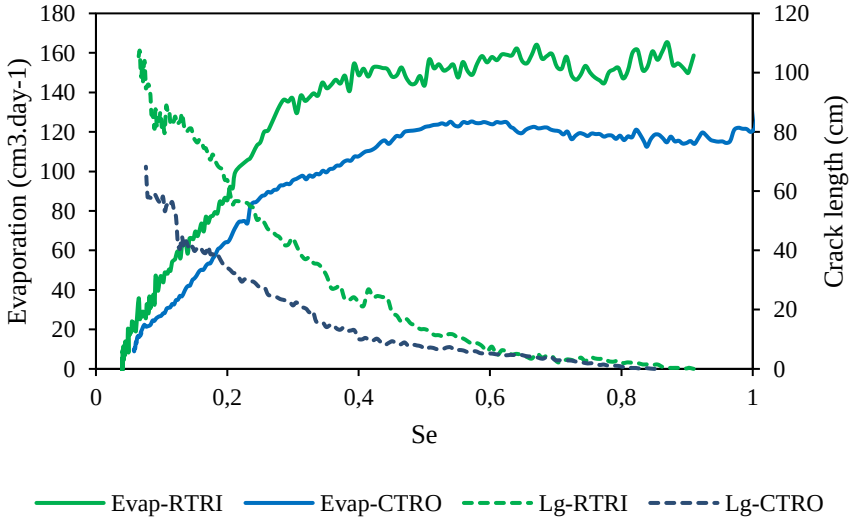

(c) Evolution of surface crack ratio and evaporation rate with water content during drying for NDS (RTRI and CTRO)

Figure 5-9 Comparing the evolution of surface crack ratio and evaporation rate between (a) observation by Tang et al. (2021) and the one from (b) DS and (c) NDS

NDS)

CHAPTER 6

How do mucilages (Chitosan, Tragacanth, and Xanthan) affect the soil evaporation and crack development?

Abstract

Soil function (water recycling, storage, etc) has been greatly fragilized due to global warming. Soil desiccation cracking can enhance the water/pollutants infiltration and also cause excess water evaporation. Mucilages (root exudates) have been commonly utilised in soil remediation. This paper investigates the effect of mucilages on crack formation and also on soil water evaporation during drying. Three types of mucilages (Chitosan (CHI), Tragacanth (TRA), and Xanthan (XAN)) are used at increasing amount: 25 % (0,9 mg/kg), 50 % (1,8 mg/kg) and 100 % (3,6 mg/kg) and compared with the reference soil (REF: no mucilage). By the help of image analysis, crack characteristics (ratio, length, probability entropy, fractal dimension) are measured. The results reveal that: (1) mucilage modifies significantly the drying characteristics of the luvisol. Soils treated with TRA and XAN retain more water (up to 75-80 %) compared to REF and CHI (only 50 %). (2) Mucilages affect also the crack propagation, as well as the probability entropy. With 3.6 g/kg (100 %) of TRA/XAN, the rate of cracking and probability entropy are decreasing by (9 % and 1%), and (59 % and 12 %), respectively. The crack formation is also delayed (by around 5 h) under TRA/XAN. (3) Xanthan remains efficient in reducing cracks (by 16 %) even at the lowest amount (25%). However, Tragacanth (at 25 %) and Chitosan (at any amount) do not change significantly the crack formation compared to REF. (4) Xanthan (and less TRA) reduces significantly the crack disorder (i.e., high entropy) and the fractal dimension compared to REF and CHI. Increasing temperature increases crack formation in REF/XAN while it is reduced (the crack formation) in TRA/XAN.

1. Introduction

In order to remediate the excessive cracking formation and propagation in the agricultural field, researchers have adopted various techniques (Xu et al., 2018; Lu et al., 2021). The major challenging techniques are to find a way to improve the soil properties in a sustainable manner. It is known that the formation and propagation of cracks depend on the soil physical (soil strength/stiffness) and hydrological properties (reducing water evaporation and/or holding more water). Previous studies add limes, fibre, biochar, and other synthetic products to increase the soil strength and reduce crack formation (Zhang et al., 2016; Lu et al., 2021). Those techniques encounter some difficulty in terms of cost-efficiency, equipment/machinery adaptability, C:N ratio disequilibrium, and some are not environmentally friendly. Recent agricultural studies are interested in mucilage application for improving the soil properties as it is a natural by-product offered by the rooting systems. This root exudate is mainly studied for its capacity to absorb water, to sorb herbicide, to store and sink carbon (Marsico et al., 2017). Other authors studied the use of mucilage to capture and attract heavy metals and other ions (Hataf et al., 2017). Recent paper reveals that mucilages could attach together soil particles located in the vicinity of the rooting system. As a consequence, the rhisospheric zones turn out to be resistant to water stress, to tensile stress (due to soil desiccation) and to water erosion (Brax et al., 2017). The gluing properties of certain mucilage (Chitosan, Tragacanth, Xanthan, Xyloglucan, AGU

etc.) has been confirmed by Naveed et al. (2018) and Galloway et al. (2018) when they rinse soil + mucilage from papers. These results advocate the possible effect of mucilage in improving the soil structural property and reduce the dynamics of cracking. Not only the type of mucilage should affect cracks; but also other parameters such as: the amount of mucilage and the environmental condition (e.g. temperature). The average quantity of mucilage in the rizhospheric zone is reported to be around 3.6g/kg soil but this value can fluctuate from on area to another (Galloway et al., 2018). Tang et al. (2010) found that temperature play some roles in crack dynamics. This is parameters need to be investigated due to the global warming. Therefore, the objective of this study is to examine the effect of mucilages (Chitosan, Tragacanth, Xanthan) at an increasing dose and temperature on desiccation cracking. Controlled laboratory experiments examine in details the soil evaporation rate (and/or water storage) as well as the process of desiccation cracking. Photogrammetry associated with image processing and analysis try to unveil the crack characteristics (physical, morphological). This research provides data and information on soil cracking and soil evaporation under different mucilage applications.

2. Materials and Methods

2.1 Study field, sample collection and experimental set-up

The physical and chemical characteristics of the soil are given in Table 6- 1 . The mucilage used in this study comes from shop online in the form of white inodorous powder. The treatment in this study is composed of: (1) Reference (REF), (2) Chitosan (CHI); Tragacanth (TRA); and Xanthan (XAN). They are chosen based on their (ready)availability, easy handling and their efficiency in sticking soil particles together (Naveed et al., 2018; Galloway et al., 2018). For the entire experiment, there are always three replicates in each treatment. Chitosan is a natural biopolymer extracted from chitin of squid pens, shrimps and crab shells. The product contains at least a deacetylation degree of 90 %. Chitosan in this study has the formula Beta-(1,4)-2-Amino-2-deoxy-D-glucose which is easily degradable and is environmentally friendly. Gum tragacanth is a natural gum extracted from the sap of the *Astragalus* tree. It is soluble in water and contains more than 90 % of polysaccharides tragacanthin and bassorin. Xanthan Gum is a (plant-based) substance produced by the *Xanthomonas campestris* bacterium during fermentation of sugar contained in maize. The gums are purified, dried and crashed into fine powder (<180 µm). Mucilages form this study are processes and issued from food and cosmetical industry from the UK.

Before the onset of the experiment, the mucilage powder is dried at 40°C for 1-2 hours, and mixed homogeneously with the soil sample. Disturbed sample is used in this experiment to assure the mixture of the soil and the mucilage. This guarantees as well the homogeneity of the soil and the similarity of each sample. An initial water content of 75-80% (weight percentage) is added to each sample mixture. The oversaturated slurry is mechanically stirred for about 10 min then placed in an open container. Two types of containers are used in this experiment: a large rectangular one

of 25 cm length x 20 cm width x 1.6 cm height or thickness (called big sample) and a smaller cylindrical container of 12.5 cm diameter and 0.8 cm height (called small sample). This is to accelerate the experimentation without compromising the quality of the study. Big sample is important since it gives the evolution of cracks with time. However, only one big sample can be accommodated in the small chamber; yet, it can contain more than three small samples. In this way, further analysis can be done on small samples such as increasing amount of mucilage and rising temperature. We decide to let the sample settle for about 2 hours before starting the drying experiment in a small chamber (55 cm side length x 65 cm height). The drying experiment takes between 7-10 days.

Table 6- 1 Soil physical and chemical characteristics of the reference sample

Category	pH	Clay, %	Silt, %	Sand, %
Samples	8,3±0,21	15.95±0.14	78.98±0.15	5.07±0.08

2.2 Water evaporation and crack progression assessment on big samples

The surface of the sample is freely opened to the atmosphere with a constant temperature of 30°C; and an initial relative humidity of 40 % for the big rectangular samples. The experiment on big sample is similar to the previous experiment (Chapter 4). For big samples, precision balance (accuracy 0.01 g) monitors the evolution of sample weight which is then used to calculate the soil water content (*Wc*) and the water evaporation rate (*E*). There are three samples without mucilage which are considered as reference, and three replicates of samples from each three types of mucilage (Chitosan, Tragacanth, and Xanthan). To minimize the number of experiments, only the maximum quantity of mucilage (3.6 g/kg = 100 %) is used for the big samples. The maximum amount (100 %) of mucilage (of about 3.6 mg/kg) corresponds to the average quantity of mucilage in the natural environment especially in the rhizospheric zone. The evolution of desiccation cracking is captured every 30 minutes by digital camera of 12 megapixels. The rate of evaporation is quantified using the following formula:

$$\boldsymbol{E} = -\frac{\mathbf{1}}{\boldsymbol{A}}\frac{\boldsymbol{\Delta m}}{\boldsymbol{\Delta t}} \quad (1)$$

Where Δm (g) indicates the variation of moisture regime during the time interval Δt (day), A is the evaporative surface area of the sample, and *E* ($cm^3.day^{-1}$) the rate of evaporation

2.3 Assessment of the effect of increasing mucilage, and temperature on cracking observed on small samples

On one hand, to investigate the effect of mucilage quantity on cracks, an increasing quantity of mucilage 0.9 g/kg (25 %); 1.8 g/kg (50 %); and 3.6 g/kg (100 %) is added to the small (spherical) samples at 30°C. On the other hand, to assess the effect of

temperature on cracks, three sets of temperatures of 25 °C, 30 °C and 50 °C are used. The choice of the temperature is from the fact that 25°C is the minimum temperature we can keep during the experiment (during summer), 30 °C is the average ambient temperature and 50 °C is the extreme temperature we can imagine to happen in the agricultural area probably not in Gembloux. This second study on temperature is done on a fix quantity (1.8 g/kg = 50 %) of mucilage (CHI, TRA, XAN). The image analysis is done at the end of the experiment (after 7-10 days) at full expanded cracks. There is no record of weight progression in small samples.

3. Results

3.1 Effect of mucilage application on water evaporation of soils (on big samples)

Figure 6-1 a,b presents the curve of water content and evaporation rate of soils treated with different types of mucilage (Chitosan, Tragacanth, and Xanthan) added at a rate of 3.6 g/kg (100 %). All curve (in each treatment) represents the average value calculated from three replicates. The curve of water content follows a linear decrease at the beginning of the experiment, then it deflects to a less decreasing a stage, before attaining an almost horizontal line of final dry stage (Figure 6-1 b). The curve of water evaporation shows two stages. However, in some treatments (REF and CHI), it starts from a decreasing curve representing an oversaturation of the sample. This indicates the presence of certain amount of free water above the sample according to Tran et al. (2019). The first stage is a relatively stable state period (Constant Rate Period = CRP) which is characterised by the maximum evaporation rate. The second stage of evaporation is shown in the section where the evaporation curve drops almost linearly (falling rate period= FRP) before reaching another stable period of residual evaporation.

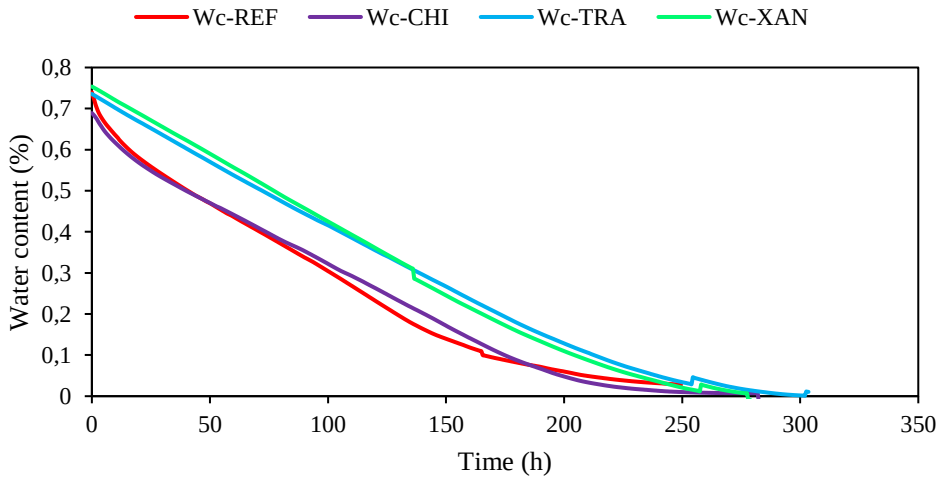

a) Curve of soil water content for all sample. Note the straight lines and late curve deflexion for TRA/XAN while concave lines for REF/CHI.

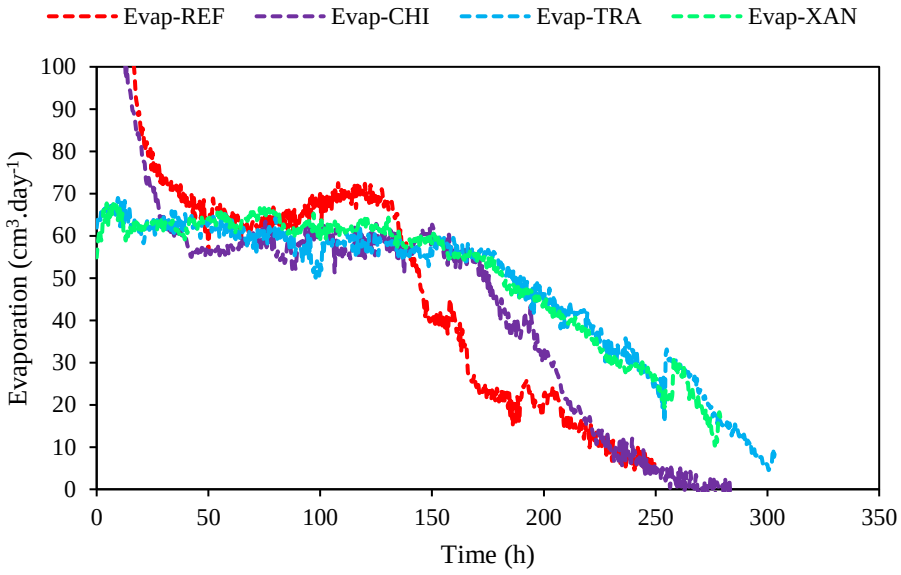

b) Evaporation curves for all sample. Note the presence of excess evaporation (before the constant rate period) for REF/CHI; long constant rate period (CRP) for TRA/XAN.

Figure 6-1 Progression of (a) water content and (b) water evaporation in function of time for the considered treatment (REF, CHI, TRA, and XAN).

The addition XAN and TRA in the soil samples affect the duration of the constant rate period (CRP). However, with an addition of 3.6 g/kg mucilage in the samples, there is almost no change in the maximum evaporation rate in the CRP period compared to the one of the reference samples (without mucilage). The maximum evaporation hovers around 60-70 $cm^3.day^{-3}$ for al treatment. Regarding the duration of the CRP period, distinction should be made between REF/CHI and TRA/XAN. For instance, by adding tragacanth and Xanthan to the samples, the duration of the maximum evaporation rate extends from 90 h (i.e., from 30-120 h in REF) to 180 h (in TRA and XAN). CHI enables to increase the CRP from 90 h (in REF) to 120 h (i.e., from 40-160 h). The time to reach the residual period increases from 250 h in REF/CHI to more than 300 h for TRA/XAN.

3.2 Cracking curve evolution after adding mucilages (on big samples)

Figure 6-2 a illustrates the crack formation and progression of each sample treated with different types of mucilage. The cracking curve presents two main periods started with a linear progression part and a second part of nearly stagnating period. The crack

development is significantly reduced in samples treated with xanthan (XAN) and tragacanth (TRA). Similarly, the cracking rate is also limited in those treatments especially in XAN as illustrated in Figure 6-2 a. The maximum crack density in CHI samples is fairly similar to the reference soil (REF). As presented in Figure 6-2 b, the fractal dimension is also affected by the use of different types of mucilage. There is difference between reference soil (REF)/chitosan (CHI) and XAN/TRA. The crack entropies seem increasing with time for all treatment showing a sort of disorderly arrangement of cracks with time (Figure 6-2 c). The highest entropy value is recorded in REF, CHI and TRA indicating that they present the lowest orderly arrangement of cracks. In other words, XAN presents the capacity of orienting cracks into an orderly manner as it has the lowest entropy value. The summary of the two cracking characteristics (probability entropy, fractal dimension) under different types of mucilage is shown in Figure 6-2 d. The data is taken at the end of cracks development (~80 h). The mucilage application reduces the cracking formation by 9 %, 59 % in TRA, XAN, respectively, compared to REF. In the contrary, CHI appears slightly increasing the forming cracks in comparison with REF. The probability entropy is decreased by 1 %, 1 %, 12 % in CHI, TRA, XAN, respectively. Therefore, the results show that addition of XAN in Luvisol creates short and narrow cracks (Figure 6-2 e). We can observe from Figure 6-2 a,e that the formation of crack is not only reduced but also delayed in TRA/XAN (by around 5 h) compared to REF/CHI. This condition can limit the formation of secondary or tertiary cracks. Therefore, this type of mucilage (XAN and slightly TRA) can be used to control (or reduce) the crack formation and propagation in the Luvisol of Belgium.

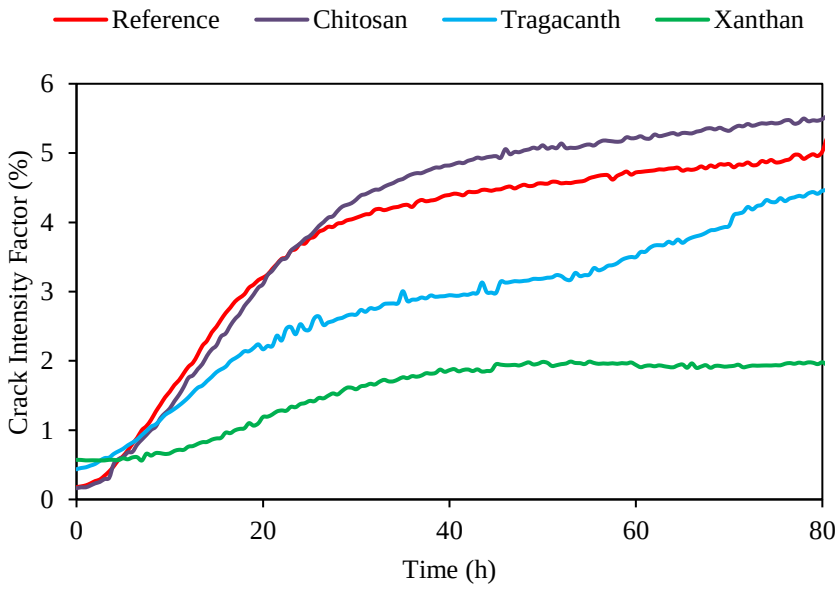

(a) Crack evolution with time in the form of crack intensity factor (CIF)

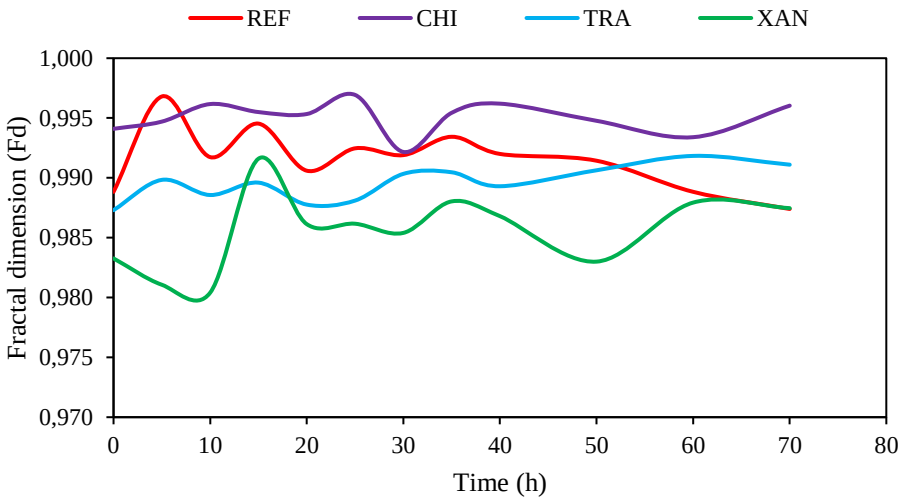

(b) Evolution of the fractal dimension (Fd) with time for all samples

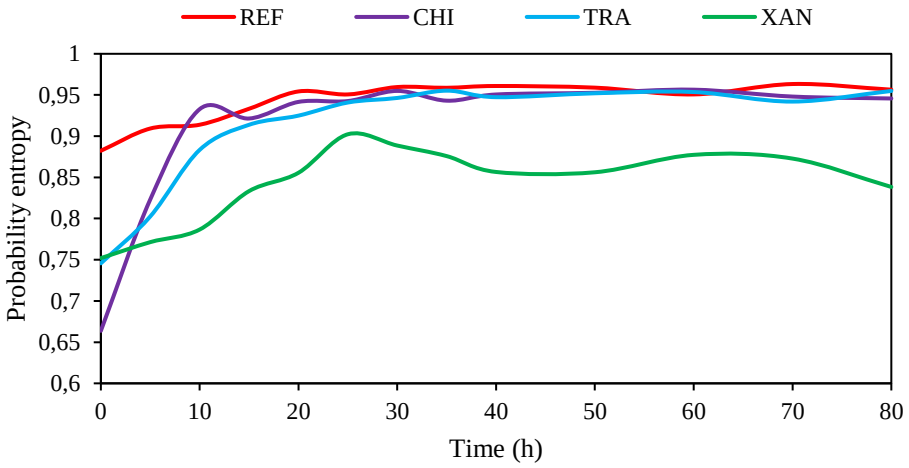

(c) Evolution of the probability entropy (H) with time for all samples

(d) Table illustrating the Fd, H and CIF at the maximum crack formation (80h)

Treatment	Fd	H	CIF
REF	0,987±0,004a	0,956±0,026a	4,9±0,484a
CHI	0,996±0,004a	0,946±0,026a	5,4±0,484a
TRA	0,991±0,004a	0,955±0,026a	4,45±0,484a
XAN	0,987±0,004a	0,838±0,026b	1,97±0,484b

**Fd: fractal dimension, H: probability entropy, CIF: Crack intensity factor*

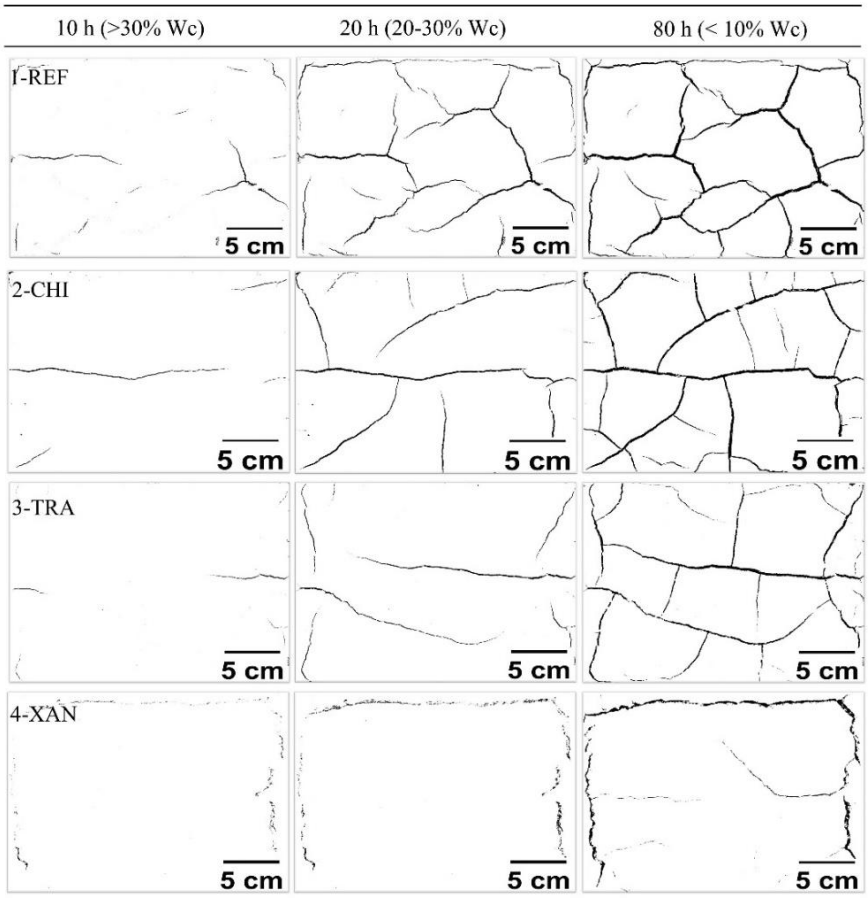

* *REF: Reference samples, CHI: Chitosan, TRA: Tragacanth, XAN: Xanthan; Wc: water content; 10h, 20h, 80h: time after crack initiation.*

(e) Crack progression captured at 10h, 20h and 80h after crack initiation. Note the earlier and higher crack formation in REF/CHI compared to TRA/XAN.

Figure 6-2 Evolution of crack characteristics (a) Cracking rate progression with time, (b) progression of the fractal dimension with time, (c) evolution of the probability entropy (H); (d) Crack characteristics at the final stage of crack expansion; (e) images of cracks

3.3 Cracking evolution at increasing mucilage and temperature (on small samples)

Crack evolution with temperature is shown in Figure 6-3 a, and Figure 6-4 b. The results show that the effect of temperature is significantly different from one treatment to another. For instance, the increasing temperature increases the crack formation in REF by 12 %. For chitosan, the length of the forming cracks is almost constant (from

25 °C-50 °C) and even decreasing from 25 °C to 30 °C. The temperature effect is also almost insignificant between 25 °C-30 °C for TRA with a fairly stagnant forming crack length. However, the crack length expansion is reduced for TRA from 30 °C to 50 °C. Similarly, XAN application reduces the crack formation (by 23 %) at an increasing temperature (25 °C to 50 °C). Therefore, the lowest crack formation is still in XAN from low to high temperature.

The increasing mucilage quantity has different effect on each treatment (Figure 6-3 b, Figure 6-4 a). It did not change significantly the size and number of cracks in CHI compared to REF. Increasing amount of TRA reduces the formation of cracks (by 19 %) only at the maximum quantity (3.6 g/kg). However, XAN can reduce the crack formation by 16 % at 0.9 g/kg (25 %), 13 % at 1.8 g/kg (50 %) and 39 % at 3.6g/kg soil (100 %) compared to REF. Therefore, at increasing amount of mucilage and rising temperature, XAN presents the highest ability to reduce cracks, followed by TRA and finally CHI.

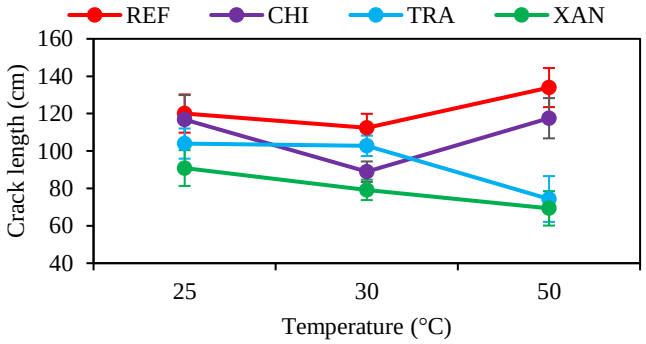

(a) Total crack length at an increasing temperature

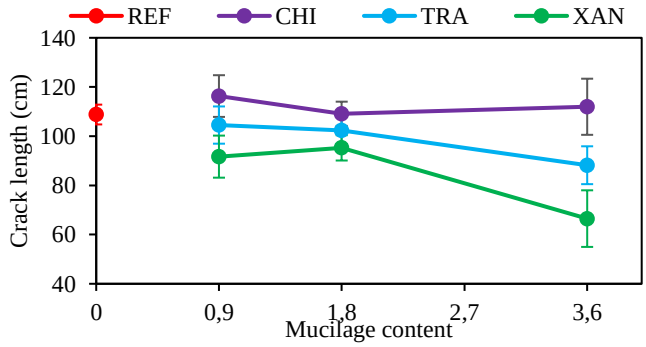

(b) Total crack length at an increasing dose of mucilage

* *REF : Reference samples (no mucilage), CHI: Chitosan, TRA: Tragacanth, XAN: Xanthan*

Figure 6-3 Evaluation of crack length modification at an (a) increasing temperature from 25 °C to 50 °C, and at (b) an increasing dose of mucilage from 0.9 g/kg, 1.8 g/kg, and 3.6 g/kg soil.

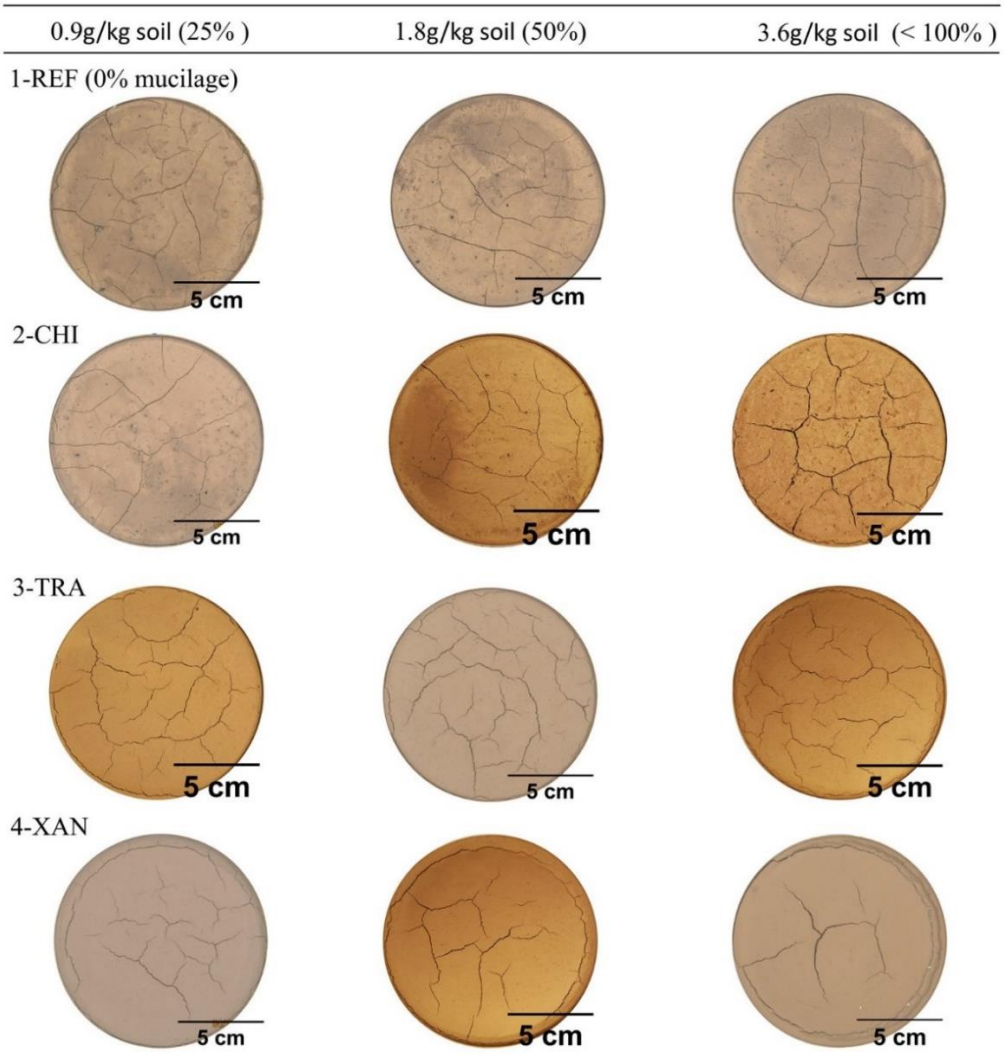

* REF: Reference samples (no mucilage), CHI: Chitosan, TRA: Tragacanth, XAN: Xanthan; Mucilage doses: 0.9 g/kg soil, 1.8g/kg soil and 3.6 g/kg soil; Temperature: 30 °C.

a) Crack development at increasing dose of mucilages (CHI, TRA, XAN) compared with the reference soil. The overall temperature is set at 30°C for all samples. Reference samples do not receive mucilage addition.

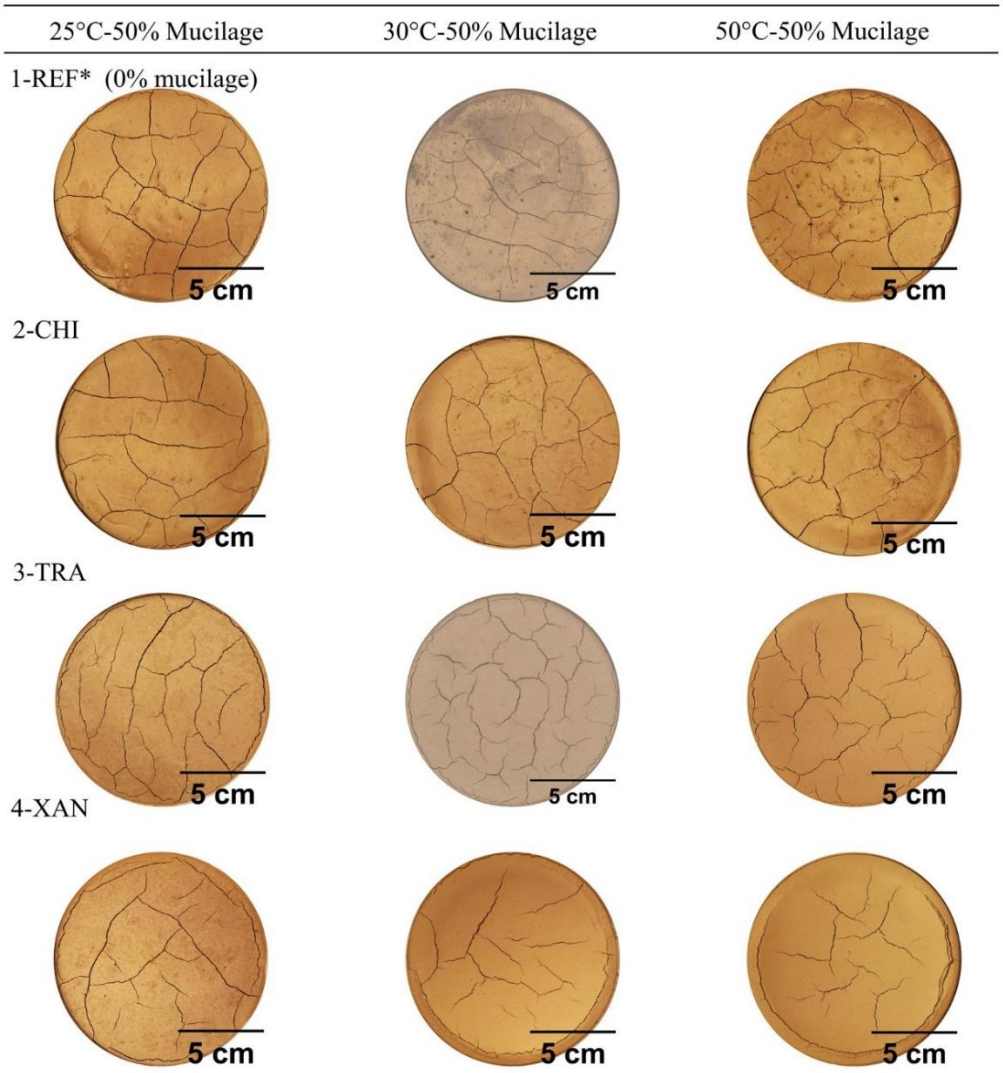

* REF: Reference samples (no mucilage), CHI: Chitosan, TRA: Tragacanth, XAN: Xanthan; Temperature: 25 °C, 30 °C, and 50°C.; Mucilage doses: 1.8g/kg soil (50%).

b) Crack development at increasing temperature under mucilages (REF (0% mucilage), CHI, TRA, XAN) addition. The dose of mucilage is 1.8 g/kg soil (50 %).

Figure 6-4 Comparing the effect of (a) an increasing dose of mucilage and (b) an increasing temperature on crack propagation. Each picture is taken out of three replicates.

4. Discussions

4.1 General discussions on crack progression and soil hydraulic properties

Figure 6-5 presents the progression of the evaporation curve against water content known as the Krisher's curve. It is clearly observed from the graph that the CRP (against water content) is also extended significantly in TRA/XAN (from 75 % to 20 %) compared to REF/CHI (from 50 % to 20 %). We can also observe that the maximum water content retained (held) by the reference soil (REF) during saturation is around 50 %. Above this water content range, water is no longer bound (held) by the soil particles and evaporates freely (as free water). This maximum water content (of 50 %) is also reported in previous study (Tran et al., 2019). This study explains the presence of excess water (free water) causing excess water evaporation (prior to the CRP) as the case (here) for REF and CH. The excess water is not seen in TRAG and XAN indicating that those mucilages enable the soil to retain (hold) more water up to 75-80 %.

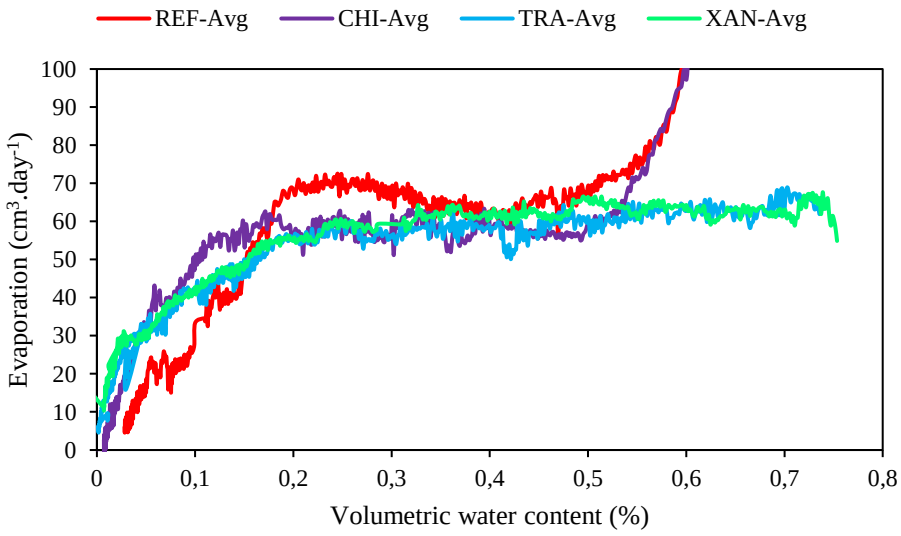

Figure 6-5 Krisher's curve presenting the progression of water evaporation rate in function of water content. Note the long range of water content during which the evaporation rate remains constant for TRA/XAN compared to REF/CHI.

The soil water retention is regulated by many factors including soil structure, soil texture, bulk density, soil pore network organisation, organic matter, the type and quantity of clay minerals and other soil composition(Zheng et al., 2018; Zhou et al., 2020; Yang et al., 2021). The textural parameters are similar for all sample leaving a room for the hydraulic property of the mucilage as the main reason for the difference in water retention. One of the main differences between the applied mucilages is the

fact that the XAN and TRA are all gum. According to Brax et al. (2017) and Saruchi et al. (2019) gums can absorb water easily and abundantly while keeping its structural stability. The same authors report that Xanthan presents more structural stability and binding strength even at very low concentration ($0.9g.kg^{-1}$ sample). In agricultural application, tragacanth gum polysaccharide is found absorbing water due to tragacanthin (and swell due to bassorin compound) and improves the soil water retention capacity (Saruchi et al., 2019). The type and also the quantity of mucilage should play a major role explaining the great efficiency of two mucilages (XAN, TRA) in this study. We assume that for chitosan, the selected amount (in this study) is not sufficient reflecting its low water holding capacity compared to other previous study (e.g., Hataf et al. (2017)).

As illustrated in Figure 6-2 a,b,c,d,e, the characteristics of the cracks varies with time. The initial cracks are always long and wide while the secondary cracks are narrow and cross the primary cracks at an almost right angle. The results reveal a strong crack formation under CHI, compared to TRA and XAN, respectively. Crack formation starts from soil volumetric shrinkage as a result of an increasing suction (stress) due to water depletion(Zeng et al., 2019; Zhang et al., 2020). The shrinkage characteristic of a given soil depends on its pore structural network, on soil composition (clays and other swell and shrinking substance) and soil mechanical strength (stiffness, compaction, etc). As illustrated before, mucilage can absorb a huge quantity of water and swell. The structural strength and stability of the mucilage (such as XAN and TRA) assure the free shrinkage of the sample during drying without forming cracks. The soil stability depends also on the interaction between soil particles and mucilages. Observation on scanning electron microscope (SEM) images by Chang et al. (2015) reveals that Xanthan can coat soil particle surfaces and increase the contact area among the soil particles. The substance creates also connection bridges between particles that are not directly in contact. This increases the strength of fine-grained soil such as silt and silt-loam soil. This property explains the low value of entropy in XAN.

This study could not assess the mechanical property of the samples; however, based on study conducted by Rosenzweig et al. (2012) and Chang et al. (2015), Xanthan was found forming strong interaction (e.g., hydrogen or electrostatic bonding) with charged soil particles. The same author found that addition of Xanthan gum brings significant increases in soil compressive strength, soil elastic modulus and soil stiffness. Xanthan was even found enhancing the cohesive property of a cohesionless sand. Concerning Tragacanth, apart from its cohesive property, this polysaccharide biodegradable hydrogel is found stable to heat which can explain its strength compared to CHI (Saruchi et al., 2019). For instance, previous study on Chitosan also shows that this biopolymer increases as well the interparticle interaction of the soil particles, leading to improved mechanical properties (Hataf et al., 2017). However, the authors found that the interparticle interactions are strong during wet condition while the bond strength is inefficient at dry condition.

The results of this study reveal an interaction between soil evaporation and mucilage addition. The evaporation mainly depends on the atmospheric condition and the organisation of the soil poral structure (Hubert et al., 2018b). Since mucilage presents

a high (dynamic) viscous solution (Omidbakhsh Amiri et al., 2015; Saruchi et al., 2019), this property can help porous soil to keep water during wetting and avail more water during soil water evaporation. The more viscous is the material, the higher the absorbed water and the longer the CRP of wer the evaporation. Saruchi et al. (Saruchi et al., 2019) reported that addition of Xanthan enhances the apparent viscosity of the mixed pastes. This phenomenon can also happen to soil mixed with Xanthan. For less reactive mucilage (as CHI), water is not retained by the mucilage resulting to similar water evaporation as REF. For TRA, at small amount, this mucilage absorbs and keep water during saturation as XAN. Finally, the rising of temperature increases the water pressure difference between the sample and the atmosphere resulting to an increasing evaporation (Zeng et al., 2019; Zhang et al., 2020). Water is removed quickly and strongly from samples increasing the suction and the soil stress. This explains the increasing of cracks in this condition. However, the structural strength of certain mucilage increases due to increasing of their viscosity according to (Saruchi et al., 2019). This could explain the decrease of crack formation in the case of XAN and TRA.

4.2 Direct effect of mucilage on crack formation

This study elucidates a possible way to prevent crack formation. In spite of the fact that this study is the beginning of experiment using mucilage. The study output has proven that addition of various types of mucilage especially Tragacanth (TRA) and Xanthan (XAN) brings positive effect on crack formation and propagation. Mucilage addition not only reduce the amount of forming crack but also the time for crack initiation and the amount of water that the soil could hold during drying. They managed to reduce the crack formation at the surface due to the characteristic of the mucilage (glue). First of all, the addition of mucilage brings better effect than the chemical additional with reduced possible environmental hazard and problem with plant growth. In fact, mucilage is a biological secretion around rizhospheric zone indicating that it cannot impinge root formation and propagation. Moreover, the products will not remove cracks completely. The contribution of mucilage on environmental hazard could come from the fact that mucilage is natural (organic) and safe for the environment. Moreover, it will reduce the transfer of pollutant to the ground water. The study shows further that mucilage increase the soil stiffness, cements the soil particles and it should perform better that fly ash, cement or silica fume. Using mucilage does not present any limits in the amount as other chemical product. However, the performance of the mucilage increases with its own amount. Cautions should be taken when dealing with small amount of mucilage. XAN presents always its high performance even at small quantity; however, small quantity of Tragacanth can be detrimental to crack control. We hypothesize that high amount of water is absorbed by the mucilage, augmenting its overall volume. The shrinkage is also enormous during drying creating wider and longer cracks. It is important to mention that mucilage should perform far better and should be stable than chemical product (Chang et al., 2015). Omidi *et al.* (1996) reported less effect of lime or cement when the initial water content was high. In the opposite, Jayanthi and Singh (2016) reported that addition of lime or cement increased the soil shrinkage and crack

propagation. There is an optimum quantity of those product and it must be homogeneous in the soil to avert cracking (difficult) according to Poncelet et al., (2021). Stabilizing soil with synthesized chemicals (e.g., sodium silicate, gypsum, and phosphoric acid) is more convenient and successful than highly reactive material (Jayanthi and Singh, 2016). Despite the fact that mucilage is only applied in silt-loam soil in this study. Based on its performance, it is highly possible that the substance works well with other types of soil such as sandy soil and highly plastic soil. The product can replace the use of microbial induced calcite precipitation (MICP) which is highly used in in sandy soil.

4.3 Temperature, mucilage and crack formation

Temperature is one of the main factors suppose affecting the desiccating crack behaviour (Tang et al., 2010; Pourhosseini et al., 2017). This is due to the fact that temperature is assumed to affect the evaporation rate, which accelerate the desiccation, the rise of suction, the shrinkage and thus the cracking. The effect of temperature (in this study) is not linear on crack formation as compared to many observations by different authors. This is mainly observed on disturbed samples without mucilage application. On samples treated with mucilage (CHI), the lower temperature (25°C) seems generating more cracks than higher temperature (35-50°C). In fact, mucilage presents two contrasting characteristics (fact) as far as crack formation is concerned. On one hand, it absorbs water significantly causing the soil to swell during wetting. This characteristic allows strong change in soil shrinkage during desiccations, creating wider and longer cracks. On the other hand, mucilage presents glue-like properties which stick soil particles upon drying. This second characteristic is important for cracks control. What may occur at lower temperature is that crack appears when soil is still highly saturated. The glue characteristics of the mucilage is not as efficient as when the soil is slightly dry for example in the case at higher temperature. Those types of mucilage are therefore proper for dry climate or utilised during dry spell or dry season. On the contrary, for samples treated with Xanthan, cracking is decreasing with increasing temperature. This suggests that the mucilage could hold soil particles at lower temperature and increase its adhesive capacity with increasing temperature and decreasing water content at pore level. The choice of mucilage is therefore crucial depending on the field condition and the study objective.

5. Conclusions

Addition of mucilages into soil affects the curve of evaporation as well as the formation and propagation of cracks. This study concludes that:

1- Two types of mucilage, Tragacanth (TRA) and Xanthan (XAN) change drastically the water retention and the evaporation of the luvisol of Belgium. Those two treatments are capable of increasing the soil water retention from 50 % to 75-80 %. Reference soil (REF) and Chitosan (CHI) present an excess water (oversaturation) when the water content (Wc) exceeds 50 %.

2- XAN and TRA delay the crack propagation by 5h and also reduce the magnitude (size) of the forming cracks, as well as the probability entropy. For instance, at 100% (3.6g/kg) of XAN and TRA, the crack intensity factor (CIF) and probability entropy (H) are reduced by (9 % and 1 %), and (59 % and 12 %), respectively.

3- By reducing the amount of the applied mucilages, it is found that XAN maintains its capacity in limiting crack propagation (drop by 16 %) until its lowest dose (25 %). However, low amount of TRA (25 %) does not affect significantly the crack formation. Chitosan additional (at any amount) does not bring significant effect as far as crack formation is concerned.

4- The effect of temperature is contrasting depending on the type of mucilage. For instance, by increasing the temperature from 25 °C to 50 °C, it is shown that crack length is increasing in REF/CHI while decreasing in TRA/XAN.

(4) Addition of XAN and TRA reduce also the crack disorder (i.e., high entropy) and the fractal dimension compared to REF and CHI.

The overall results confirm certain literature illustrating that mucilage increases the overall strength of the soil sample due to formation of chemical and physical bounds with soil particles. This study reveals however that the strength of the bound could be highly dependent on the type and the amount of mucilage, as well as the ambient temperature. Here, XAN (and lesser TRA) are the most important mucilages which reduce the crack formation and propagation, and also increase the water retention and maintain the maximum evaporation rate (CRP) for longer time. This study calls for wide perspective studies such as: use of other types of mucilage, analysis of the mucilage at field scale, observation of soil+mucilage at micro-scale etc.

CHAPTER 7

General discussions and perspective

1. Discussions and perspective

There are three major questions that come to researchers concerning cracks preponderance in the agricultural fields: 1) what is their process of formation and propagation (how they take place?)and how can we measure/quantify them, 2) what are their consequences (on water evaporation, water content) and 3) how to deal with them? (Figure 6-6).

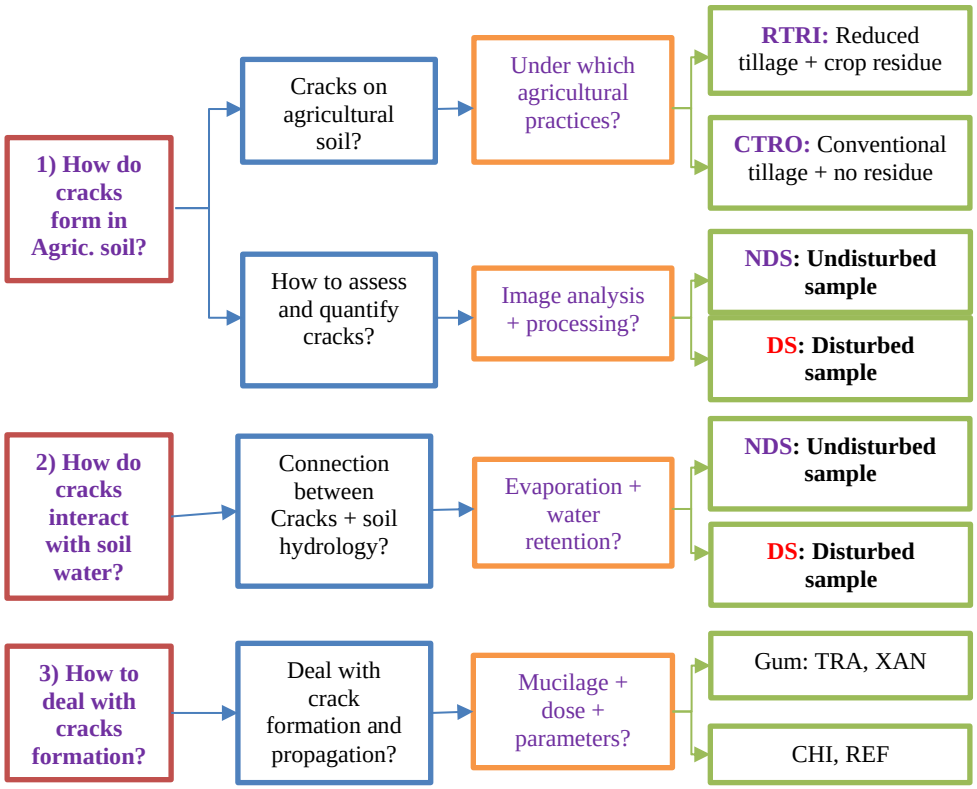

Figure 6-6 Different challenges when dealing with crack study starting from (1) analysis of crack formation on agricultural soil based on digital image analysis and processing, (2) assessment of crack effects on water content, water evaporation, and water retention, (3) and control of cracking using mucilage?

The challenge is enormous since answering all questions calls for a broad knowledge and understanding from different branches in science. Moreover, the study should include different aspect of spatial and temporal analysis. For that matter, the first step in this study consists of monitoring any modification (shrinkage, and cracking) from the sample surface during the drying experiment. The second step

searches for an adequate computational approach which could quantify cracks directly from 2d image processing and analysis. This should eventually be converted to a model which is hold to validate the observation and hypothesis alleged during the laboratory experiment. The final step includes various ways to encompass or reduce the possible negative effect of cracks propagation. In all, this study requires knowledge in image analysis, data processing, statistical analysis, soil hydropedology, and computer programming/modelling.

This study aimed at understanding the processes of crack formation and its propagation under agricultural field in Gembloux taking account of agricultural practices, residue management and soil disturbance. The main idea is to quantify cracks and their effect on soil hydrodynamic in order to optimise water use efficiency, improve crop production and modelized adequate and environmentally friendly land management. It is observed that cracks are omnipresent in the field including in loamy soil. It is important therefore not only to measure and quantify cracks but also to characterise and include them in predictive models. The main characteristics include the shape and size (area, length, width) as well as the intensity and density. This is because, those are the first observable and quantifiable features when dealing with cracks. Moreover, those parameters are crucial to explain soil physical processes (strain, stress, shear, compaction, shrinkage rate etc) and change in hydraulic properties (infiltration rate, evaporation, rate of solute contamination, recharge of groundwater) during drying/wetting (Fredlund et al., 2010; Li et al., 2016; Naveed et al., 2018). Other properties such as fractal dimension, probability entropy come later from further analysis based on digital image analysis. Secondly, the link between cracks and soil water dynamic should also be investigated. Thirdly, it is also important to investigate the possible remedy for extra-cracking in the field. Next to the overall discussion which engages important conclusions from the dissertation; it is worth to carry out a broad view and new perspective out of the current research. By identifying the possible weaknesses of the process utilised for cracks identification (based on ROI methods); it brings us to explore different possibilities, a room for improvement of the methodology to be developed in the upcoming future. The discussion and perspective are divided in three to four parts: it starts with 1) a general discussion and perspective debating the overall processes and methodology used in this study, followed by 2) Various proposition to improve the methodology, and ended with 3) Discussion and perspective on the interaction between crack formation and the soil hydrodynamic, and 4) Discussion and perspective on the use of mucilage to control cracks.

2. General discussions and perspective on the applied methodology in this experiment

2.1 Clear image processing but use of many software, many programs (script) and manual ROI

It is important to remind us that the core element of this study lays upon digital image processing and analysis. The accuracy and the liability of the output is so

important that we decide to dedicate an important part of the study (Chapter 2, 4 and 5) to dig and cultivate more upon the process. Concerning the methodology for crack extraction and interpretation. We agree that the crack analysis (in this study) is accurate enough to spot and quantify the crack differences following the specific define sequence of computer-implementable instructions (i.e., algorithm). However, we mentioned that the image processing also requires the use of two-three software in which GIMP corrects the image distortion (by perspective program), then ImageJ creates the ROI (Region of interest), noise reduction, image segmentation and thresholding, then PCAS finalises the (task) process by conducting thinning, skeletonization and crack/clod identification. We admit that using only one software would facilitate and reduce the time for analysis. There is possible way to collect all the program (scripts) in one software such as ImageJ or Matlab. However, the use of many software could delay the analysis but not reduce the quality of the output. This can be seen from the distinct crack evolution with time, the small variation between repetitions and the quality of this study compared to other research using sophisticated materials. The result has spotted pattern reported in other studies and gave more detailed information on crack initiation and propagation thanks to stable/clear data input (camera of good quality + good exposure of sample surface) and the narrow time (and fix) interval of observation. In this study, the time monitoring was performed using intervalometer program which is adapted specifically for Canon camera. Other program uses different scripts (in Python, Matlab, etc) or datalogger (e.g., Arduino®, CR800®) to be able to record time and command the camera in a fix time interval.

One crucial part of the image analysis was the use of ROI which aimed at reducing the noise from image background especially for intact samples. As mentioned in the dissertation, the ROI technique averts the use of median filter (Auvray et al., 2014) which requires a reduction of the image resolution (quality) and needs huge amount of time to process. This technique manages to improve greatly the quality of the output; however, the conception and the drawing of ROI was done manually. This could have been done automatically by detecting the crack and other object boundary during image segmentation. Nevertheless, this would require further analysis in order to find the right filter (for each image) and the most effective thresholding algorithm to all samples.

2.2 Difficult choice of sample thickness and friction grid

One of the most important decisions we made during this research is the choice of the sample thickness. We agree that thickness plays an important role in cracks apparition. For that matter we conducted a pre-analysis with samples thickness moving from 4cm to 2 cm with and without friction at the base of the sample. We realised that the wider and thinner the samples, the greater (number and width) the forming cracks. Taking account of the size of the tensiometer (~ 0.5cm diameter), we decided to keep a thickness of 1.6cm which is the minimum size in which the apparatus (tensiometer) could be inserted and monitor properly the soil suction without any damage (i.e., opening or forming air bubble). We believe that it did not affect the soil hydrodynamic measurement and did not reduce the sample air entry value. For not shaking too much the sample during the sample preparation, the

insertion of tensiometer was done carefully. This includes creation of hole with special apparatus and saturation of the hole before inserting the tensiometer. The extension of the tensiometer was fixed with glue to the sample metallic box. There was possibility of early cavitation due to occurrence of crack formation above the tensiometer. This was the reason why we used two tensiometers and take the average value or chose the one which performed the best. This can be one of the limits of the study because there is a large distance between the tensiometer and the centre of the sample, which is not the case for HYPROP ® or other devices as the case in Chapter 2. Moreover, as we discussed in the previous section, NDS could not present vivid clod formation due to the chosen thickness. Therefore, it is normal to suggest the use of thinner samples for undisturbed samples and use other device (such as pressure plate) to measure water suction. It is also possible to increase the sample size in order to have sufficient ratio surface/thickness.

Concerning the frictional grid (1mm height in form of square) applied at the base of each sample (RTRI, CRTO and DS) to increase the soil interfacial friction at the bottom. It is worth to mention that despite the fact that the friction is not too high (1mm) compared to the soil thickness; it was enough to hold part of the soil matrix during shrinkage and imitate some field reality (i.e., hold at the base of the soil and form crack). As we mentioned in the previous section, each type of frictional-grid (squared and diamond) produces huge different forming cracks. The squared-form produced almost squared shape cracks (clod) while diamond grid gave branchy type and polygonal clods. Until now, it is difficult to reproduce exactly the form and size of crack found in the field. This calls for various crack analysis only based on different size, thickness and form of frictional element. Further analysis should be conducted using different type of grid and assess which grid represents (mimics) more the field condition.

2.3 Discussion about the sample size and number of replicates

The discussion which could be raised in this study is the choice of the sample size as well as the number of replicates. The sample size is extremely variable in the literature starting from around 10 cm in length or diameter to few meters in laboratory studies (Tang et al., 2008; Lakshmikantha et al., 2009). Tang et al. (2021) summarise the overall size used by different authors which falls around our chosen size. Therefore, we chose the actual size (20 cm x 25 cm) based on three main facts: the first one is based on the literature. The second one consists of the possible extraction of the samples from the field without disturbing the sample structure. This requirement is very challenging since too large samples will require specific tools to dig and carry them from the field to the laboratory. Moreover, it will create difficulties during storage in the laboratory; not mentioning the struggle during handling, sample preparation and the experimental set-up. The last reason for the sample size is the ratio between the size of surface and thickness. The literature reveals that sample around 10-30 cm has a thickness from few mm up to 3-4 cm (Tang et al., 2008; Lakshmikantha et al., 2009; Zhang et al., 2020). The final thickness of 1.6 cm is set after conducting pre-tests with increasing thickness as explained in the previous section. We agree that change in sample size would change the cracks output both for

disturbed and undisturbed samples. However, the chosen size gives distinctive information between the considered treatments.

There is also discussion about the number of replicates in this study which is around 3 in average. The limited number of replicates reside from the fact that analysing one sample takes 7 days of material preparation (water degassing, tensiometer preparation and filling, sample saturation/preparation), plus 7-10 days of experiment. Moreover, increasing in replicates will increase exponentially the time for image analysis and processing since one sample could produce more than 400 pictures.

However, we agree that multiple experiments (high number of replicates) and analyses would enable us to give (and generate) global crack network and pattern characteristics (which could not be attained in this observational study). The representative data would be adequate to simulate water evaporation and infiltration as well as biological activities and chemical reaction. It would be efficient to connect soil physics, fluid mechanics and soil biochemical analysis.

2.4 Possible interaction between factors considered in the treatment

The first objective of this dissertation is the use of image processing to evaluate the difference between desiccating cracks from three treatments such as RTRI, CTRO, and DS. For that matter, we hypothesised that crack formation would be different depending on land-use or agricultural management/practices (such as conservation tillage and conventional tillage) due to difference in soil structure (porosity, aggregate) and composition (organic matter, organisms). The first idea was to have contrasted samples to portray the crack difference amongst treatment. The difference that we observe between treatment could not tell us which specific parameters (are involve and) explain the crack difference. For instance, it is hard to conclude with sufficient evidence the separate effect of tillage alone and residue management alone. Nonetheless, we agree that as far as agricultural field is concerned, those two parameters are almost inseparable. No tillage and return of residue are often time coming together. However, based on the study output, and for the sake of a scientific research, it is possible to focus on specific (separately) treatment (for example: tillage/no-tillage; residue/no-residue, disturbed/not-disturbed). We believe that all those parameters are affecting crack formation and propagation at different specific level. For sure, the parameters interaction can be positive or negative in some cases. This is another reason for further investigation of desiccating cracking on specific and combined parameters.

2.5 Actual image analysis (and set-up) seems more adapted for indoor experiment

The methodologies applied in this dissertation are more adequate to laboratory experiment due to the fact that all sensors and tools require permanent use of loggers and connected computer. It should be noted however, that the set-up in the field should be different (in size) from the structure in laboratory. For example, balance should be replaced by sensors (neutron scattering, Time Domain Reflectometry (TDR), Frequency Domain Reflectometry (FDR), etc) in the field to measure soil water

content. It may cost in time and in terms of financial aspect. Therefore, it could also affect the quality of the images, their accuracy and the way to analyse the images. For instance, concerning image processing, it is still hard to create a single standardised process which can work for any crack analysis. This is due to the huge variation in terms of image quality, soil type/colour/composition, material quality, etc. An open-source structured procedure should be created engaging possible modification/adaptation by the end-user. However, we are in favour of standardised crack analysis and characterization. Till this day, ImageJ plugin can go up to the thinning and skeletonization processes as far as crack analysis is concerned. Therefore, the algorithm found in PCAS should be transferred into imageJ plugin in order to manipulate the data easily using script and macro.

2.6 Other features (signs of biological activities) which are omitted due to the chosen methodology (ROI)

It is worth noticing that great differences in soil structure could be visible between treatment. Soil from reduced tillage presents many worm holes reflecting high biological activity while the conventional tillage samples contained some visible fresh crop residues (small stem and roots) which were left in the field and mixed with the soil. There are many possibilities to extract the hole (pore) information from the soil surface based on visual identification (Naveed et al., 2018), or under geometrical differentiation using plugin available on ImageJ (e.g., BoneJ, Beat, Feature tracker (Mosaic), etc.). The worm holes might have influence on crack formation and development and also on soil function. For instance, according to some researchers holes on a soil could reduce the tensile strength of the material (Tan et al., 2019; Saravanan et al., 2020). In some cases, some holes became the centre of crack initiation while others deviated the crack path (Saravanan et al., 2020). We did not consider the worn holes in this research project due to the fact that most of them were located outside the chosen crack-ROI (i.e. they are located on the image background) and for that matter removed from the analysis. Including holes in the study would increase and complicate considerably the image analysis. In fact, noises would be mingled with the background and undiscerned from the cracks. We believe that the effect of those holes is already projected in the global perspective of crack percentage (CIF). After all, the output was successfully demonstrated the different stages of crack evolution. Moreover, we could highlight the sharp crack distinction amongst treatments especially between intact and disturbed samples.

This observation (on holes) emphasizes as well the drawback of using disturbed samples in the laboratory to present crack occurrence in the agricultural field. The output of this study could serve correcting some extrapolating models founded on laboratory experiment. We encourage more experiments and analyses relating intact agricultural soil and disturbed samples. However, the finding may indicate the evolution of crack formation after time series tillage practices. From this perspective, disturbed samples (DS) indicate the period just after the tillage (plough), while undisturbed tilled (CTRO) and reduced tillage (RTRI) samples represent the soil state after one year and more than 4 years tillage, respectively. We could conclude that

crack formation is not linearly decreasing with tillage events. This finding invites multiple experiment to discern the moment of inflexion of crack formation.

3. Various ways to improve the methodology (by some modification and new suggestion)

The first improvement consists of standardizing the methodology for crack assessment. It is quite difficult to make comparison of cracking data unless the measurement techniques were performed identically. We argue in favour of unified measurement that would allow us to compare data, use them in modelling and confront them with the data from the field (ground truth). Nowadays, there are only few studies conducting laboratory study and observe the reality in the field. It renders obsolete all output from laboratory-based modelling.

The second improvement is to strengthen the quality of the study output. Possible ways to improve the accuracy of the output is to whether 1) increase the image resolution or 2) call for sophisticated material such as SEM, X-ray tomography. On one hand, increasing the resolution of the image will give more details about the crack characteristics but increase the amount of data and the time for data treatment. It may include however, some part of cracks which were omitted in our current resolution (very thin cracks < 5µm) as discussed in the dissertation. On the other hand, images from X-ray tomography would give simultaneously information on cracks and on soil macro/micropores in 3D instead of 2D. This was part of the study objective at the start of the project. However, the idea (concerning tomography) was aborted due to the fact that there is an inverse relationship between the image resolution and the sample size. Thus, a greater resolution around 400 µm was the maximum quality we can obtain from our sample size (20 cm x 25 cm). The resolution (voxel) could be reduced to 200µm x 200µm using the improved version of the scanner at Ghent University; however, the process is too expensive (>150 Euro/observation) while the resolution is not small enough to discern the average forming crack from the background. A better solution would consider smaller sample (size <5 cm) extracted from the bigger one. But this also will require sophisticated apparatus to keep the sample structure (addition of resin, use of sharp cutting tools, etc) intact. For the time being, it looks like we attain the optimum limit as far as crack analysis is concerned. However, there is great room for improvement since computer hardware and software are the more and more performing if we are not reciting the short-coming of super-computer and development of quantum-computer. Moreover, the improvement of cameras and X-ray tomography give more hope of new advanced technology at micro-nano-resolution. The limits in terms of sample scale could no longer be problematic in the near future.

Concerning crack analysis in the fields, there are many different suggestions (method and tools) which can be applied. The first one is the use of ground penetration radar (GPR) which is a non-destructive and indirect technique that uses electromagnetic pulses to map (in 3D) the soil different constituents. The soil map gives the reflections of different electromagnetic waves which are very sensitive to change in soil structure (macropore, and void) (Levatti et al., 2019). GPR is currently

used for estimating/detecting water content (Klotzsche et al., 2018), shrinkage, plant rooting structure (Stokes et al., 2002), and desiccation test (Levatti et al., 2019). Crack could be analysed using this method since the accuracy of the materials can go up to 1-2 mm wide (Tang et al., 2021). The second one is the use of electrical resistivity tomography (ERT). This method offers huge range of possibility starting from laboratory to field scale. Despite its main use in monitoring soil moisture regime (Chambers et al., 2010), some authors prove its utility as far as volume change and crack analysis is concerned (Jones et al., 2014). The third tool is the use of electromagnetic induction (EMI). This tool was not yet used for crack analysis; however, it has its potential to study cracks since it has been used in mapping soil salinity (Corwin and Lesch, 2005), clay content (Benedetto et al., 2010), and water content (Doolittle and Brevik, 2014).

Study on cracks should consider not only the soil structure as elaborated before (using X-ray scanning), but also the parameters which contribute to the formation of crack (i.e., parameters which affect the soil function). One of the most repeated factors in this study is the presence of roots in the intact samples. The roots are very important because they contribute to the stability and the strength of the soil. They can also bring store some elements (e.g., carbon) to the soil matrix. The importance of roots resides both on its overall quantity (in amount and size) and also in its structural pattern (architecture) in the soil. Previous study proves that roots have strong effect on soil stabilization and of crack formation and propagation (Azadegan et al., 2012; Hudek et al., 2017). Roots increase the soil strength and limit the crack development (Li et al., 2016a). Grass species were found decreasing the crack density by 20% (Azadegan et al., 2012) . Roots can be observed using X-ray scanning but also with other tools such as GPR as mentioned above (Stokes et al., 2002).

Last but not least, concerning the use of model to simulate soil drying and water evaporation. The used model in this study simulates adequately the drying of the Luvisol due to the fact that model takes account of thermo-hydro-mechanical conditions. However, this model can be improved by simulating the drying from 2D to 3D boundary condition. This will consider the variability in terms of soil porosity distribution. The 3D pore information can be obtained from scanning the soil using X-ray tomography. For sure, this will require stronger computer (a super computer) due to significant increase of calculation time. Moreover, crack should be considered in the simulation as well since this is the core of the study. The study should be similar to the work of Tran et al., (2019) but in 3D. According to Matsubara et al., (2016), it is possible to simulate soil desiccation shrinkage/cracking using a three-dimensional finite element model.

4. Discussions and perspective on the interaction between crack formation and the soil hydrodynamic

Concerning the interaction between crack formation and the soil hydrodynamic, it is important to affirm that the influences can go to both directions. In one hand, the drying process induced crack formation when a threshold is reached. This part was

observed when the study correlates water suction/content and crack formation. The output of the study showed a strong positive relationship between soil hydrology and crack variables. The tensiometer reading could go up to 500 kPa (pF 3.5) which was significantly higher compared to other study (Hyprop, with maximum around 200kPa). This was due to the fact that special attention was made during the tensiometer preparation. For instance, we made sure that the vacuum tube was hermetic enough to avoid air entering the system during degassing of water and materials (tensiometer, tubes). This was performed by covering the system with glue. Moreover, the time for removing gas (under vacuum) was extended from 48h to more than 72hours. This assures the total gas removal in the system. Last but not least, we proceeded to a further degassing process when filling the tube close to (around) the sensor. This degassing process consists of exerting strong negative pressure to water inside syringe and removing gas by tapping the syringe. This procedure was inspired from Hyprop ® device preparation.

As a result, most part of the crack formation in DS could be correlated well with the suction reading. Moreover, the tensiometer cavitate only when most part of the cracks was visible for the case of undisturbed sample (RTRI and CTRO). We advise however the use of solid apparatus which could stand stronger suction (e.g., using pressure chamber (-1500 kPa< h < -10 kPa), vapour pressure chamber (h < -1500 kPa), etc) when dealing with cracks especially for intact agricultural samples. Indeed, special care should be added during crack monitoring.

The result output could show distinct periods during soil evaporation. We could even spot the effect of cracks on soil evaporation. All crack parameters (CIF, width, length) were found to be correlated to soil hydraulic properties. More data from similar studies will give precious tools to predict accurately the soil hydrodynamic just by observing cracks. It was observed however that soil structure is also important (e.g., RTRI Vs. CTRO) for water evaporation, for example. Therefore, a combination of soil structural (Ks, SWRC, etc) and crack characteristics will improve a predicting model. The attempt on relating the occurrence of crack and the SWRC was successful. Indeed, crack formation was able to modify the trend of the curve as far as DS and RTRI were concerned. This was observed by the formation of bimodal curves and higher extrapolated macropore above 500µm.This points out the importance of cracks in predicting water retention curve both for disturbed and undisturbed samples. This emphasizes as well the need for 3D sample analysis in order to observe the change of soil structural characteristics during cracks formation. An attempt for structural monitoring was made from the soil surface. The results could not be interpreted due to need of special programming skills to extract and analyse the data. We could observe however that there was strong structural change (shrinkage) for DS before the appearing of cracks, explaining the crack influence on SWRC before they appear on the surface.

5. Discussions and perspective on the use of mucilage to control cracks

The idea of controlling cracks with mucilage come from the fact that mucilage acts like a glue in the rhizosphere. The literature reveals that mucilages can augment the soil tensile strength/toughness, and inter-particle bond while keep the soil structure after several wet-and-drying cycles. They contribute to the soil aggregate-formation, microbial growth, water/nutrients uptakes, and plant-soil-atmosphere interaction. Until this day, we did not find any agricultural study using mucilage in order to control cracks. Therefore, our challenge was to find the right substances and the right quantity. First of all, the substance was selected from few studies which worked on soil stability (with mucilage) upon drying-wetting cycle. We decided as well to choose readily available substances and efficient in holding soil particles together. We planned to extract mucilage from chia seed since the substance was commonly used as equivalent to root exudate. However, the mucilage extraction is still a debate among researcher (cold Vs warm, rotating Vs filtrating) and it is difficult to guess its equivalence to other dry product (substance). Therefore, we selected three products (Xanthan, Tragacanth, and Chitosan) out of the study of Caesar-Tonthat (2002), Galloway et al. (2018) which are readily available from the market and seem adequate (powder) to the study. After all, this is just the beginning of the assessment; further studies are invited to inquire more products and parameters which may have importance in the agricultural environment. Though, this research tries to obtain the optimum information concerning the interaction between mucilage and cracks. For that matter, deep assessment was conducted in terms of crack observation/characterisation, and soil hydraulic behaviour thanks to previous topic which covered already all the processing component. We agree that the technique we use was not perfect (possible leak of heat, and disturbed sample); however, it gives important information on how mucilage addition could control cracks. The objective was not to find substance that stops cracking completely (as crack may have also positive effect in agriculture), but rather avert excess cracking. At this stage, the exact process on how to apply the mucilage in the field was not investigated. This invites more research on how the mucilage behaviour will be adapted and change with time in the field. Due to limited time frame, the current research is also limited to disturbed sample. As mentioned in the previous chapter, soil structure is very important for crack analysis. However, reference samples were added in the study in order to help us to compare the results with the previous topic without addition of mucilage (disturbed and undisturbed samples).

The result output revealed that rhizospheric substances exert principally two contradictory effects on the physical property of the soil. They could increase the particle cohesion and at the same time (they) swallow water and expand upon wetting. This last property is the very reason why clayed soil expands and cracks. The effect on crack depends therefore on the ratio between the two properties. For instance, when the cohesion forces are not affected much by the expansion, cracking is limited (case of Xanthan). The inverse case is also possible when the soil expands but could not cohere particles upon drying; then the cracking could get even larger than the

reference (e.g., Chitosan and Tragacanth at low quantity less than 1.8 mg/kg soil). In the absence of both properties, mucilage has no effect on cracking (e.g., Chitosan at low quantity). The result on soil hydrology shows the capacity of mucilage to hold water that could influence the SWRC. This study could not analyze the effect of mucilage on SWRC due to limited time. However, as we discussed earlier, the ability of mucilage to hold water has an effect of delaying crack formation and development. Moreover, it will alleviate the negative effect of cracks on water evaporation. The result output reveals as well decreasing effect of temperature on crack formation. The mucilage application seems having stronger effect on reducing crack formation.

6. General conclusion

Crack formation is an important process which can impact the soil function (water recycling, storage, etc). The overall objective of this study is to monitor the process of desiccation cracking, associate this process with the soil water retention and evaporation, and then find appropriate method to alleviate the effect of cracks on soil function.

Firstly, the soil desiccation cracking was monitored (at 25°C) under laboratory set-up using undisturbed samples (RTRI and CTRO) and disturbed samples. Cracks evolution was assessed through series of image recording, image processing and analysis (using ImageJ, and PCAS). The results show that:

- Assessing crack under undisturbed sample (NDS) requires more steps in the image analysis since there are too much noise in the images (background) especially when the soils are wet. The proposed method in this study is the use of ROI in order to remove the background noise. The use of ROI is not compulsory for DS; however, for the sake of uniformity, this method is also applied for DS.

- Cracks (length and area) measured on DS are significantly higher (6 times) than on NDS (RTRI and CTRO) despite the delay of crack initiation in DS. Crack length and area are higher in DS>> RTRI > CTRO. We assume soil structure, soil organic/fibre content as the main elements controlling cracks in this study. The difference between DS and NDS is stronger than the difference among the NDS (CTRO and RTRI).

Secondly, when observing the interaction between cracks and soil hydrodynamic, it is concluded that:

- There is strong influence of soil suction and water content on crack formation. Starting from its initiation, crack initiation in DS requires stronger suction (>100 kPa) and lower water content (< 30 %) compared to NDS. The interaction crack-suction is in linear relationship for both DS and NDS. Since cracks rise faster in DS, the correlation crack-suction is limited to lower suction (300 kPa) compared to NDS (> 15 000 kPa). The fast crack expansion after its initiation in DS illustrates the lack of sample structure, and lack of frictional materials (fibres, coarse material). As consequence, DS absorb water, swell/shrink easily creating larger and thicker cracks.

- For NDS, crack fast expansion coincides with the end of the constant evaporation rate period: (CRP) and the time to reach the critical water content. The general pattern

of evaporation curve (as the Krisher's curve) shows that DS does not present CRP. Therefore, the soil permeability (and evaporation) seems related to the pore size >50 µm and likely the appearance of cracks at lower suction (<100 kPa).

- It was difficult to make a connection between cracks and the SWRC due to the fact that full grown crack appears late (>100 kPa) in the curve. This is valid even for the undisturbed samples (for CTRO and DS). However, the new forming crack change the pore size distribution of the samples. By combining the pore size distribution before and after crack formation, it was found that crack influences the SWRC subsequent to dryings.

Thirdly, by looking for an ecological mean for controlling crack using mucilages, the results conclude that:

- Not all mucilage presents the same effect (on drying and cracks) at different amount and during increasing temperature. For instance, when the soil is mixed with Tragacanth (TRA) and Xanthan (XAN), its capacity to absorb water increased from 50 % (in reference soil: REF) to 75-80 %. This is not the case for soil treated with chitosan (CHI); which is oversaturated beyond 50 % of Wc. This water excess is presented in the curve as high-water evaporation before CRP.

- At a rate of 3.6g/kg of soil, XAN and TRA could reduce significantly the rate of cracking and postpone the initiation of cracks. Those two mucilages reduce as well the crack disorder (i.e., high entropy) and the fractal dimension.

- On one hand, Xan presents certain stability in terms of efficiency (from controlling cracks) compared to TRA when the mucilage drops to 0.9g/kg soil. On the other hand, the effect of CHI is very similar to the one of REF at different amount. This could indicate that the quantity of CHI needs to be increased to control cracks.

- The efficiency (reduction of cracks) of XAN and TRA continue to take place when the temperature is raised from 25 °C to 50 °C. The opposite scenario happens for CHI and REF showing and increasing of the forming cracks with temperature.

Therefore, we can conclude that despite certain imperfection, challenge and difficulty encountered during the research study (Covid, research of materials and new methodology, change of certain objective etc) as discussed and presented in the perspective; the chosen methodology could bring adequate crack information from the samples. However, deeper and automated analyses need to be adopted in order to avoid errors during manual manipulation. Manual procedure can be biased based on end-user appreciation. Use of sophisticated tools such as X-ray tomography can unveil important pore and crack properties in 3 dimensions. This will give more information on the correlation between SWRC and cracks progression. Other analysis such as column experiment is also important to observe the direct effect of crack on water infiltration and pollutant transport. The chosen treatment (DS and NDS) could be well differentiated in terms of crack formation as well as hydraulic parameters. However, this study calls for field experimentation and consideration of other agricultural practices (Tillage + residue, type of organic amendment, types and amount of tillage etc). The current research manages as well to propose ways to deal with crack by the help of three types of mucilages (Chitosan, Tragacanth and Xanthan). However, it is known that there are many other types of mucilages in the agricultural fields.

Therefore, it is also important to know how they perform (individually or interaction) on cracks; moreover, how long they keep their efficiency in the field? Therefore, this study opens doors for many future research topics: improvement of the methodology, assessment of other crack factor/parameters related to SWRC and evaporation, use of other types (or quantity) of mucilage, assessment of mucilage in the field and for longer time frame, etc.

References

Acharya, R., Pedarla, A., Bheemasetti, T. V., Puppala, A.J., 2017. Assessment of Guar Gum Biopolymer Treatment toward Mitigation of Desiccation Cracking on Slopes Built with Expansive Soils | Enhanced Reader. J. Transp. Res. Board 2657, 78–88. https://doi.org/http://dx.doi.org/10.3141/2657-09

Aguilar Torres, M.A., De Luna Armenteros, E., Ordóñez Fernández, R., González Fernández, P., 2004. Digital image analysis for the estimation of cracked areas and the soil shrinkage characteristic curve in clay soils amended with composted sewage sludge. Spanish J. Agric. Res. 2, 473–479. https://doi.org/10.5424/sjar/2004023-101

Al-Awsi, M., Abbas, I., Hassan, A., 2015. 3D Electrical Resistivity Tomography Method for Simulating of Polygonal Soil Cracks. Int. J. Sci. Eng. Res. 6, 155–160.

Al-Dakheeli, H., Bulut, R., Clarke, C.R., Nevels, J.B., 2018. Hydro-mechanical analysis of crack initiation in expansive soils, in: Geotechnical Special Publication. Ascelibrary, Dallas, Texas, pp. 332–340. https://doi.org/10.1061/9780784481707.033

Al-Jeznawi Marcelo Sanchez Abbas Al-Taie, D.J., 2021. Using Image Analysis Technique to Study the Effect of Boundary and Environment Conditions on Soil Cracking Mechanism. Geotech. Geol. Eng. 39, 25–36. https://doi.org/10.1007/s10706-020-01376-5

Al-Taie, A., Disfani, M.M., Evans, R., Arulrajah, A., Horpibulsuk, S., 2016. Swell-shrink Cycles of Lime Stabilized Expansive Subgrade. Procedia Eng. 143, 615–622. https://doi.org/10.1016/J.PROENG.2016.06.083

Albrecht, B.A., Benson, C.H., 2001. Effect of Desiccation on Compacted Natural Clays. J. Geotech. Geoenvironmental Eng. 127, 67–75. https://doi.org/10.1061/(ASCE)1090-0241(2001)127:1(67)

Alwahab, R.M., Alqedra, M., 1995. Using Fibres to Reduce Tension Cracks and Shrink/Swell Cycles in a Compacted Clay. Proc. Spec. Conf. Geotech. Pract. Waste Disposal, Volume: 1, Number: 2.

An, N., Hemmati, S., Cui, Y.-J., Tang, C.-S., 2018. Numerical investigation of water evaporation from Fontainebleau sand in an environmental chamber. Eng. Geol. 234, 55–64. https://doi.org/10.1016/j.enggeo.2018.01.005

An, N., Tang, C.S., Cheng, Q., Wang, D.Y., Shi, B., 2020. Application of electrical resistivity method in the characterization of 2D desiccation cracking process of clayey soil. Eng. Geol. 265, 105416. https://doi.org/10.1016/j.enggeo.2019.105416

Atique, A., Sanchez, M., 2011. Analysis of cracking behavior of drying soil. Int. Conf. Environ. Sci. Technol. 1, 66–70.

Auvray, R., Rosin-Paumier, S., Abdallah, A., Masrouri, F., 2014. Quantification of soft soil cracking during suction cycles by image processing. Eur. J. Environ. Civ. Eng. 18, 11–13. https://doi.org/10.1080/19648189.2013.840250

Azadegan, O., Kaffash, E.A., Yaghoubi, M.J., Pourebrahim, G.., 2012. (PDF) Laboratory Study on the Swelling, Cracking and Mechanical Characteristics of the Palm Fiber Reinforced Clay. Electron. J. Geotech. Eng. 17, 47–54.

Baer, J.U., Kent, T.F., Anderson, S.H., 2009. Image analysis and fractal geometry to characterize soil desiccation cracks. Geoderma 154, 153–163. https://doi.org/10.1016/j.geoderma.2009.10.008

Benedetto, D. de, Castrignanò, A., Sollitto, D., Modugno, F., 2010. Spatial relationship between clay content and geophysical data. Clay Miner. 45, 197–207. https://doi.org/10.1180/CLAYMIN.2010.045.2.197

Bernstein, L., Bosch, P., Canziani, O., Chen, Z., Christ, R., Davidson, O., Hare, W., Huq, S., Karoly, D., Kattsov, V., Kundzewicz, Z., Liu, J., Lohmann, U., Manning, M., Matsuno, T., Menne, B., Metz, B., Mirza, M., Nicholls, N., Nurse, L., Pachauri, R., Palutikof, J., Parry, M., Qin, D., Ravindranath, N., Reisinger, Andy, Ren, J., Riahi, K., Rosenzweig, C., Rusticucci, M., Sch-Neider, S., Sokona, Y., Solomon, S., Stott, P., Stouffer, R., Sugiyama, T., Swart, R., Tirpak, D., Vogel, C., Yohe, G., Pachauri, R.K., Reisinger, A, Nottage, R., Madan, P., 2007. Climate Change 2007 Synthesis Report. Geneva, Switzerland.

Bishop, A.W., 1960. The principle of effective stress, in: Teknisk Ukeblad 39. Norges Geotekniske Institutes, Oslo, pp. 859–863.

Boivin, P., Schäffer, B., Temgoua, E., Gratier, M., Steinman, G., 2006. Assessment of soil compaction using soil shrinkage modelling: Experimental data and perspectives. Soil Tillage Res. 88, 65–79. https://doi.org/10.1016/J.STILL.2005.04.008

Bordoloi, S., Gopal, P., Boddu, R., Wang, Q., Cheng, Y.F., Garg, A., S, S., 2019. Soil-biochar-water interactions: Role of biochar from Eichhornia crassipes in influencing crack propagation and suction in unsaturated soils. J. Clean. Prod. 210, 847–859. https://doi.org/10.1016/J.JCLEPRO.2018.11.051

Braudeau, E., Frangi, J.-P., Mohtar, R.H., 2004. Characterizing Nonrigid Aggregated Soil–Water Medium Using its Shrinkage Curve. Soil Sci. Soc. Am. J. 68, 359–370. https://doi.org/10.2136/SSSAJ2004.3590

Brax, M., Buchmann, C., Schaumann, G.E., 2017. Biohydrogel induced soil–water interactions: how to untangle the gel effect? A review. J. Plant Nutr. Soil Sci. 180, 121–141. https://doi.org/10.1002/JPLN.201600453

Bronick, C.J., Lal, R., 2004. Soil structure and management: a review. Geoderma 124, 3–22. https://doi.org/10.1016/j.geoderma.2004.03.005

Bronswijk, J.J.B., 1991. Relation between Vertical Soil Movements and Water-Content Changes in Cracking Clays. Soil Sci. Soc. Am. J. 55, 1220–1226. https://doi.org/10.2136/SSSAJ1991.03615995005500050004X

Caesar-Tonthat, T.C., 2002. Soil binding properties of mucilage produced by a basidiomycete fungus in a model system. Mycol. Res. 106, 930–937. https://doi.org/10.1017/S0953756202006330

Cardoso, R., Pires, I., Duarte, S.O.D., Monteiro, G.A., 2018. Effects of clay's chemical interactions on biocementation. Appl. Clay Sci. 156, 96–103.

https://doi.org/10.1016/j.clay.2018.01.035

Chaduvula, U., Viswanadham, B.V.S., Kodikara, J., 2017. A study on desiccation cracking behavior of polyester fiber-reinforced expansive clay. Appl. Clay Sci. 142, 163–172. https://doi.org/10.1016/j.clay.2017.02.008

Chambers, J.E., Wilkinson, P.B., Weller, A., Meldrum, P.I., Kuras, O., Ogilvy, R.D., Aumonier, J., Bailey, E., Griffiths, N., Matthews, B., Penn, S., Wardrop, D., 2010. Characterising sand and gravel deposits using electrical resistivity tomography (ERT) : case histories from England and Wales , in: Hunger, E., Walton, G. (Eds.), 16th Extractive Industry Geology Conference. Extractive Industry Geology Conference, University of Portsmouth , pp. 166–172.

Chang, C.-C., Cheng, D.-H., 2018. Predicting the soil water retention curve from the particle size distribution based on a pore space geometry containing slit-shaped spaces. Hydrol. Earth Syst. Sci. 22, 4621–4632. https://doi.org/10.5194/hess-22-4621-2018

Chang, I., Im, J., Kharis Prasidhi, A., Cho, G.-C., 2015. Effects of Xanthan gum biopolymer on soil strengthening. Constr. Build. Mater. 74, 65–72. https://doi.org/10.1016/j.conbuildmat.2014.10.026

Chartin, C., Stevens, A., Goidts, E., Krüger, I., Carnol, M., Van Wesemael, B., 2016. Mapping Soil Organic Carbon stocks and estimating uncertainties at the regional scale following a legacy sampling strategy (Southern Belgium, Wallonia). https://doi.org/10.1016/j.geodrs.2016.12.006

Chen, Z., Ti, J., Chen, F., 2017. Soil aggregates response to tillage and residue management in a double paddy rice soil of the Southern China. Nutr. Cycl. Agroecosystems 109, 103–114. https://doi.org/10.1007/s10705-017-9864-8

Cheng, Q., Tang, C.-S., Zeng, H., Zhu, C., An, N., Shi, B., 2020. Effects of microstructure on desiccation cracking of a compacted soil. Eng. Geol. 265, 105418. https://doi.org/10.1016/j.enggeo.2019.105418

Cochrane, B.H.W., Reichert, J.M., Eltz, F.L.F., Norton, L.D., 2005. Controlling soil erosion and runoff with polyacrylamide and phosphogypsum on subtropical soil. Trans. Am. Soc. Agric. Eng. 48, 149–154. https://doi.org/10.13031/2013.17958

Collin, F., Li, X.L., Radu, J.P., Charlier, R., 2002. Thermo-hydro-mechanical coupling in clay barriers. Eng. Geol. 64, 179–193. https://doi.org/https://doi.org/10.1016/S0013-7952(01)00124-7

Consoli, N.C., Arcari Bassani, M.A., Festugato, L., 2010. Effect of fiber-reinforcement on the strength of cemented soils. Geotext. Geomembranes 28, 344–351. https://doi.org/10.1016/J.GEOTEXMEM.2010.01.005

Cornelis, W.M., Corluy, J., Medina, H., Díaz, J., Hartmann, R., Van Meirvenne, M., Ruiz, M.E., 2006. Measuring and modelling the soil shrinkage characteristic curve. Geoderma 137, 179–191. https://doi.org/10.1016/j.geoderma.2006.08.022

Corte, A.E., Higashi, A. 1922-, 1960. Experimental research on desiccation cracks in soil, This Digital Resource was created from scans of the Print Resource. U.S. Army Snow, Ice, and Permafrost Research Establishment., Illinois.

Corwin, D.L., Lesch, S.M., 2005. Apparent soil electrical conductivity measurements in agriculture. Comput. Electron. Agric. 46, 11–43. https://doi.org/10.1016/j.compag.2004.10.005

costa, S., Kodikara, J., Shannon, B.N., 2013. Salient factors controlling desiccation cracking of clay in laboratory experiments. Geotechnique 63, 18–29. https://doi.org/10.1680/geot.9.P.105

Coumans, W.J., 2000. Models for drying kinetics based on drying curves of slabs. Chem. Eng. Process. 39, 53–68.

Coussy, O.P., Brisard Volume, S., 2009. Prediction of drying shrinkage beyond the pore isodeformation assumption . J. Mech. Mater. Struct. 4, 263–279.

Dang, L.C., Fatahi, B., Khabbaz, H., 2016. Behaviour of Expansive Soils Stabilized with Hydrated Lime and Bagasse Fibres. Procedia Eng. 143, 658–665. https://doi.org/10.1016/J.PROENG.2016.06.093

Daraghmeh, O.A., Jensen, J.R., Petersen, C.T., 2009. Soil structure stability under conventional and reduced tillage in a sandy loam. Geoderma 150, 64–71. https://doi.org/10.1016/j.geoderma.2009.01.007

DeCarlo, K.F., Caylor, K.K., 2019. Biophysical effects on soil crack morphology in a faunally active dryland vertisol. Geoderma 334, 134–145. https://doi.org/10.1016/j.geoderma.2018.07.042

Decarlo, K.F., Shokri, N., 2014. Effects of substrate on cracking patterns and dynamics in desiccating clay layers. Water Resour. Res. 50, 3039–3051. https://doi.org/10.1002/2013WR014466

Degrune, F., Theodorakopoulos, N., Colinet, G., Hiel, M.P., Bodson, B., Taminiau, B., Daube, G., Vandenbol, M., Hartmann, M., 2017. Temporal dynamics of soil microbial communities below the seedbed under two contrasting tillage regimes. Front. Microbiol. 8, 1127. https://doi.org/10.3389/fmicb.2017.01127

Dejong, J.T., Fritzges, M.B., Nüsslein, K., 2006. Microbially Induced Cementation to Control Sand Response to Undrained Shear. J. Geotech. Geoenviron. Eng. 132, 1381–1392. https://doi.org/10.1061/ASCE1090-02412006132:111381

Demagistri, A., Ledesma, A., Cordero, J., Jacinto, A., 2018. Effects of compaction on desiccation cracking of clayey soils, in: Unsaturated Soils: UNSAT 2018 (Ed.), The 7th International Conference on Unsaturated Soils. The Hong Kong University of Science and Technology (HKUST), pp. 1273–1278.

Doolittle, J.A., Brevik, E.C., 2014. The use of electromagnetic induction techniques in soils studies. Geoderma 223–225, 33–45. https://doi.org/10.1016/j.geoderma.2014.01.027

Drumm, E.C., Boles, D.R., Wilson, G. V, 1997. Desiccation Cracks Result in Preferential Flow. Geotech. News, Vancouver 15, 22–26.

Durner, W., 1994. Hydraulic conductivity estimation for soils with heterogeneous pore structure. Water Resour. Res. 30, 211–223. https://doi.org/10.1029/93WR02676

Eberemu, A.O., Amadi, A.A., Sule, J., 2011. Desiccation Effect on Compacted Tropical Clay Treated with Rice Husk Ash. Geotech. Spec. Publ. 6, 45–64.

https://doi.org/10.1061/41165(397)122

Edil, T.B., Motan, S.E., 1979. Soil-Water Potential and Resilient Behavior of Subgrade Soils, in: 58th Annual Meeting of the Transportation Research Board. Transportation Research Board, Washington District of Columbia, United States, pp. 54–63.

Fang, H.-Y., Chaney, R.C., 2016. Shrinkage, Swelling, and Cracking Characteristics of Soil, in: Introduction to Environmental Geotechnology. CRC Press, p. 40. https://doi.org/10.1201/9781315374734

Fredlund, D.G., Bergan, A.T., Wong, P.K., Mcfarlane Brentnall, M., Kong, H., 1977. Relation Between Resilient Modulus and Stress Conditions for Cohesive Subgrade Soils. Transp. Res. Rec. 642, 73–81.

Fredlund, D.G., Houston, S.L., Nguyen, Q., Fredlund, M.D., 2010. Moisture movement through cracked clay soil profiles. Geotech. Geol. Eng. 28, 865–888. https://doi.org/10.1007/s10706-010-9349-x

Freibauer, A., Rounsevell, M.D.A., Smith, P., Verhagen, J., 2004. Carbon sequestration in the agricultural soils of Europe. Geoderma 122, 1–23. https://doi.org/10.1016/j.geoderma.2004.01.021

Gallipoli, D., Wheeler, S.J., Karstunen, M., 2003. Modelling the variation of degree of saturation in a deformable unsaturated soil. Geotechnique 53, 105–112.

Galloway, A.F., Pedersen, M.J., Merry, B., Marcus, S.E., Blacker, J., Benning, L.G., Field, K.J., Knox, J.P., 2018. Xyloglucan is released by plants and promotes soil particle aggregation. New Phytol. 217, 1128–1136. https://doi.org/10.1111/nph.14897

Gao, L., Becker, E., Liang, G., Houssou, A.A., Wu, H., Wu, X., Cai, D., Degré, A., 2017. Effect of different tillage systems on aggregate structure and inner distribution of organic carbon. Geoderma 288, 97–104. https://doi.org/10.1016/j.geoderma.2016.11.005

Gargiulo, L., Mele, G., Terribile, F., 2015. The role of rock fragments in crack and soil structure development: A laboratory experiment with a Vertisol. Eur. J. Soil Sci. 66, 757–766. https://doi.org/10.1111/ejss.12263

Gentile, A.R., Barceló-Cordón, S., Van Liedekerke, M., 2009. JRC Publications Repository - Soil Country Analyses - Belgium [WWW Document]. EUR 23959 EN/2. Luxemb. OP; 2009. JRC53315. https://doi.org/10.2788/27334

Gerard, P., Léonard, A., Masekanya, J.-P., Charlier, R., Collin, F., 2010. Study of the soil–atmosphere moisture exchanges through convective drying tests in non-isothermal conditions. Int. J. Numer. Anal. Methods Geomech. 34, 1297–1320. https://doi.org/10.1002/NAG.866

Gerard, P., Mahdad, M., Mccormack, A.R., François, B., 2015. A unified failure criterion for unstabilized rammed earth materials upon varying relative humidity conditions. Constr. Build. Mater. 95, 437–447. https://doi.org/10.1016/j.conbuildmat.2015.07.100

Ghavami, K., Toledo Filho, R.D., Barbosa, N.P., 1999. Behaviour of composite soil

reinforced with natural fibres. Cem. Concr. Compos. 21, 39–48. https://doi.org/10.1016/S0958-9465(98)00033-X

Guo, Y., Han, C., Yu, X.B., 2018. Laboratory characterization and discrete element modeling of shrinkage and cracking in clay layer. Can. Geotech. J. https://doi.org/10.1139/cgj-2016-0674

Gupta, S. Das, Mohanty, B.P., Köhne, J.M., 2006. Soil Hydraulic Conductivities and their Spatial and Temporal Variations in a Vertisol. Soil Sci. Soc. Am. J. 70, 1872–1881. https://doi.org/10.2136/SSSAJ2006.0201

Han, J., Gabr, M.A., 2002. Numerical analysis of geosynthetic-reinforced and pile-supported earth platforms over soft soil. J. Geotech. Geoenvironmental Eng. 128, 44–53.

Harianto, T., Hayashi, S., Du, Y.-J., Suetsugu, D., 2008. Effects of Fiber Additives on the Desiccation Crack Behavior of the Compacted Akaboku Soil as A Material for Landfill Cover Barrier. Water Air Soil Pollut 194, 141–149. https://doi.org/10.1007/s11270-008-9703-2

Haruna, G.Y., Gofar, N., 2012. Influence of evaporation on transient suction distribution in unsaturated soil. Int. J. Phys. Sci. 7, 508–518. https://doi.org/10.5897/IJPS11.1651

Hataf, N., Ghadir, P., Ranjbar, N., 2017. Investigation of soil stabilization using chitosan biopolymer. https://doi.org/10.1016/j.jclepro.2017.09.256

Hejazi, S.M., Sheikhzadeh, M., Abtahi, M., Zadhoush, A., 2012. A simple review of soil reinforcement by using natural and synthetic fibers. Constr. Build. Mater. 300, 100–116. https://doi.org/10.1016/j.conbuildmat.2011.11.045

Hubert, J., Plougonven, E., Prime, N., Léonard, A., Collin, F., 2018a. Comprehensive study of the drying behavior of Boom clay: Experimental investigation and numerical modeling. Int. J. Numer. Anal. Methods Geomech. 42, 211–230. https://doi.org/10.1002/NAG.2715

Hubert, J., Plougonven, E., Prime, N., Léonard, A., Collin, F., 2018b. Comprehensive study of the drying behavior of Boom clay: Experimental investigation and numerical modeling. Int. J. Numer. Anal. Methods Geomech. 42, 211–230. https://doi.org/10.1002/nag.2715

Hudek, C., Sturrock, C.J., Atkinson, B.S., Stanchi, S., Freppaz, M., 2017. Root morphology and biomechanical characteristics of high altitude alpine plant species and their potential application in soil stabilization. Ecol. Eng. 109, 228–239. https://doi.org/10.1016/J.ECOLENG.2017.05.048

Hulimka, J., Dawczyński, S., Krzywoń, R., 2019. Common thermal and shrinkage cracking of ceiling slabs. MATEC Web Conf. 284. https://doi.org/10.1051/matecconf/201928

Ikeagwuani, C.C., Nwonu, D.C., 2019. Emerging trends in expansive soil stabilisation: A review | Elsevier Enhanced Reader. J. Rock Mech. Geotech. Eng. 11, 423–440.

Inan Sezer, G., Ramyar, K., Karasu, B., Burak Göktepe, A., Sezer, A., 2008. Image

analysis of sulfate attack on hardened cement paste. Mater. Des. 29, 224–231. https://doi.org/10.1016/j.matdes.2006.12.006

Jayanthi, P.N. V., Singh, D.N., 2016. Utilization of Sustainable Materials for Soil Stabilization: State-of-the-Art. Adv. Civ. Eng. Mater. 5, 46–79. https://doi.org/10.1520/ACEM20150013

Jones, G., Sentenac, P., Zielinski, M., 2014. Desiccation cracking detection using 2-D and 3-D Electrical Resistivity Tomography: Validation on a flood embankment. J. Appl. Geophys. 106, 196–211. https://doi.org/10.1016/j.jappgeo.2014.04.018

Kan, Z.R., Ma, S.T., Liu, Q.Y., Liu, B.Y., Virk, A.L., Qi, J.Y., Zhao, X., Lal, R., Zhang, H.L., 2020. Carbon sequestration and mineralization in soil aggregates under long-term conservation tillage in the North China Plain. Catena 188, 104428. https://doi.org/10.1016/j.catena.2019.104428

Keey, R.B., Suzuki, M., 1974. On the characteristic drying curve. Int. J. Heat Mass Transf. 17, 1455–1464. https://doi.org/10.1016/0017-9310(74)90055-6

Khattak, M.J., Alrashidi, M., 2006. Durability and mechanistic characteristics of fiber reinforced soil-cement mixtures. Int. J. Pavement Eng. 7, 53–62. https://doi.org/10.1080/10298430500489207

Khelifi, H., Lecompte, T., Perrot, A., Ausias, G., 2015. Mechanical enhancement of cement-stabilized soil by flax fibre reinforcement and extrusion processing. Mater. Struct. 49, 1143–1156. https://doi.org/10.1617/S11527-015-0564-Z

Kleppe, J., Olson, R., 1985. Desiccation Cracking of Soil Barriers. Hydraul. Barriers Soil Rock 263-263–13. https://doi.org/10.1520/STP34583S

Klotzsche, A., Jonard, F., Looms, M.C., Van Der Kruk, J., Huisman, J.A., 2018. Measuring Soil Water Content with Ground Penetrating Radar: A Decade of Progress; Measuring Soil Water Content with Ground Penetrating Radar: A Decade of Progress. Vadose Zo. J. 17, 1–9. https://doi.org/10.2136/vzj2018.03.0052

Konrad, J.-M., Ayad, R., 1997. A idealized framework for the analysis of cohesive soils undergoing desiccation. Can. Geotech. J. 34, 477–488. https://doi.org/10.1139/T97-015

Kowalski, S.J., 2012. Thermomechanics of Drying Processes, Lecture Notes in Applied and Computational Mechanics. Springer Berlin Heidelberg, Berlin, Heidelberg.

Kowalski, S.J., 2003. Thermomechanics of Drying Processes, 1st ed. ed, Lecture Notes in Applied and Computational Mechanics. Springer Berlin Heidelberg, Berlin, Germany. https://doi.org/10.1007/978-3-540-36405-4

Kumar, M., Arora, V., 2015. Cracking in liner behavior and desiccation of compacted landfill liner soils - inpressco. Int. J. Curr. Eng. Technol. 5, 3921–3925.

Kutilek, M., 1996. “Water relations and water management of vertisols,” in Vertisols and Technologies for their Management, in: Ahmad, N., Mermut, A. (Eds.), Developments in Soil Science. Elsevier, pp. 201–230.

Lachenbruch, A.H., 1962. Mechanics of Thermal Contraction Cracks and Ice-Wedge Polygons in Permafrost. Spec. Pap. Geol. Soc. Am. 70, 1–65.

https://doi.org/10.1130/SPE70-P1

Lakshmikantha, M.R., Prat, P.C., Ledesma, A., 2018. Boundary Effects in the Desiccation of Soil Layers with Controlled Environmental Conditions. Geotech. Test. J. 41, 675–697. https://doi.org/10.1520/GTJ20170018

Lakshmikantha, M.R., Prat, P.C., Ledesma, A., 2009. Image analysis for the quantification of a developing crack network on a drying soil. Geotech. Test. J. 32, 505–515. https://doi.org/10.1520/GTJ102216

Le Bray, Y., Prat, M., 1999. Three-dimensional pore network simulation of drying in capillary porous media. Int. J. Heat Mass Transf. 42, 4207–4224. https://doi.org/https://doi.org/10.1016/S0017-9310(99)00006-X

Le Roux, S., Medjedoub, F., Dour, G., Rézaï-Aria, F., 2013. Image analysis of microscopic crack patterns applied to thermal fatigue heat-checking of high temperature tool steels. Micron 44, 347–358. https://doi.org/10.1016/j.micron.2012.08.007

Lehmann, P., Assouline, S., Or, D., 2008. Characteristic lengths affecting evaporative drying of porous media. Phys. Rev. E - Stat. Nonlinear, Soft Matter Phys. 77, 056309. https://doi.org/10.1103/PhysRevE.77.056309

Léonard, A., 2002. Étude du séchage convectif de boues de station d'épuration-suivi de la texture par microtomographie à rayons X. Université de Liège.

Léonard, A., Blacher, S., Marchot, P., Pirard, J.-P., Crine, & M., 2005. Convective Drying of Wastewater Sludges:Influence of Air Temperature, Superficial Velocity,and Humidity on the Kinetics. Dry. Technol. An Int. J. 23, 1667–1679. https://doi.org/10.1081/DRT-200065082

Levatti, H.U., Prat, P.C., Ledesma, A., 2019. Numerical and experimental study of initiation and propagation of desiccation cracks in clayey soils. Comput. Geotech. 105, 155–167. https://doi.org/10.1016/J.COMPGEO.2018.09.015

Li, J., Guo, L.B., Cai, C.Z., 2012. Influence of water content and soil type on soil cracking, in: The 2012 World Congress on Advances in Civil, Environmental, and Materials Research (ACEM' 12). Seoul, Korea, pp. 1543–1553.

Li, J., Tang, C., Wang, D., Pei, X., Shi, B., 2014. Effect of discrete fibre reinforcement on soil tensile strength. J. Rock Mech. Geotech. Eng. 6, 133–137. https://doi.org/10.1016/J.JRMGE.2014.01.003

Li, J.H., Li, L., Chen, R., Li, D.Q., 2016a. Cracking and vertical preferential flow through landfill clay liners. Eng. Geol. 206, 33–41. https://doi.org/10.1016/j.enggeo.2016.03.006

Li, J.H., Li, L., Chen, R., Li, D.Q., 2016b. Cracking and vertical preferential flow through landfill clay liners. Eng. Geol. 206, 33–41. https://doi.org/10.1016/j.enggeo.2016.03.006

Li, J.H., Zhang, L.M., 2011. Study of desiccation crack initiation and development at ground surface. Eng. Geol. 123, 347–358. https://doi.org/10.1016/j.enggeo.2011.09.015

Li, X., Zhang, K., 2018. Numerical analysis of drying process of soils using finite

volume method. Int. J. Pavement Res. Technol. 11, 813–818. https://doi.org/10.1016/j.ijprt.2018.06.005

Liu, B., Zhu, C., Tang, C.S., Xie, Y.H., Yin, L.Y., Cheng, Q., Shi, B., 2020. Bio-remediation of desiccation cracking in clayey soils through microbially induced calcite precipitation (MICP). Eng. Geol. 264, 105389. https://doi.org/10.1016/j.enggeo.2019.105389

Liu, C., Shi, B., Zhou, J., Tang, C., 2011. Quantification and characterization of microporosity by image processing, geometric measurement and statistical methods: Application on SEM images of clay materials. Appl. Clay Sci. 54, 97–106. https://doi.org/10.1016/j.clay.2011.07.022

Lloret, A., Ledesma, A., Lorenzo, R., Pacheco, R., Sanchez, M., 1998. Crack initiation in drying soils, in: Technical Committee of the Second International Conference on Unsaturated soils (Ed.), Proceedings of the Second International Conference on Unsaturated Soils. International Academic Publishers, Beijing, China, pp. 497–502.

Lomeling, D., Kenyi, M.C., Lodiong, M.A., Kenyi, M.S., Silvestro, G.M., Yieb, J.L.L., 2016. Characterizing dessication cracking of a remolded clay (eutric Vertisol) using the fractal dimension approach. Open J. Soil Sci. 6, 68–80. https://doi.org/10.4236/ojss.2016.64008

Lu, Y., Gu, K., Zhang, Y., Tang, C., Shen, Z., Shi, B., 2021. Impact of biochar on the desiccation cracking behavior of silty clay and its mechanisms. Sci. Total Environ. 794, 148608. https://doi.org/10.1016/j.scitotenv.2021.148608

Mallory, J.J., Mohtar, R.H., Heathman, G.C., Schulze, D.G., Braudeau, E., 2011. Evaluating the effect of tillage on soil structural properties using the pedostructure concept. Geoderma 163, 141–149. https://doi.org/10.1016/j.geoderma.2011.01.018

Marsico, A. Di, Scrano, L., Amato, M., Gàmiz, B., Real, M., Cox, L., 2017. Mucilage from seeds of chia (Salvia hispanica L.) used as soil conditioner; effects on the sorption-desorption of four herbicides in three different soils. Sci. Total Environ. 625, 531–538. https://doi.org/10.1016/j.scitotenv.2017.12.078

Marto, A., Othman, B.A., 2011. The Potential Use of Bamboo as Green Material for Soft Clay Reinforcement System, in: IPCBEE vol.8 (Ed.), International Conference on Environment Science and Engineering . IACSIT Press, Singapore, pp. 129–133.

Matsubara, H., Hirose, K., Edo, T., Tamanaha, K., Hara, H., Yamada, T., 2016. Numerical modelling of mudcrack growth. Japanese Geotech. Soc. Spec. Publ. 2, 1143–1147. https://doi.org/10.3208/JGSSP.ATC1-3-17

Merlin, O., Stefan, V., Amazirh, A., Chanzy, A., Ceschia, E., Er-Raki, S., Gentine, P., Tallec, T., Ezzahar, J., Bircher, S., Stefan, V.G., Beringer, J., Khabba, S., 2016. Modeling soil evaporation efficiency in a range of soil and atmospheric conditions using a meta-analysis approach. Water Resour. Res. 52, 3663–3684. https://doi.org/10.1002/2015WR018233ï

Mesri, G., Ali, S., 2002. Undrained shear strength of a glacial clay overconsolidated by desiccation | Enhanced Reader. Geotechnique 52, 65–69. https://doi.org/10.1680/geot.52.1.65.40827

Mihashi, H., Ahmed, S.F.U., Mizukami, T., Nishiwaki, T., 2006. Quantification of crack formation using image analysis and its relationship with permeability TT - Bauinstandsetzen und Baudenkmalpflege: eine internationale Zeitschrift. Restor. Build. Monum. an Int. J. = Bauinstandsetz. und Baudenkmalpfl. eine Int. Zeitschrift 12, 335–348.

Mishra, A.K., Dhawan, S., Rao, S.M., 2008. Analysis of swelling and shrinkage behavior of compacted clays. Geotech. Geol. Eng. 26, 289–298. https://doi.org/10.1007/S10706-007-9165-0

Mitchell, J.K., Asce, H.M., Santamarina, J.C., Asce, M., 2005. Biological Considerations in Geotechnical Engineering. J. Geotech. Geoenviron. Eng. 131, 1222–1233. https://doi.org/10.1061/ASCE1090-02412005131:101222

Morris, P.H., Graham, J., Williams, D.J., 1992. Cracking in drying soils. Can. Geotech. J. 29, 263–277. https://doi.org/10.1139/t92-030

Mousavi, S.F., Moazzeni, M., Mostafazadeh-Fard, B., Yazdani, M.R., 2012. Effects of Rice Straw Incorporation on Some Physical Characteristics of Paddy Soils. J. Agr. Sci. Tech 14, 1173–1183.

Mualem, Y., 1976. A new model for predicting the hydraulic conductivity of unsaturated porous media. Water Resour. Res. 12, 513–522. https://doi.org/10.1029/WR012i003p00513

Murray, H.H., 1991. Overview — clay mineral applications. Appl. Clay Sci. 5, 379–395. https://doi.org/10.1016/0169-1317(91)90014-Z

Nahlawi, H., Kodikara, J.K., 2006. Laboratory experiments on desiccation cracking of thin soil layers. Geotech. Geol. Eng. 24, 1641–1664. https://doi.org/10.1007/s10706-005-4894-4

Nandan, R., Singh, V., Singh, S.S., Kumar, V., Hazra, K.K., Nath, C.P., Poonia, S.P., Malik, R.K., Bhattacharyya, R., McDonald, A., 2019. Impact of conservation tillage in rice–based cropping systems on soil aggregation, carbon pools and nutrients. Geoderma 340, 104–114. https://doi.org/10.1016/j.geoderma.2019.01.001

Nasrallah, S. Ben, Perre, P., 1988. Detailed study of a model of heat and mass transfer during convective drying of porous media. Int. J. Heat Mass Transf. 31, 957–967. https://doi.org/10.1016/0017-9310(88)90084-1

Naveed, M., Brown, L.K., Raffan, A.C., George, T.S., Bengough, A.G., Roose, T., Sinclair, I., Koebernick, N., Cooper, L., Hallett, P.D., 2018. Rhizosphere-scale quantification of hydraulic and mechanical properties of soil impacted by root and seed exudates. Vadose Zo. J. 17, 1–12. https://doi.org/10.2136/vzj2017.04.0083

Nunes, M.R., Karlen, D.L., Moorman, T.B., 2020. Tillage Intensity Effects on Soil Structure Indicators-A US Meta-Analysis. Sustainability 12, 2071. https://doi.org/10.3390/su12052071

Omidbakhsh Amiri, E., Nayebzadeh, K., Amin Mohammadifar, M., 2015. Comparative studies of xanthan, guar and tragacanth gums on stability and rheological properties of fresh and stored ketchup. J. Food Sci. Technol. Vol. 52, 7123–7132. https://doi.org/10.1007/s13197-015-1837-9

Omidi, G.H., Prasad, T. V, Thomas, J.C., Brown, K.W., 1996. The influence of amendments on the volumetric shrinkage and integrity of compacted clay soils used in landfill liners. Water, Air, Soil Pollut. Vol. 96, 263–274.

Parvin, N., Beckers, E., Plougonven, E., Léonard, A., Degré, A., 2017. Dynamic of soil drying close to saturation: What can we learn from a comparison between X-ray computed microtomography and the evaporation method? Geoderma 302, 66–75. https://doi.org/10.1016/j.geoderma.2017.04.027

Peng, X., Horn, R., 2007. Anisotropic shrinkage and swelling of some organic and inorganic soils. - OceanRep. Eur. J. Soil Sci. 58, 98–107.

Peron, H., Hueckel, T., Laloui, L., Hu, L.B., 2009. Fundamentals of desiccation cracking of fine-grained soils: Experimental characterisation and mechanisms identification. Can. Geotech. J. 46, 1177–1201. https://doi.org/10.1139/T09-054

Pillai, R.R., Ayothiraman, R., 2012. An Innovative Technique of Improving the Soil Using Human Hair Fibers, in: Third International Conference on Construction In Developing Countries (ICCIDC–III). Bangkok, Thailand, pp. 428–434.

Poncelet, N., Herrier, G., François, B., 2021. An effective stress constitutive framework for the prediction of desiccation crack in lime-treated soil: Experimental characterization and constitutive prediction. Geomech. Energy Environ. 100265. https://doi.org/10.1016/j.gete.2021.100265

Poulos, S.J., 1971. The Stress-Strain Curve of Soils. Massachusetts.

Pourhosseini, R., Mossavi, M., Nassiri, N., 2017. Amirkabir Journal of Civil Engineering Influence of Temperature on Desiccation Cracking of Clay Soil. Civ. Eng 49, 161–64. https://doi.org/10.22060/ceej.2016.711

Pouya, A., Vo, T.D., Hemmati, S., Tang, A.M., Minh, A., 2019. Modeling soil desiccation cracking by analytical and numerical approaches. Int. J. Numer. Anal. Methods Geomech. 43, 738–763. https://doi.org/10.1002/nag.2887ï

Prabakar, J., Sridhar, R.S., 2002. Effect of random inclusion of sisal fibre on strength behaviour of soil. Constr. Build. Mater. 16, 123–131. https://doi.org/https://doi.org/10.1016/S0950-0618(02)00008-9

Prat, M., 1991. 2D modelling of drying of porous media: influence of edge effects at the interface. Dry. Technol. An Int. J. 9, 1181–1208. https://doi.org/10.1080/07373939108916748

Prat, P.C., Ledesma, A., Lakshmikantha, M.R., 2006. SIZE EFFECT IN THE CRACKING OF DRYING SOIL, in: Gdoutos E.E. (eds) (Ed.), Fracture of Nano and Engineering Materials and Structures. Springer, Dordrecht, pp. 1373–1374. https://doi.org/https://doi.org/10.1007/1-4020-4972-2_682

Prat, P.C., Ledesma, A., Lakshmikantha, M.R., Levatti, H., Tapia, J., 2008. Fracture Mechanics for Crack Propagation in Drying Soils, in: The 12th International Conference of International Association for Computer Methods and Advances in Geomechanics (IACMAG). IACMAG, Goa, India.

Prime, N., Housni, Z., Fraikin, L., Léonard, A., Charlier, R., Levasseur, S., 2014. On Water Transfer and Hydraulic Connection Layer During the Convective Drying

of Rigid Porous Material. Transp. Porous Media 106, 47–72. https://doi.org/10.1007/S11242-014-0390-8

Qi, W., Zhang, Zhan yu, Wang, C., Chen, Y., Zhang, Ze min, 2020. Crack closure and flow regimes in cracked clay loam subjected to different irrigation methods. Geoderma 358, 113978. https://doi.org/10.1016/j.geoderma.2019.113978

Qiang, X., Lu, H.-J., Li, Z.-Z., Lei, L., 2014. Cracking, water permeability and deformation of compacted clay liners improved by straw fiber. Eng. Geol. 178, 82–90. https://doi.org/10.1016/j.enggeo.2014.05.013

Rayhani, M.H.T., Yanful, E.K., Fakher, A., 2008. Physical modeling of desiccation cracking in plastic soils. Eng. Geol. 97, 25–31. https://doi.org/10.1016/j.enggeo.2007.11.003

Rayhani, M.H.T., Yanful, E.K., Fakher, A., 2007. Desiccation-induced cracking and its effect on the hydraulic conductivity of clayey soils from Iran. Can. Geotech. J. 44, 276–283. https://doi.org/10.1139/T06-125

Rieu, M., Sposito, G., 1991. Fractal Fragmentation, Soil Porosity, and Soil Water Properties: I. Theory. Soil Sci. Soc. Am. J. 55, 1231–1238. https://doi.org/10.2136/SSSAJ1991.03615995005500050006X

Rosenzweig, R., Shavit, U., Furman, A., 2012. Water Retention Curves of Biofilm-Affected Soils using Xanthan as an Analogue. Soil Sci. Soc. Am. J. 76, 61–69. https://doi.org/10.2136/SSSAJ2011.0155

Saravanan, Sachin, S., Ramesh, K., 2020. Study on the effect of porosity on crack propagation. Mater. Today Proc. 28, 825–829. https://doi.org/10.1016/j.matpr.2019.12.306

Saruchi, Kumar, V., Mittal, H., Alhassan, S.M., 2019. Biodegradable hydrogels of tragacanth gum polysaccharide to improve water retention capacity of soil and environment-friendly controlled release of agrochemicals. Technology. https://doi.org/10.1016/j.ijbiomac.2019.04.023

Sawangsuriya, A., Edil, T.B., Bosscher, P.J., 2009. Modulus-Suction-Moisture Relationship for Compacted Soils in Postcompaction State. J. Geotech. Geoenviron. Eng 135, 1390–1403. https://doi.org/10.1061/ASCEGT.1943-5606.0000108

Schäffer, B., Schulin, R., Boivin, P., 2013. Shrinkage Properties of Repacked Soil at Different States of Uniaxial Compression. Soil Sci. Soc. Am. J. 77, 1930–1943. https://doi.org/10.2136/SSSAJ2013.01.0035

Schäffer, B., Schulin, R., Boivin, P., 2008. Changes in shrinkage of restored soil caused by compaction beneath heavy agricultural machinery. Eur. J. Soil Sci. 59, 771–783. https://doi.org/10.1111/J.1365-2389.2008.01024.X

Scherer, G.W., 1990. Theory of Drying. J. Am. Ceram. Soc. 73, 3–14. https://doi.org/10.1111/J.1151-2916.1990.TB05082.X

Schlüter, S., Großmann, C., Diel, J., Wu, G.M., Tischer, S., Deubel, A., Rücknagel, J., 2018. Long-term effects of conventional and reduced tillage on soil structure, soil ecological and soil hydraulic properties. Geoderma 332, 10–19. https://doi.org/10.1016/j.geoderma.2018.07.001

Seki, K., 2007. SWRC fit – a nonlinear fitting program with a water retention curve for soils having unimodal and bimodal pore structure. Hydrol. Earth Syst. Sci. Discuss. 4, 407–437. https://doi.org/10.5194/hessd-4-407-2007

Şenol, A., 2012. Effect of fly ash and polypropylene fibres content on the soft soils. Bull. Eng. Geol. Environ. 2011 712 71, 379–387. https://doi.org/10.1007/S10064-011-0391-6

Shepidchenko, T., Zhang, J., Tang, X., Liu, T., Dong, Z., Zheng, G., Yang, L., 2020. Experimental study of the main controlling factors of desiccation crack formation from mud to shale. J. Pet. Sci. Eng. 194, 107414. https://doi.org/10.1016/j.petrol.2020.107414

Shin, H., Santamarina, J.C., 2011. Desiccation cracks in saturated fine-grained soils: particle-level phenomena and effective-stress analysis. Geotechnique 61, 961–972. https://doi.org/10.1680/geot.8.P.012

Shit, P.K., Bhunia, G.S., Maiti, R., 2015. Soil crack morphology analysis using image processing techniques. Model. Earth Syst. Environ. 1, 1–7. https://doi.org/10.1007/s40808-015-0036-z

Simaůnek, J.S., Jarvis, N.J., Van Genuchten, M.T., Gärdenäs, A., Brown, G.E., 2003. Review and comparison of models for describing non-equilibrium and preferential flow and transport in the vadose zone. J. Hydrol. 272, 14–35. https://doi.org/https://doi.org/10.1016/S0022-1694(02)00252-4

Smet, S., Plougonven, E., Leonard, A., Degré, A., Beckers, E., 2018. X-ray micro-CT: how soil pore space description can be altered by image processing. Vadose Zo. J. 17, 1–14. https://doi.org/10.2136/vzj2016.06.0049

Somasundaram, J., Lal, R., Sinha, N.K., Dalal, R., Chitralekha, A., Chaudhary, R.S., Patra, A.K., 2018. Cracks and potholes in Vertisols: characteristics, occurrence, and management, in: Advances in Agronomy. pp. 93–159. https://doi.org/10.1016/bs.agron.2018.01.001

Song, W.K., Cui, Y.J., 2020. Modelling of water evaporation from cracked clayey soil. Eng. Geol. 266, 105465. https://doi.org/10.1016/j.enggeo.2019.105465

Sridharan, A., Jayadeva, M.S., 1982. Double layer theory and compressibility of clays. Géotechnique 32, 133–144. https://doi.org/10.1680/GEOT.1982.32.2.133

Stokes, A., Fourcaud, T., Hruska, J., Cermak, J., Nadyezdhina, N., Nadyezhdin, V., Praus, L., 2002. An evaluation of different methods to investigate root system architecture of urban trees in situ: I. ground-penetrating radar. J. Arboric. 28, 1–10.

Stoops, G., Langohr, R., Ranst, E. Van, 2020. Micromorphology of soils and palaeosoils in Belgium. An inventory and meta-analysis. https://doi.org/10.1016/j.catena.2020.104718

Stull, R., 2011. Wet-Bulb Temperature from Relative Humidity and Air Temperature. J. Appl. Meteorol. Climatol. 50, 2267–2269. https://doi.org/10.1175/JAMC-D-11-0143.1

Style, R.W., Peppin, S.S.L., Cocks, A.C.F., 2011. Mud peeling and horizontal crack formation in drying clays. J. Geophys. Res 116, 1025.

https://doi.org/10.1029/2010JF001842

Taallah, B., Guettala, A., Guettala, S., Kriker, A., 2014. Mechanical properties and hygroscopicity behavior of compressed earth block filled by date palm fibers. Constr. Build. Mater. 59, 161–168. https://doi.org/10.1016/j.conbuildmat.2014.02.058

Tan, H., Chen, F., Chen, J., Gao, Y., 2019. Direct shear tests of shear strength of soils reinforced by geomats and plant roots. Geotext. Geomembranes 47, 780–791. https://doi.org/10.1016/j.geotexmem.2019.103491

Tang, C., Shi, B., Liu, C., Zhao, L., Wang, B., 2008. Influencing factors of geometrical structure of surface shrinkage cracks in clayey soils. Eng. Geol. 101, 204–217. https://doi.org/10.1016/j.enggeo.2008.05.005

Tang, C.S., Cheng, Q., Leng, T., Shi, B., Zeng, H., Inyang, H.I., 2020. Effects of wetting-drying cycles and desiccation cracks on mechanical behavior of an unsaturated soil. CATENA 194, 104721. https://doi.org/10.1016/J.CATENA.2020.104721

Tang, C.S., Cui, Y.J., Shi, B., Tang, A.M., Liu, C., 2011a. Desiccation and cracking behaviour of clay layer from slurry state under wetting-drying cycles. Geoderma 166, 111–118. https://doi.org/10.1016/j.geoderma.2011.07.018

Tang, C.S., Cui, Y.J., Tang, A.M., Shi, B., 2010. Experiment evidence on the temperature dependence of desiccation cracking behavior of clayey soils. Eng. Geol. 114, 261–266. https://doi.org/10.1016/j.enggeo.2010.05.003

Tang, C.S., Shi, B., Liu, C., Suo, W. Bin, Gao, L., 2011b. Experimental characterization of shrinkage and desiccation cracking in thin clay layer. Appl. Clay Sci. 52, 69–77. https://doi.org/10.1016/j.clay.2011.01.032

Tang, C.S., Zhu, C., Cheng, Q., Zeng, H., Xu, J.J., Tian, B.G., Shi, B., 2021. Desiccation cracking of soils: A review of investigation approaches, underlying mechanisms, and influencing factors. Earth-Science Rev. 216, 103586. https://doi.org/10.1016/J.EARSCIREV.2021.103586

Tay, Y.Y., Stewart, D.I., Cousens, T.W., 2001. Shrinkage and desiccation cracking in bentonite-sand landfill liners. Eng. Geol. 60, 263–274.

Terzaghi, K., 1943. Theoretical Soil Mechanics, Theoretical Soil Mechanics. John Wiley & Sons, Inc., London,. https://doi.org/10.1002/9780470172766

Tollenaar, R.N., van Paassen, L.A., Jommi, C., 2017. Observations on the desiccation and cracking of clay layers. Eng. Geol. 230, 23–31. https://doi.org/10.1016/j.enggeo.2017.08.022

Tran, D.K., Ralaizafisoloarivony, N., Charlier, R., Mercatoris, B., Léonard, A., Toye, D., Degré, A., 2019. Studying the effect of desiccation cracking on the evaporation process of a Luvisol – From a small-scale experimental and numerical approach. Soil Tillage Res. 193, 142–152. https://doi.org/10.1016/j.still.2019.05.018

Vail, M., Zhu, C., Tang, C.-S., Maute, N., Tababa, M., Lomboy, M.-, 2020. TRR Desiccation Cracking Behavior of Clayey Soils Treated with Biocement and Bottom Ash Admixture during Wetting-Drying Cycles. Transp. Res. Rec. 2674, 441–454. https://doi.org/10.1177/0361198120924409

Valadez-Gonzalez, A., Moreno-Chulim, M. V., Herrera-Franco, P.J., 2009. Modification of the fibre surface for the optimisation of mechanical properties in natural-fibre reinforced polymers. Int. J. Mater. Prod. Technol. 36, 417–430. https://doi.org/10.1504/IJMPT.2009.027846

van Genuchten, M.T., 1980. A Closed-form Equation for Predicting the Hydraulic Conductivity of Unsaturated Soils. Soil Sci. Soc. Am. J. 44, 892–898. https://doi.org/10.2136/sssaj1980.03615995004400050002x

Vanapalli, S.K., Fredlund, D.G., Pufahl, D.E., Clifton, A.W., 1996. Model for the prediction of shear strength with respect to soil suction. Can. Geotech. J. 33, 379–392. https://doi.org/10.1139/T96-060

Vo, T.D., Pouya, A., Hemmati, S., Tang, A.M., 2017. Numerical modelling of desiccation cracking of clayey soil using a cohesive fracture method. Comput. Geotech. 85, 15–27. https://doi.org/10.1016/j.compgeo.2016.12.010

Vogel, H.-J., Hoffmann, H., Roth, K., 2005. Studies of crack dynamics in clay soil I. Experimental methods, results, and morphological quantification. Geoderma 125, 203–211. https://doi.org/10.1016/j.geoderma.2004.07.009

Wakao, N., Yagi, S., Yagi, ; S, Kunii, D., 1968. On the mechanism of drying of granular beds. J. Chem. Eng. Japan 1, 26–31.

Wan, Y., Wu, C., Xue, Q., Hui, X., 2019. Effects of plastic contamination on water evaporation and desiccation cracking in soil. Sci. Total Environ. 654, 576–582. https://doi.org/10.1016/j.scitotenv.2018.11.123

Wang, L.L., Tang, C.S., Shi, B., Cui, Y.J., Zhang, G.Q., Hilary, I., 2018. Nucleation and propagation mechanisms of soil desiccation cracks. Eng. Geol. 238, 27–35. https://doi.org/10.1016/j.enggeo.2018.03.004

Wang, M., Pande, ; G N, Kong, ; L W, Feng, Y.T., 2016. Comparison of Pore-Size Distribution of Soils Obtained by Different Methods. https://doi.org/10.1061/(ASCE)GM.1943-5622.0000696

Wang, X., Yang, B., Jin, L., Zhang, Z., Xu, X., 2020. Management and Fractal Analysis of Desiccation Cracks of Soils with Acid Contamination. Adv. Civ. Eng. 2020, 1–9. https://doi.org/10.1155/2020/6678620

Weinberger, R., 1999. Initiation and growth of cracks during desiccation of stratified muddy sediments. J. Struct. Geol. 21, 379–386. https://doi.org/10.1016/S0191-8141(99)00029-2

Weninger, T., Julich, S., Feger, K.-H., Schwärzel, K., Bodner, G., Schwen, A., 2019. Effects of tillage intensity on pore system and physical quality of silt-textured soils detected by multiple methods. Soil Res. 57, 703–711. https://doi.org/10.1071/SR18347

WRB, 2014. World Reference Base for Soil Resources 2014, update 2015. International soil classification system for naming soils and creating legends for soil maps. World Soil Resources Reports No. 106, World Soil Resources Reports No. 106. FAO, Rome, Italy. https://doi.org/10.1017/S0014479706394902

Xu, G.X., Wang, Z.F., Gao, M., Tian, D., Huang, R., Liu, J., Li, J.C., 2018. Effects

of straw and biochar return in soil on soil aggregate and carbon sequestration. Huanjing Kexue/Environmental Sci. 39, 355–362. https://doi.org/10.13227/j.hjkx.201705217

Xu, Xu tang, Shao, L. jin, Huang, J. bin, Xu, Xiang, Liu, D. qi, Xian, Z. xing, Jian, W. bin, 2021. Effect of wet-dry cycles on shear strength of residual soil. Soils Found. 61, 782–797. https://doi.org/10.1016/J.SANDF.2021.03.001

Yang, B., Li, D., Yuan, S., Jin, L., 2021. Role of biochar from corn straw in influencing crack propagation and evaporation in sodic soils. CATENA 204, 105457. https://doi.org/10.1016/J.CATENA.2021.105457

Ye, Y., Xiao, S., Liu, S., Zhang, W., Zhao, J., Chen, H., Guggenberger, G., Wang, K., 2020. Tillage induces rapid loss of organic carbon in large macroaggregates of calcareous soils. Soil Tillage Res. 199, 104549. https://doi.org/10.1016/j.still.2019.104549

Yiotis, A.G., Tsimpanogiannis, I.N., Stubos, A.K., Yortsos, Y.C., 2006. Pore-network study of the characteristic periods in the drying of porous materials. J. Colloid Interface Sci. 297, 738–748. https://doi.org/10.1016/j.jcis.2005.11.043

Yoshida, S., Adachi, K., 2001. Soil Science and Plant Nutrition Effects of cropping and puddling practices on the cracking patterns in paddy fields. Soil Sci. Plant Nutr. 47, 519–532. https://doi.org/10.1080/00380768.2001.10408416

Yost, J.L., Palmer, C.E., Egerton-Warburton, L.M., 2014. The Contribution of Soil Aggregates to Carbon Sequestration in Restored Urban Grasslands. Soil Carbon 147–154. https://doi.org/10.1007/978-3-319-04084-4_15

Zeng, H., Tang, C. sheng, Cheng, Q., Inyang, H.I., Rong, D. zheng, Lin, L., Shi, B., 2019. Coupling effects of interfacial friction and layer thickness on soil desiccation cracking behavior. Eng. Geol. 260, 105220. https://doi.org/10.1016/j.enggeo.2019.105220

Zhang, X., Xin, X., Zhu, A., Zhang, J., Yang, W., 2017. Effects of tillage and residue managements on organic C accumulation and soil aggregation in a sandy loam soil of the North China Plain. Catena 156, 176–183. https://doi.org/10.1016/j.catena.2017.04.012

Zhang, Y., Gu, K., Li, J., Tang, C., Shen, Z., Shi, B., 2020. Effect of biochar on desiccation cracking characteristics of clayey soils. Geoderma 364, 114182. https://doi.org/10.1016/j.geoderma.2020.114182

Zhang, Z.B., Zhou, H., Lin, H., Peng, X., 2016. Puddling intensity, sesquioxides, and soil organic carbon impacts on crack patterns of two paddy soils. Geoderma 262, 155–164. https://doi.org/10.1016/j.geoderma.2015.08.030

Zhang, Z.B., Zhou, H., Zhao, Q.G., Lin, H., Peng, X., 2014. Characteristics of cracks in two paddy soils and their impacts on preferential flow. Geoderma 228–229, 114–121. https://doi.org/10.1016/j.geoderma.2013.07.026

Zheng, W., Zeng, S., Bais, H., LaManna, J.M., Hussey, D.S., Jacobson, D.L., Jin, Y., 2018. Plant Growth-Promoting Rhizobacteria (PGPR) Reduce Evaporation and Increase Soil Water Retention. Water Resour. Res. 54, 3673–3687. https://doi.org/10.1029/2018WR022656

Zhou, H., Chen, C., Wang, D., Arthur, E., Zhang, Z., Guo, Z., Peng, X., Mooney, S.J., 2020. Effect of long-term organic amendments on the full-range soil water retention characteristics of a Vertisol. Soil Tillage Res. 202, 104663. https://doi.org/10.1016/j.still.2020.104663

Zhu, L., Fan, D., Ma, R., Zhang, Y., Zha, Y., Russo, S. Lo, 2018. Experimental and Numerical Investigations of Influence on Overland Flow and Water Infiltration by Fracture Networks in Soil. Geofluids ID 7056858, 1–16. https://doi.org/10.1155/2018/7056858

Zhu, L., Shen, T., Ma, R., Fan, D., Zhang, Y., Zha, Y., 2020. Development of cracks in soil: An improved physical model. Geoderma 366, 114258. https://doi.org/10.1016/j.geoderma.2020.114258

Ziegler, S., Leshchinsky, D., Ling, H.I., Perry, E.B., 1998. Effect of Short Polymeric Fibers on Crack Development in Clays. Soils Found. 38, 247–253. https://doi.org/10.3208/SANDF.38.247

Appendices

Appendix under Chapter 4

Appendix A: Parameters of soil water evaporation curve

Treatment	α (m.s-1)	Wcrit (%)	Qmax ($cm^3.day^{-1}$)
RTRI	0.00221±0.00017a*	0.2±0.016	181.28±14.09a*
CTRO	0.00161±0.00017ab	0.2±0.016	131.68±14.09ab
DS	0.00111±0.00017b		90.56±14.09b

** Wcrit: critical water content; α: Mass transfer coefficient α (m/s); qmax: Maximum drying rate (cm3.day-1), N/A: not enough data*

Appendix B: ANOVA of pore size distribution (PSD) class

Source	DF	Sum of squares	Mean squares	F	Pr > F
Model	2	0.0083	0.0042	11.9010	0.0056
Error	7	0.0025	0.0004		
Corrected Total	9	0.0108			

Appendix C: Model parameters of van Genuchten (van Genuchten, 1980) and Durner (Durner, 1994):

Treatment	θs	θr	$w1^a/m^b$	R^2
RTRI (DB)	0.477±0.033	0.053±0.046	0.24±0.182	0.999±0.001
CTRO (VG)	0.499±0.004	6.58E-06±8.72E-06	1.275±0.055	0.989±0.009
DS (DB)	0.467±0.046	0.16±0.083	0.217±0.204	0.998±0.002

** [a]DB: Bimodal model of Durner, [b]VG: Monomodal model of van Genuchten. θs: saturated water content, θr: residual water content, R^2: determination coefficient. The value indicates mean ± standard error*

Details information about the model's parameters

Treatment	θs	θr	w1	a1/a	n1/m	a2	n2	R2
RTRI-1	0.443	0.000	0.033	0.005	7.94	0.0016	1.30	0.99776
RTRI-2	0.481	0.075	0.315	0.019	1.7847	0.0008	1.46	0.99998
RTRI-3	0.508	0.083	0.372	0.018	1.5398	0.0006	1.48	0.99996
CTRO-1	0.496	8.85E-07	N/A	0.002	1.3284	N/A	N/A	0.99829
CTRO-2	0.503	2.24E-06	N/A	0.004	1.219	N/A	N/A	0.98094
CTRO-3	0.498	1.55E-05	N/A	0.002	1.2786	N/A	N/A	0.98678
DS-1	0.471	0.050	0.294	0.079	1.3723	0.0003	1.33	0.99810
DS-2	0.428	0.145	0.470	0.038	1.4387	0.0004	1.42	0.99930
DS-3	0.531	0.205	0.038	0.122	27.659	0.0179	1.19	0.99775

Appendix D: Correlation coefficient and RMSE between observed and fitted water suction from SWRC

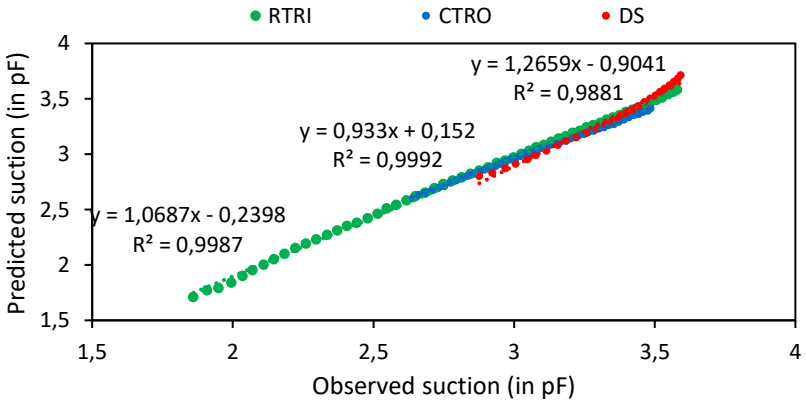

(**a**) Graph showing the linear correlation between predicted (from SWRC) and observed data. Slope=1: perfect estimation, Slope > or < 1: over and underestimation.

b) Characteristic and error between predicted/observed suction data

Treatment	Nb-Obs	Slope	R^2	RMSE
RTRI	58	1.07	0.9987	0.0603
CTRO	47	0.93	0.9992	0.0575
DS	27	1.27	0.9881	0.0696

** Nb-Obs: number of observations, Slope: slope of the correlation between predicted versus observed data, R2: correlation coefficient of determination, RMSE: Root Mean Square Error*

Appendix under Chapter 6

Appendix E: Methods for calculating cracks characteristics such as fractal dimension (Fd) and the probability entropy (H) (Yang et al., 2021)

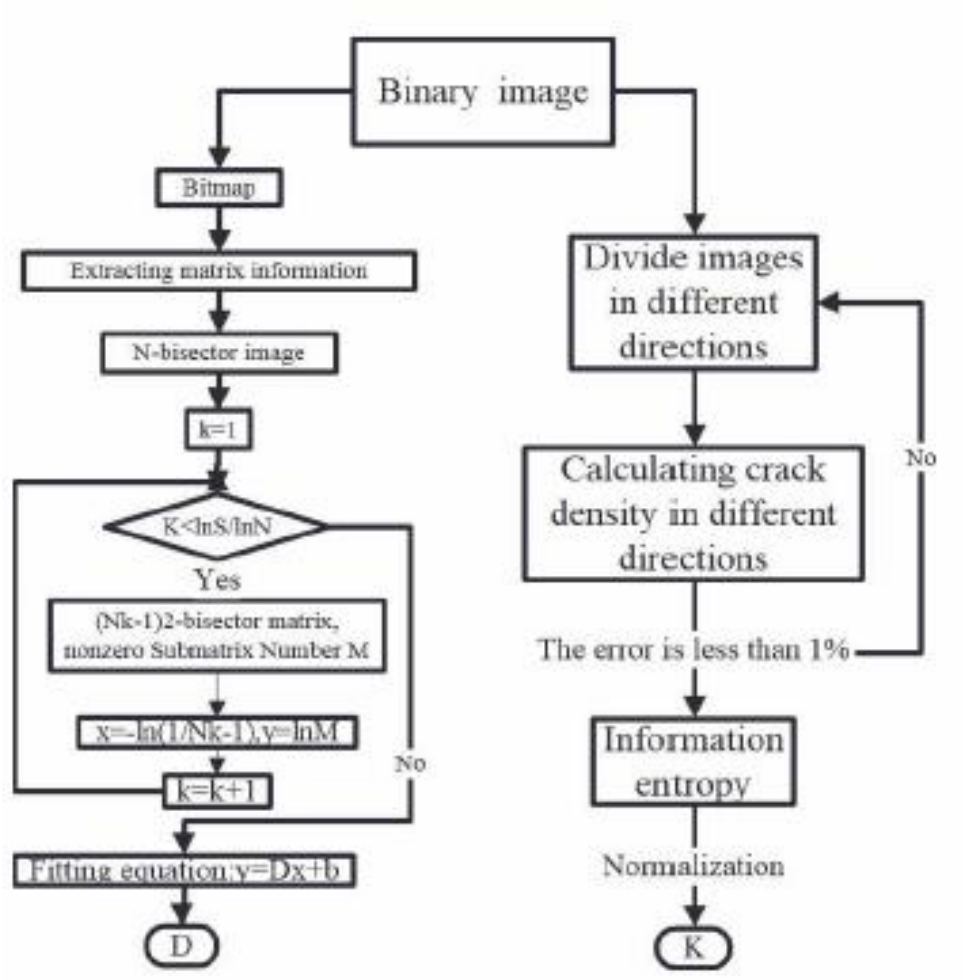

Appendix F: Explanation of fractal dimension

a) Fractal Dimensions of Geometric Objects

In the last section, we learned how scaling and magnification relate to dimension, and we saw that the dimension, D, can be seen as the log of the number of pieces divided by the log of the magnification factor. Expressed as an equation, we have D

= log(N) / log(r). Now let's apply this idea to some geometric fractals. We'll examine the Koch Curve fractal below:

Geometric fractals can be made by starting with a simple generator pattern and replacing every section of the pattern with a smaller copy of the generator. Let's look at the way the length of the curve changes as we iterate the fractal. The generator (order 1) is made of 4 sections, and each section is 1/3 of the length of the initiator (order 0), which has a unit length of 1. The second order of the Koch Curve has had each of the 4 sections of the generator replaced with the same shape, so it has 16 small segments, and each segment is 1/9 of the unit length. That means the total length of the second order curve is 16/9. The third order curve follows the same pattern, and it has 64 tiny segments, each of which is 1/27 of the unit length, making a total length of 64/27. As the progression continues, the curve gets longer and longer, and eventually becomes infinitely long! Now, it is not very useful to know that a curve is infinitely long, and this is where the concept of Fractal Dimension becomes very useful.

Remembering that D = log(N) / log(r), we can calculate the dimension D by seeing how the number of units, N, changes with the magnification factor, r. In this case, we can see that the number of pieces in the generator, N, is 4, and the magnification factor is 3, because each section of the generator is 1/3 of the unit length. This same relationship holds between each of the orders of the curve. Order 4 has four times as many pieces as order 3, and each piece is 1/3 the scale.

So according to the formula D = log(N) / log(r), we can say that D = log(4) / log(3) = 1.26

b) But what does this mean?!

We're used to dimensions that are whole numbers, 1,2 or 3. What could a fractional dimension mean?

Fractional dimensions are very useful for describing fractal shapes. In fact, all fractals have dimensions that are fractions, not whole numbers. We can make some sense out of the dimension, by comparing it to the simple, whole number dimensions. If a line is 1-Dimensional, and a plane is 2-Dimensional, then a fractional dimension of 1.26 falls somewhere in between a line and a plane. And this describes the Koch Curve - it's wigglier than a straight line, but it doesn't fill up a whole 2-Dimensional plane either. As we'll see soon, the more of a plane that a fractal covers the closer its dimensions is to 2.

Source: http://fractalfoundation.org/OFC/OFC-10-2.html

Another way to calculate Fd is from calculation of the angle between the two lines which starts from 0° for a line and increases to 90° when two lines are at right angle.

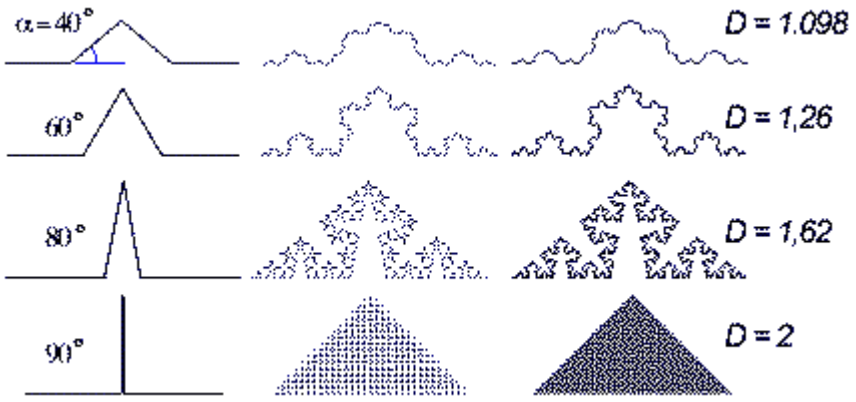

e.g. D = log 2 / log (2 cos a / 2),
Source : http://charles.vassallo.pagesperso-orange.fr/fr/art/dimension.html